Image-guided radiotherapy using 2D and 3D ultrasound combined with Monte Carlo dose calculations in prostate treatments

Clarisse Ildikó Mark

Department of Medical Physics
McGill University, Montreal
December 2005

A thesis submitted to the Faculty of Graduate and Postdoctoral Studies in partial fulfillment of the requirements of the degree of Master of Science in Medical Radiation Physics

Your file Votre référence
ISBN: 978-0-494-24733-4
Our file Notre référence
ISBN: 978-0-494-24733-4

Abstract

Two ultrasound systems were studied to investigate the effects of positional and volumetric prostate variations on dosimetry over the course of external radiation therapy. A 2D system, currently used at the Montreal General Hospital for patient repositioning, was compared to a 3D system invented recently. Prostate variations were quantified from ultrasound images acquired daily during a 2003 clinical study. A method was devised to introduce ultrasound information in a Monte Carlo Treatment Planning System previously developed at McGill. Patient repositioning was evaluated for both systems using dose-volume histograms of Voxel Monte Carlo dose calculation. Repositioning with the 3D system, neglecting volume changes, was found to bring the target dose to within 1 % of the planned dose, rather than the 12 % of the clinical 2D system. However, when considering the varying 3D volumes, the dose could only be corrected to within 7 %. These results indicate that the 3D system provides not only a more accurate assessment of prostate displacements, but also volumetric information that significantly affects the dosimetry.

Résumé

Deux systèmes ultrasons ont été étudiés dans le but d'examiner les effets que peuvent avoir sur la dosimétrie les changements de position et de volume de la prostate durant la radiothérapie externe. Un système 2D, présentement utilisé à l'Hôpital Général de Montréal pour le repositionnement des patients, a été comparé à un système 3D nouvellement inventé. Les variations de la prostate ont été quantifiées à partir d'images ultrasons acquises quotidiennement durant une étude clinique effectuée en 2003. Une méthode a été conçue pour introduire l'information ultrasons dans un Système de Planification de Traitement Monte Carlo développé antérieurement à McGill. Le repositionnement des patients a été évalué pour chacun des systèmes en utilisant des histogrammes dose-volume sur des calculs de dose de Voxel Monte Carlo. On a constaté que le repositionnement avec le système 3D, en gardant des volumes constants, ramène la dose à la cible à 1 % de la dose planifiée, plutôt qu'à 12 % comme l'indique le système clinique 2D. Cependant, il y été établi qu'en considérant les variations de volumes 3D, la dose peut seulement être corrigée à 7 %. Ces résultats indique que le système 3D procure non seulement une évaluation plus exacte des déplacements de la prostate, mais aussi de l'information volumétrique qui affecte la dosimétrie de façon marquée.

Acknowledgements

I would like to thank my supervisor, Dr. Frank Verhaegen, for his valuable expertise, guidance, support and editorial help. Thanks for the opportunity he gave me to attend an international workshop on medical imaging technologies as well as his encouragements in making me see the value of pursuing Doctoral level studies.

I want to thank Dr. Ervin Podgorsak for his broad knowledge in the field and for providing me the opportunity to study in a world-class department.

I would like to thank Dr. Tony Falco and all of the Resonant Medical Inc team for support with the RESTITU ultrasound prototype and for providing me with their ultrasound data from a 2003 clinical study.

Thanks to Dr. Te Vuong and Dr. Fabio Biagini Cury for their valuable expertise in medical related matters. For computer and programming support, special thanks to Dr. François Deblois & Dr. Wamied Abdel-Rahman.

I also want to take this opportunity to recognize the advices given to me by Geneviève Jarry concerning Monte Carlo simulations. Special thanks to Aichu Chang for assisting me in collecting a tremendous amount of patient clinical data.

I thank also all of the medical staff and the Medical Physics students for making the past two years memorable.

This research has been founded by an NSERC Post-Graduate Scholarship.

Table of Contents

Abstract I
Résumé II
Acknowledgements III
Table of Contents IV

Chapter 1: Objectives of the research

1.1. Background 1
1.1.1 Prostate cancer 1
1.1.2 External Beam Radiation Therapy 1

1.2. Organ motion 3
1.2.1 Image Guided Radiation Therapy 4

1.3. Dose accuracy 5
1.3.1 Monte Carlo method 6
1.3.2 McGill Monte Carlo Treatment Planning system 7

1.4. Purpose and structure of the thesis 7

References 9

Chapter 2: Methods and Material
Ultrasound as a tumor localization device

2.1. Rational for daily measurements with ultrasound 13
2.1.1 Ultrasound imaging fundamentals 13

2.2. Prostate motion and volume 18

2.3. Obtaining ultrasound daily prostate motion data 19
2.3.1 BAT system 20
2.3.2 RES system 23
2.3.3 2003 clinical study 27

References 28

Chapter 3: Methods and Material Patient Dose Calculation

3.1. Treatment Planning Systems **31**
3.1.1 CADPLAN 31
3.1.2 Monte Carlo simulations 31
3.1.2.1 BEAMnrc *32*
3.1.2.2 XVMC and DOSXYZ *33*

3.2. Introducing motion changes in TPS **36**
3.2.1 CADPLAN 37
3.2.2 Monte Carlo 39

3.3. McGill Monte Carlo Treatment Planning system **40**
3.3.1 State of the art system capabilities 40
3.3.2 Methods of DVH analysis 40
3.3.3 System adaptations to introduce ultrasound data 49
3.3.3.1 Positional variations *50*
3.3.3.2 Volumetric variations *56*

References **63**

Chapter 4: Results and discussion 2D versus 3D Ultrasound

4.1. Quantification of daily positional measurements **65**

4.2. Quantification of daily volumetric measurements **73**

References **76**

Chapter 5: Results and discussion Monte Carlo dose calculations

5.1. XVMC versus CADPLAN **79**
5.1.1 CADPLAN without heterogeneity correction 79
5.1.2 CADPLAN with heterogeneity correction 87
5.1.3 Conclusion 93

5.2. XVMC versus DOSXYZ 94
5.2.1 CT density and materials ... 94
5.2.2 Water density and material ... 96
5.2.3 Conclusion ... 98

References 99

Chapter 6: Results and discussion
Introducing ultrasound information

6.1. Introducing positional variations 101
6.1.1 CADPLAN ... 101
6.1.2 XVMC ... 105
6.1.3 Conclusion ... 108

6.2. Introducing volumetric variations 109
6.2.1 CADPLAN ... 109
6.2.2 XVMC ... 114
6.2.3 Conclusion ... 117

References 118

Chapter 7: Conclusions and future work

7.1. Summary of the work performed 119
7.1.1 Quantification of prostate variations ... 119
7.1.2 XVMC versus CADPLAN ... 120
7.1.3 XVMC versus DOSXYZ ... 120
7.1.4 Dosimetric impact of prostate variations ... 121

7.2. Future work 121

Chapter 1: Objectives of the research

1.1 Background

1.1.1 Prostate cancer

There are approximately 11 000 prostate cancer cases every year in Canada [4]. This disease involves the uncontrolled growth of cells in the prostate that culminate in a malignant tumor. If left untreated, this tumor tends to metastasize to other body parts and can lead to death. It is estimated that one in 7 men will develop prostate cancer and one in 26 men will die from it [3]. Several different modalities can be used alone or in combination to provide curative or palliative treatments; radiotherapy (RT), brachytherapy, radical prostatectomy or hormone therapy. The majority of prostate cases are treated with external beam radiation therapy (EBRT). From April 1st 2004 to March 31st 2005, the McGill University Health Center (MUHC) and its affiliated hospitals diagnosed 349 prostate cases and treated 200 of them with RT; 93 % with EBRT alone and the rest with a combination of EBRT and brachytherapy. The research described here involves data collected from a clinical study performed in 2003 on a group of 26 prostate patients who underwent EBRT at the Montreal General Hospital (MGH).

1.1.2 External Beam Radiation Therapy

Radiotherapy (RT) uses ionizing radiation to eradicate malignant cells within cancerous tissues and organs. Depending on where the radiation source is situated, RT can be classified into: brachytherapy or external beam radiation therapy (EBRT). In brachytherapy, the radioactive source is placed inside the body. In EBRT, the radiation is provided by a medical linear accelerator (Linac) external to the patient. By tightly conforming to tumor tissues, 3D conformal RT (3D-CRT) can deliver a higher dose of radiation to the tumor while reducing the dose to normal tissues to lessen side effects. At the MGH, typical prostate EBRT treatment plans (TP) involve irradiating the prostate to 50-70 Gy by five 3D-CRT photon beams by rotating the Linac head around the patient and stopping at the 5 required positions: One anterior (A), two lateral (RT and LT) and

two posterior obliques (RPO and LPO) (Figure 1.). The amount of time spent in each position is dictated by the prescribed number of Monitor Units (MU) corresponding to a certain amount of dose delivered; typically 1cGy for 1 MU under specific conditions.

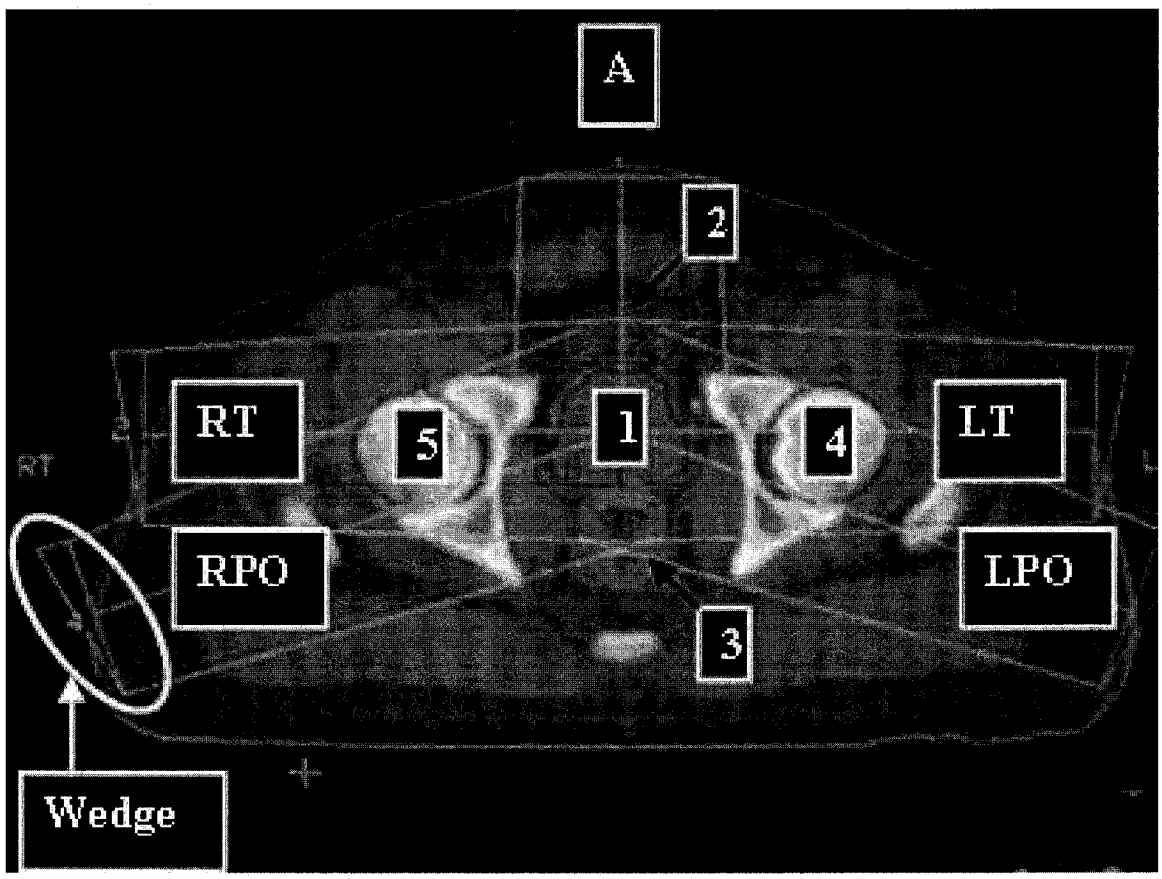

Figure 1.1: Axial CT image and 3D-CRT photon beam arrangement for typical prostate patient treated by EBRT at the MGHThe co ntours indicated are: (1) the prostate, (2) the bladder, (3) the rectum, (4) the left femoral head and (5) the right femoral head.

An arrangement with no posterior field is necessary to protect the radiation sensitive rectum. To spare the bladder and the femurs, physical blocks of angled lead or steel, called wedges (Figure 1.), are placed in the beam to produce a gradient in the radiation intensity. In order to cover the prostate from all directions while sparing healthy tissues, the radiation fields are irregularly-shaped through static MultiLeaf Collimators (MLC) in the Linac head. The MLC typically consist of 26 pairs of individually computer-

controlled tungsten leaves that partially block the fields [21]. The photon beam energy is typically 18 MV. Using a high energy increases the effective treatment depth while decreasing the surface dose [14], a requirement to treat the deeply seated prostate.

In preparation for a treatment plan (TP), patients diagnosed and staged with prostate cancer must undergo a scan, typically through a Computed Tomography Simulator (CT-Sim), a month prior to the start of treatment. Based on segmentations of pelvic organs on every CT slice, a 3D treatment planning system (TPS) is used to generate an optimum TP. The MGH uses the CADPLAN TPS (Varian Oncology System, CA) for 3D-CRT. To be found are; (1) the recognition and localization of 3D clinical and planning target volumes (CTV and PTV) and neighboring organs at risk (bladder, rectum and femoral heads), (2) the direction, shape and weight of each beam, (3) the prescription dose, fractional dose value, dose distribution and limitation, (4) the patient positioning and (5) the Linac beam energy and MUs.

The total prescribed dose in EBRT is usually delivered in a series of small fractions of equal sizes. Dose fractionation has shown to achieve better control of cancerous tumors while minimizing damages to surrounding healthy tissues [15,20,21]. Typical prostate patients receive five fractions per week over 4-8 weeks for a total of 22-36 treatments. The conventional daily set-up uses skin marks on the patient and lasers on the walls of the treatment room to recreate the correct planned couch position every day.

1.2 Organ motion

As a dose fractionation treatment progresses, tumors can vary in volume and position due to (1) patient setup uncertainties and errors arising in slightly different positions of immobilization devices on subsequent days and (2) internal organ motion due to different daily bladder and rectal fill or weight gain or loss. Table 1. shows that the typical variations expected for the prostate, bladder and rectum over a single week can be quite significant [10].

Organ/Tumor	△ Volume	△ Position (mm)
Prostate	20 % / 2 weeks	0.4 – 6
Bladder	6 % / week	15
Rectum	4 % / week	13 – 20

Table 1.1: Typical magnitudes of variations in organ volume and position during the course of EBRT for prostate patients.

Currently in TP, organs are assumed to remain fixed in position and volume over the entire course of treatment. The organ contours are based on the single CT-scan taken prior to the start of treatment. Following geometrical definitions by the International Commission on Radiation Units and Measurements (ICRU) [9], the planning target volume (PTV) must account for internal organ motion and treatment setup uncertainty to ensure adequate coverage of the gross palpable or visible tumor defined by the radiation oncologist as the clinical target volume (CTV). Studies have shown that for the PTV to emcompass prostate position and volume variations with a 95 % probability, margins of 7 mm are required around the CTV in the lateral and cranial-claudal directions and of 11 mm in the superior-inferior and anterior-posterior directions [22,1]. These large margins can lead to undesirable rectal and bladder complications. The solution to organ motion lies in Image-Guided RT (IGRT).

1.2.1 Image-Guided Radiation Therapy

Radiation delivery accuracy can be improved by localizing and realigning the prostate in the fields prior to daily treatments. Knowing precisely where the target is allows EBRT to hit tumor cells while sparing healthy tissues, effectively positioning the dose accurately inside the treated volume. Image-guidance of organs could potentially allow (1) to reduce margins, (2) a higher dose delivery and (3) to reduce side effects [24]. In fact, based on a ultrasound (US) localization device used by Lattanzi *et al* [11], Price *et al* [13] reduced their localization uncertainty to 3 mm on Intensity-Modulated RT (IMRT) prostate patients, for a total margin around the GTV of only 5 mm instead of the conventional 7 mm.

Several different imaging modalities can be used for IGRT, the most common ones being: Electronic portal imager, CT scanner, Magnetic Resonance Imaging (MRI) and US. Electronic portal imaging can be integrated into the Linac to verify the position of the prostate on a daily basis. During a short fraction of the treatment time, the beam is used to expose an electronic imaging system for real-time imaging of radiopaque markers or bony anatomies. The main drawbacks are marker migration from their original position and poor soft tissue contrast due to the high Linac energy. CT-scans, on the other hand, are taken with lower beam energy for higher contrast images. However, these are usually taken only at the planning stage since daily scans would result in an unacceptably large dose of radiation to healthy tissues. Moreover, CT-scanners have low availability, high costs and are usually in a different room than the Linac. To avoid exposing patients to harmful radiation, MRI would be an option but not a viable one due to the very high costs and low availability of the equipment.

Given the limitations of the above methods, the currently accepted imaging technique used for daily prostate repositioning is US [6,19,23]. US imaging has the benefits of being a simple and non-invasive procedure, offering good soft tissue contrast and high spatial resolution. The equipment is very compact and relatively cheap, making it the only imaging procedure which can be easily integrated in the RT treatment room.

1.3 Dose accuracy

Because tumor control is tightly related to dose, accurate dose delivery is critical in RT. The overall accuracy of the dose delivered to patients is recommended to be ± 5 % [8]. Since there are many sources of errors in the RT process, the uncertainty in the dose calculation should be within ± 2 %. This goal is hard to achieve in the presence of heterogeneities such as soft tissue, bone and air found in the prostate region. Differences of 10-30 % have been reported when comparing calculations to measurements at interfaces between materials of different densities [12,26]. Unfortunately, in current practice TPS calculate the dose to be delivered without considering heterogeneous regions in patients. Details of complex internal organs are neglected. As a result of

these severe inaccuracies, dose calculations are approximates to the actual delivered dose [2]. The solution to these inaccuracies lies in Monte Carlo (MC) dose calculations.

1.3.1 Monte Carlo method

The Monte Carlo method is based on the fundamentals of radiation physics to simulate accurate trajectories of individual particles. It contains algorithms to simulate both photon and electron transport in Linacs and patient geometries. The transport algorithms start with a particle shower described by position, energy and direction. To find which interaction the particle will undergo after, a pseudo random number generator (RNG) samples probability distribution functions (PDFs) describing physical processes. The energy, direction and distance of travel of any particle resulting from this interaction are sampled from predetermined angular distribution of material dependent cross sections [17]. The path of the incident particle in a medium including all secondary particles is defined as a history. The larger the numbers of histories simulated the better the precision of the resulting macroscopic behavior.

MC is capable of calculating accurate dose distributions in complex geometries such as Linacs, including MLC and wedges [16] as well as patients including heterogeneities. Previous work in our research team has shown excellent agreement between results of MC simulations and measurements as well as significant errors in conventional dose calculations based on analytical techniques [5,7,18]. As MC simulations become faster, MC will be integrated in the clinic for TP. Such a system, still at the research stage, is described in the following section.

1.3.2 McGill Monte Carlo Treatment Planning system

In the view that MC will soon become fast enough for clinical implementation, the McGill Medical Physics Unit has integrated it into a state of the art research software for TP; the McGill Monte Carlo Treatment Planning system (MMCTP). McGill is unique in Canada on this front as it held an "International Workshop on Current Topics in Monte Carlo Treatment Planning" in May 2004 [25]. This tool integrates CT images used for TP, MC dose calculations as well as TP from clinical TPS. As described in section 1.3.1, MC can model heterogeneities in patient geometries and hence provide dose distributions that are closer to reality than conventional TPS. Hence, with its superior dose calculations, MMCTP can minimize discrepancies between planned dose and real delivered dose. MMCTP can also serve as a gold standard to compare empirical heterogeneity corrections of conventional TPS.

1.4 Purpose and structure of the thesis

The purpose of the thesis is to evaluate the extent to which planned dose distributions are degraded by prostate motion and volumetric changes. To this date, there are no publications on the comparison of 2D and 3D US data for IGRT that also include a dose calculation analysis. The goal of the proposed research is to analyse US image data, obtained from a 2003 clinical study, for every treatment fraction for 26 prostate patients. 2D and 3D US data are quantified for prostate motion and volume variations. The acquired US data is then integrated into our MMCTP system. This tool permits MC recalculation of the dose delivered at every treatment fraction, taking into account positional and volumetric prostate changes. This allows a more accurate assessment of the real dose delivered to the different organs over the course of a treatment. This also enables an investigation into the effects of inter-fraction variations on the clinically planned dose. By providing a new 4D dose distribution analysis tool for TP, this thesis project opens the door to important advances in adaptive RT. MMCTP could be used to replan a treatment an optimized number of times to decrease treatment outcome complications.

In the following chapter, the rational for using US for daily motion and volumetric measurements of the prostate is reviewed. A description of the equipment used in the 2003 clinical study is also given. Then, chapter 3 discusses the methods of patient dose calculations in clinical TPS and MC. The MMCTP system is detailed, along with its extension to include US positional and volumetric data. The results and discussions are divided into three separate chapters. Chapter 4 covers the quantification of the US measurements. Chapter 5 dives into the MMCTP analysis and comparisons to conventional TPS without the US information taken into account. Chapter 6 presents the MMCTP analysis with the US positional and volumetric data. In the last chapter, an overall conclusion is given and potential future work is discussed.

References

[1] Antolak J.A., Rosen I.I., Childress C.H., Zagars G.K. and Pollack A. "Prostate Target Volume Variations during the course of Radiotherapy", Int. J. Radiat. Oncol. Biol. Phys., 42 (3), pp. 661-672, 1998.

[2] Brahme A. "Dosimetric precision requirements in radiation therapy". Acta Radiol. Oncol., 23, pp. 379-91, 1984.

[3] Canadian Cancer Society
http://www.cancer.ca/ccs/internet/standard/0,3182,3172_14471__langId-en,00.html

[4] Canadian Cancer Society:
http://www.cancer.ca/ccs/internet/standard/0,3182,3172_15268__langId-en,00.html

[5] Doucet R., Olivares M., DeBlois F., Podgorsak E.B. , Kawrakow I. and Seuntjens J. "Comparison of measured and Monte Carlo calculated dose distributions in inhomogeneous phantoms in clinical electron beams". Phys. Med. Biol., 48, pp. 2339-2354, 2003.

[6] Falco T., Shenouda G., Kaufmann C., Belanger I., Procaccini C., Charrois C. and Evans M. "Ultrasound imaging for external-beam prostate treatment setup and dosimetric verification". Medical Dosimetry, 27 (4), pp. 271-273, 2002.

[7] Heath E., Parker W., Curran B. and Seuntjens J.P. "Clinical Evaluation of the PEREGRINE Monte Carlo Dose Calculation System for 6MV photon Beams". World Congress on Medical Physics, Sydney, Australia, August 24-29, [paper No. 1800], 2003.

[8] ICRU "Determination of absorbed dose in patient irradiated by beams of X or gamma rays in radiotherapy procedure". International Commission on Radiation Units and Measurements, 1976, Report #24, Washington, D.C.

[9] ICRU "Prescribing, recording, and reporting photon beam therapy". Bethesda: International Commission on Radiation Units and Measurements, Sept. 1. 1993, Report #50.

[10] Langen K.M. and Jones D.T.L. "Organ Motion and its management". Int. J. Radiat. Oncol. Biol. Phys., 50 (1), pp. 265-278, 2001.

[11] Lattanzi J., McNeeley S., Pinover W., Horwitz E., Das I., Schultheiss T.E. and Hanks G.E. "A comparison of Daily CT localization to a daily Ultrasound-based system in prostate cancer", Int. J. Radiat. Oncol. Biol. Phys., 43 (4), pp. 719-725, 1999.

[12] Photon treatment planning collaborative working group "Role of inhomogeneity corrections in three-dimensional photon treatment planning". Int. J. Radiat. Oncol. Biol. Phys., 21, pp. 59-69, 2001.

[13] Price R.A., Hanks G.E., McNeeley S.W., Horwitz E.M. and Pinover W.H. "Advantages of using noncoplanar versus axial beam arrangements when treating prostate cancer with intensity-modulated radiation therapy and the step-and-shoot delivery method". Int. J. Radiat. Oncol. Biol. Phys., 53 (1), pp. 236-243, 2002.

[14] Podgorsak E.B., ed. "Review of radiation oncology physics: a handbook for teachers and students". Vienna, International Atomic Energy Agency, 2003.

[15] Regaud C. and Ferroux R. "Discordance des effets de rayons X, d'une part dans le testicule, par le fractionnement de la dose". C. R. Soc. Biol., 97, pp. 431–434, 1927.

[16] Rogers D.W. O., Faddegon B.A., Ding G.X., Ma C.-M., We J. and Mackie T.R. "BEAM: a Monte Carlo code to simulate radiotherapy treatment units", Med. Phys, 22 (5), pp. 503-524, 1995.

[17] Rogers D.W. O., Walters B. and Kawrakow I. "BEAMnrc user manual", NRCC report PIRS-0590B, 2003.

[18] Seco J., Verhaegen F. and Bidmead M. "Development and commissioning of a Monte Carlo dose calculation engine for clinical IMRT beams". World conference on Medical Physics, Sydney Australia, 2003.

[19] Serago C.F., Chungbin S.J., Buskirk S.J., Ezzell G.A., Collie A.C. and Vora S.A. "Initial experience with ultrasound localization for positioning prostate cancer patients for external beam radiotherapy". Int. J. Radiat. Oncol. Biol. Phys., 53 (5), pp. 1130–1138, 2002.

[20] Suit H. and Witte R. "Radiation dose fractionation and tumor control probability". Radiat Res., 29, pp. 267–73, 1966.

[21] Thames H.D., ed. "Fractionation and radiotherapy". New York, Taylor and Francis, 1997.

[22] Tinger A., Michalski J.M., Cheng A., Low D.A., Zhu R., Bosch W.R., Purdy J.A. and Perez C.A. "A critical evaluation of the planning target volume for 3-D conformal radiotherapy of prostate cancer". Int. J. Radiat. Oncol. Biol. Phys., 42 (1), pp. 213–221, 1998.

[23] Trichter F. and Ennis R.D. "Prostate localization using transabdominal ultrasound imaging". Int. J. Radiat. Oncol. Biol. Phys., 56, pp. 1225-1233, 2003.

[24] Varian Medical Systems Annual Report: "Dynamic Targeting IGRT: What's next ?", pp. 5-8, 2003.

[25] Verhaegen F. and Seuntjens J.P., "Special issue: International Workshop on Current Topics in Monte Carlo Treatment Planning", Phys. Med. Biol., 50 (5), 2005.

[26] Wong W.J. and Purdy J.A. "On methods of inhomogeneity corrections for photon transport" Med. Phys, 17, pp. 807-817, 1990.

Chapter 2: Methods and Material
Ultrasound as a tumor localization device

2.1 Rational for daily measurements with ultrasound

Ultrasound (US) has been used for many years in the medical field for qualitative diagnostic purposes; the most well known application being obstetrics. Recently, US imaging has found a niche in correcting setup errors during internal or external radiotherapy (RT). As these corrections are generally required on a daily basis, US is truly the best imaging modality for this purpose: it is non-invasive, non-harmful, fast and easy to use. US offers real-time imaging while being relatively cheap and easily integrated in any oncology room. By selecting the proper probe and frequency, US can achieve a higher resolution than most imaging modalities. US also has a very high sensitivity to differences in soft tissues, a key feature in tracking internal organs such as the prostate.

2.1.1 Ultrasound imaging fundamentals

The basic principle of medical US imaging relies on the interactions of mechanical US waves with a patient. Most diagnostic US is used in pulse-echo operation, based on the transmission of US pulses rather than continuous waves (CW) [5]. An US transducer fills in a dual function; it acts as a transmitter of the US beam and as a receiver of the US echoes. Figure 2.1 shows the process involved in US image formation; the transducer produces high-frequency pulses that are transmitted into the human body. These US waves then get reflected off internal structures and are received as echoes.

The typical pulse-repetition frequency (PRF) is 5 kHz and the frequency of the US pulse is 2-10 MHz in common clinical practice. A typical prostate probe is at the low end of this range, because the prostate is a deep seated tumor and attenuation increases by 0.5 dB per cm per MHz in human soft tissues.

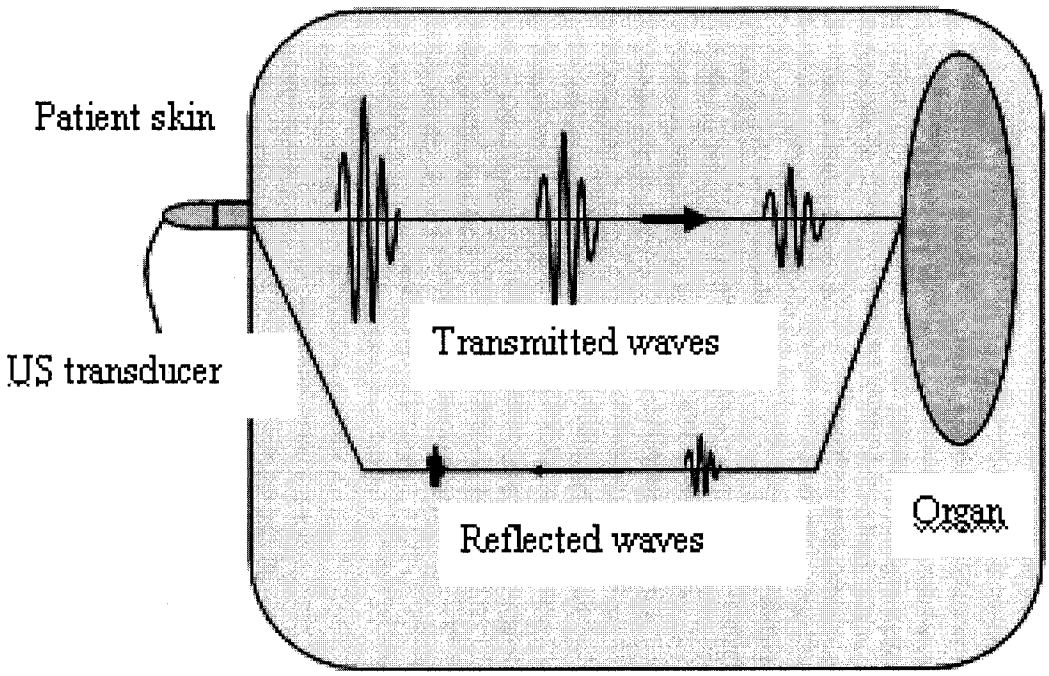

Figure 2.1: US data acquisition process.

An US image of the patient anatomy is built by sending waves in different directions. The image is assembled one bit at a time on a monitor, where each bit is generated by one returning echo. Many modalities can be used to construct an US image; (1) A-Mode, (2) M-Mode, (3) B-Mode and (4) 3D-Mode. The amplitude-mode (A-mode) is now obsolete in medical imaging. Figure 2.2 shows the 1D image obtained through this mode, where the amplitude of the US echoes are displayed with regard to position when a single beam passes through objects of different composition. The height of a spike is proportional to the echo intensity. The size of a brain can be measured accurately by dividing the speed of sound in soft tissue (1540 m/sec) by half of the sound travel time.

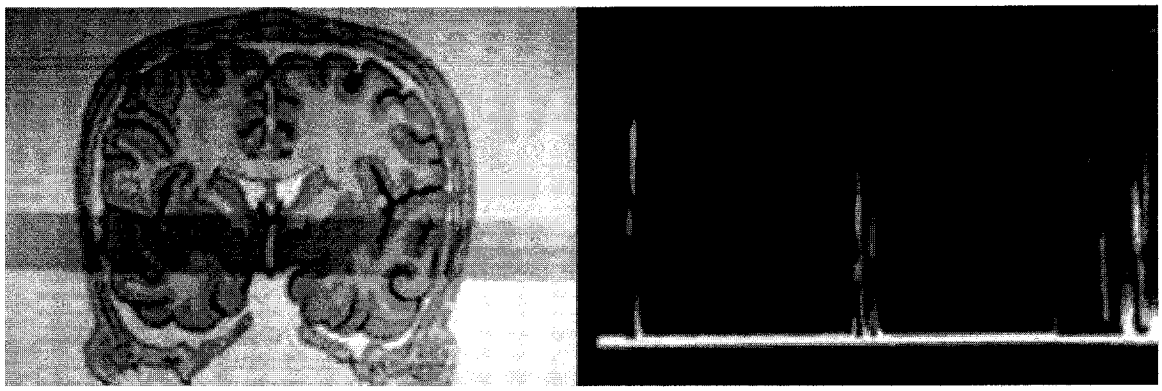

Figure 2.2: Example of an A-mode US image of the brain. [6]

M-mode is the motion-mode, where a single beam is held fix in position to measure very fast motions inside a patient. For example, Figure 2. shows the movement of a heart valve depicted in a wave-like manner (shown on the right) from a cross-sectional view of the heart (shown on the left) over time. This 1D mode, the oldest form of cardiac US, is still used extensively in cardiac and fetal cardiac imaging.

Figure 2.3: Example of M-mode US image of the heart. [3]

B-mode, also called brightness mode or 2D US, is commonly used. It is the same as A-mode, but the amplitudes are represented as image pixels, where the brightness of a pixel relates to the echo strength. The resulting gray-scale image gives a 2D graphical representation of the patient anatomy that provides good anatomic details. A series of such 2D US images can then be used in various imaging reconstruction techniques to form 3D US images.

The velocity (c) at which US waves transmit energy to a medium is independent of frequency (*f*). It mainly depends on the medium composition, with the most important characteristics being compressibility (κ) and mean density (ρ_0):

$$c(cm/\sec) = f(Hz)\ \lambda(cm) = \sqrt{1/\rho_0(g/cm^3)\ \kappa(cm\sec^2/g)} \tag{2.1}$$

where λ is the US wavelength [8]. Since US imaging relies on the reflection of US waves from internal structures, equation 2.2 gives the fraction of reflected energy at the boundary of two media with different acoustic impedances Z_1 and Z_2.

$$R(\%) = \left[\frac{Z_1 - Z_2}{Z_1 + Z_2}\right]^2 X\ 100 \tag{2.2}$$

The acoustic impedance (Z) is described by the density of the medium (ρ) and the velocity (c) of the wave in the medium:

$$Z(10^{-5} g/cm^2 \sec) = \rho(g/cm^3) \times c(cm/\sec) \tag{2.3}$$

Table 2.1 lists different types of human body tissues along with their velocities and impedances. The speed of sound is inversely proportional to the material compressibility (κ); sound travels slowest in gases as they are very compressible while it travels fastest in solids like bone, which are less compressible. In the middle of these two extremes lie human tissues that behave like liquids and transmit sound at around the same velocity. Hence, a velocity of 1540 m/sec is used in US systems as an average for human tissues. Tissues that have a velocity larger than this are imaged smaller than reality on the US image while tissues with a velocity smaller than this appear larger.

Material	US velocity (m/s)	US impedance ($\times 10^{-5}$ g/cm^{2}sec)
Air	331	0.0004
Fat	1450	1.38
Soft tissue	1540	1.54
Brain	1541	1.58
Liver	1549	1.65
Kidney	1561	1.62
Blood	1570	1.61
Muscle	1585	1.70
Lens of the eye	1620	1.84
Skull bone	4080	7.8

Table 2.1: Velocities and impedances of US signals in different body tissues. [5]

As image formation is based on reflection, the greater the difference between the impedances of two tissues the larger the reflection (equation 2.2). For example, from the impedances given in Table 2.1, a kidney/fat interface would yield a 0.64 % reflection while a kidney/muscle interface would result in only 0.06 % reflection. These interfaces would hence form different echo strengths that would appear as different pixel image contrast clearly distinguishable. Note that an almost 100 % reflection would result from an air/tissue interface. This reverberation would keep any useful signal from being transmitted inside a patient. Therefore, an acoustic coupling gel is applied on the patient skin before scanning to fill the air gap. This gel matches the impedances between the transducer and the skin to reduce the reflection and maximize the energy transmitted.

A number of pharmaceutical companies have developed contrast agents to enhance diagnostic US imaging. Most agents produced today are encapsulated gas-filled microbubbles less than 10 μm in diameter. They have specific physical and acoustical properties depending on bubble size, shell composition and inner gas. The bubbles can alter the echo amplitude by up to 25 dB by changing any or all of the following: (1) the US absorption, (2) the US reflection and (3) the US refraction. They provide acoustic

windows by filling body cavities. For example, by supplying the blood stream with an US contrast agent reflections from the blood-filled chambers of the heart significantly increase and the chambers can be clearly differentiated from those of the heart muscle itself. For prostate patients, filling the rectum or bladder with such an agent can improve visualization. However, none of the patients considered in this study were injected with contrast agents.

2.2 Prostate motion and volume

As mentioned in chapter 1, a prostate can move and change volume during the course of RT. These variations can be classified into two categories: intra-fraction and inter-fraction. Intra-fraction refers to prostate motion occurring while the radiation beam is on. Inter-fraction, the focus of the research presented herein, refers to organ changes on subsequent days. These variations have been under study using several different imaging modalities. In 1998, a research group at the M.D. Anderson Cancer Center used a CT-scanner to measure the mobility of the prostate CTV with respect to the pelvic anatomy during the course of RT [1]. In addition to the standard pre-treatment CT-scan, each of 17 patients was CT-scanned at 2-weeks intervals during therapy for a total of 4 scans. The rate of setup errors found was not much different from that observed in patients using portal images [7]. The pre-treatment CT study was found not to be representative of the prostate position during therapy. The research group concluded this was due to the bladder and rectum being emptier during RT as a consequence of irradiation. This systematic setup error could have also come from the different couches used on pre-treatment and on-treatment CT-scanners. Compared to CT-scanners, US and portal imagers remove this potential source of error by imaging the prostate at the Linac in the treatment position. Compared to CT-scanners or portal imagers, US allows a larger collection of data sets since no dose is delivered to the patient. For example, using CT for localization would expose patients to an extra dose of approximately 2-4 cGy every day [5]. Following this train of thoughts, Lattanzi *et al* evaluated the feasibility and accuracy of daily US-guided localization in prostate patients utilizing daily CT as a standard [11]. After 5 weeks of 3D-CRT, 23 patients underwent a second CT-scan. Out

of these, 10 patients were also scanned with the BAT US system (described in section 2.3.1). Significant correlation was found between the measured CT and US isocenter shifts in all three dimensions. They concluded US to be functionally equivalent to CT in terms of targeting purposes, while being more convenient to use than CT, which require significantly more human and technical resources.

2.3 Obtaining ultrasound daily prostate motion data

This research is based on a 2003 clinical study involving 26 prostate patients scanned with two different US systems. One system is 2D and part of the conventional setup procedure used at the MGH to track daily prostate positional shifts. The other system is a 3D prototype that can not only track positional shifts but also volumetric changes. Table 2.2 introduces some features of the US systems. The sections following detail the scanning procedures involved.

	US device	
	BAT system	**Restitu™ system**
Company	NAS/NOMOS, California	Resonant Medical, Quebec
Installed at the MGH in	2000	2003
Rooms	Linac	CT-Sim & Linac
Modality	Inter-modality (CT/US)	Intra-modality (US/US)
Type	2D B-mode	3D B-mode
Probe f (MHz)	3.5	3.5 to 13
Types of cancer	Prostate	Head and Neck & Prostate
Position sensors	Robotic arm	Polaris
Precision (cm)	± 0.07	± 0.1
Applications	Spatial Shifts	Spatial Shifts & Dose recalculation

Table 2.2: US systems used in the 2003 clinical prostate study

2.3.1 BAT system

The BAT system, short for B-mode Acquisition and Targeting, was purchased by the MUHC in winter 2000. The system is installed in the treatment room adjacent to the Linac to obtain daily prostate spatial shifts. Manufactured by the NOMOS Radiation Oncology Division of North American Scientific (NAS), it was the first commercial US-guided targeting device to be developed. It is a 2D US system that produces real-time US images in axial and sagittal planes. The system is made up of a 2D probe and a 3D robotic arm (Figure 2..a), a touch screen and a computer system coupled to the hospital network.

The procedure to obtain US images of a prostate patient is as follows. First the US probe is oriented to the Linac isocenter through a docking device on the collimator (Figure 2.. b). The probe then recognizes its position in 3D space and can be moved in any direction while maintaining its orientation with respect to the Linac isocenter.

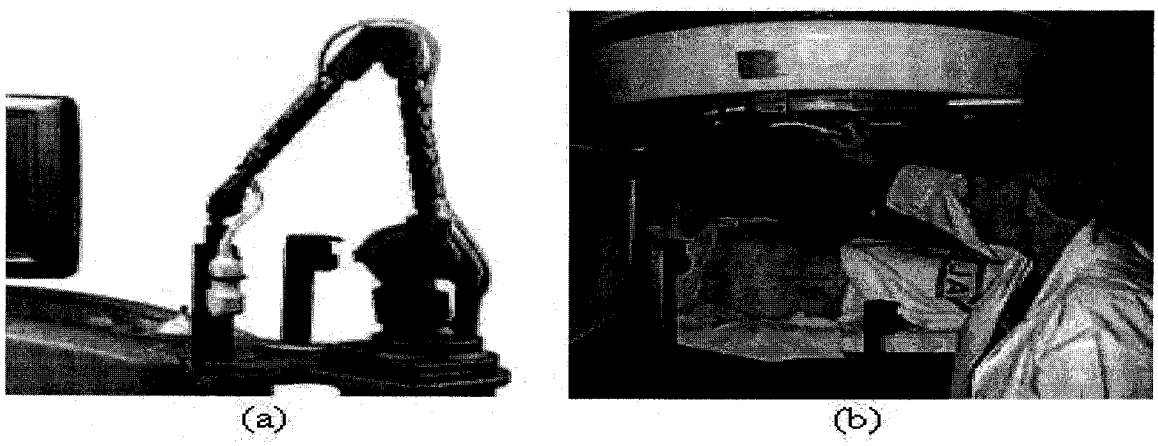

Figure 2.4: BAT system showing (a) the probe and the robotic arm and (b) the probe calibration position in the Linac docking system.

The system is then ready to scan the patient, who gets positioned by aligning his skin dye marks with lasers on the wall. Two perpendicular US images, one axial and one sagittal, are acquired and displayed on the screen (Figure 2.3). These images have known orientation since the probe is aware of where it lies in space. After importing the CT information through DICOM, it is hence possible to overlay the CT prostate contour

along with the TP isocenter position onto the corresponding US images. The misalignment between the CT contours and the US images is corrected manually by the technologist in both the axial and sagittal views. The magnitude and direction of the required shifts are recorded by the BAT system.

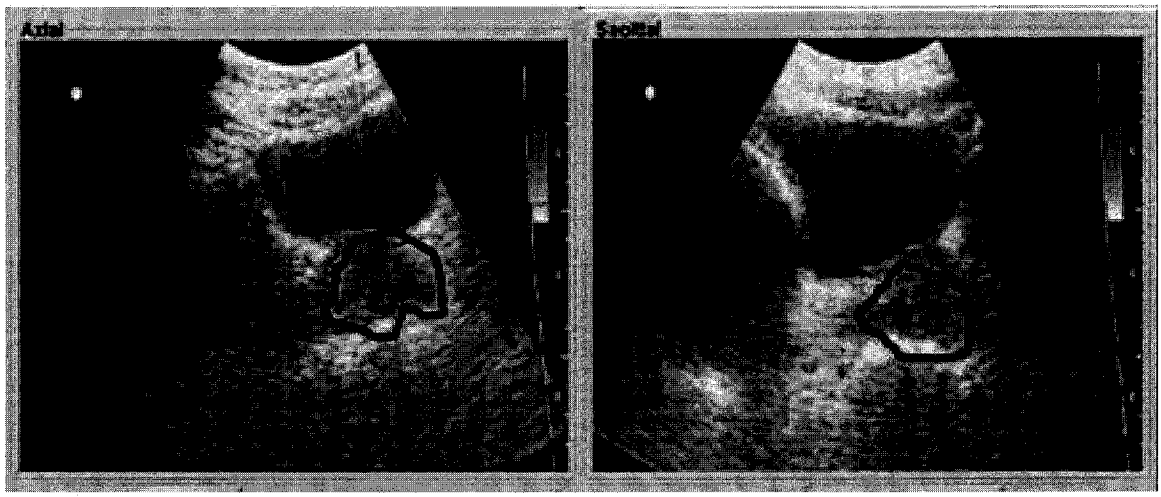

Figure 2.3: BAT US axial and sagittal images and contours used for couch alignment. The CT prostate contour is shown in heavy dark line.

The technologist can then make the required couch shifts to position the prostate back to the desired TP position, effectively correcting for daily prostate motion. By inserting the probe in the couch docking system (Figure 2.4) BAT tracks the couch position to within 0.7 mm of the desired position. As it is performed after conventional setup, the measured shift includes setup errors which have been shown to have a standard deviation on the order of 2-3 mm [2]. The BAT displacements shown on the screen are recorded in the patient charts. This procedure was performed daily for all the patients in the clinical study.

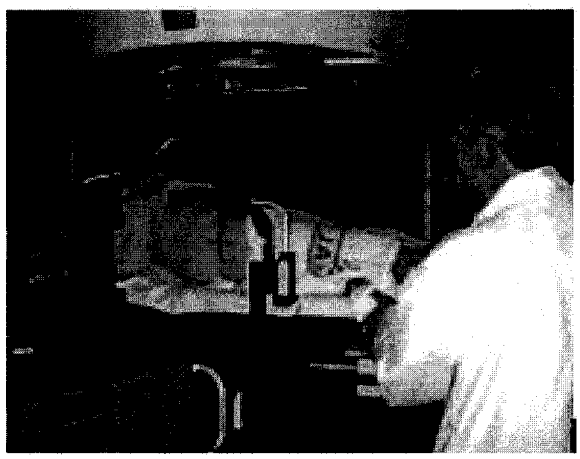

Figure 2.4: BAT US probe installed in the couch cradle for couch movements.

To use the US information for quantification and dose calculations a coordinate transformation has to be applied. Of interest are the actual prostate displacements rather than the required couch movements displayed in the charts. These are inversely related. For example, if the technologist moves the couch upward to re-align the prostate to the treatment isocenter, it means that the prostate on that day was located posterior to the isocenter.

The couch coordinate system (Figure 2.5.a) and the patient anatomical coordinate system in the supine position (Figure 2.5.b) are related by the simple relationship given in Table 2.3. RT/LT stands for Right/Left Transverse, A/P for Anterior/Posterior and Sup/Inf for Superior/Inferior.

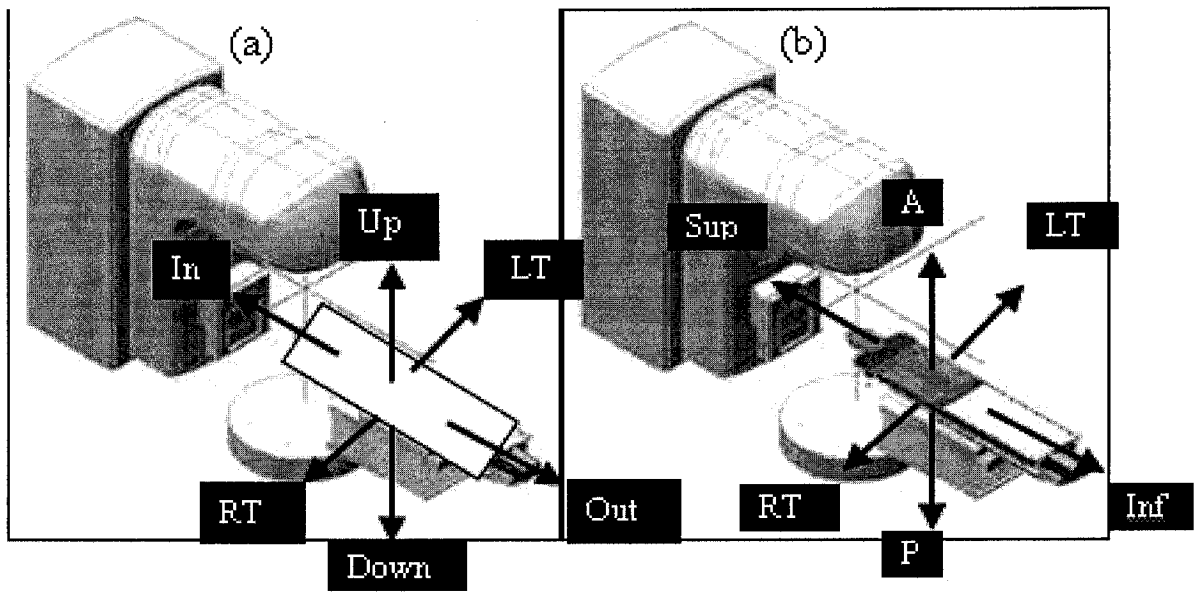

Figure 2.5: (a) Couch coordinate system and (b) Patient anatomical coordinate system for prostate patients treated in the supine position at the MGH [12].

	Translation and corresponding transformation					
Couch	LT	RT	Down	Up	In	Out
Patient anatomical	RT (+)	LT (-)	A (+)	P (-)	Inf (-)	Sup (+)

Table 2.3: Transformation from couch to patient coordinate system, including the sign convention described in chapter 3.

2.3.2 *RES system*

While most clinics use 2D US imaging, the Restitu^{TM} system (RES) is a 3D research tool soon to be made commercial. The prototype is from an ongoing collaboration with the Quebec-based company Resonant Medical Inc. It is a platform that can support several types of probes for different cancer sites. This is an advantage over the BAT system, which is at the moment dedicated to scanning prostates. RES also has the advantage over BAT of providing 3D rather than 2D images, giving not only daily positional changes but also volumetric changes. For these reasons, RES was chosen to evaluate inter-fraction positional as well as volumetric changes variations over the course of RT. As described in Table 2.1, compared to BAT which resides only in the treatment room, RES is an intra-modality imaging system found in both the CT and the treatment room (Figure 2.6).

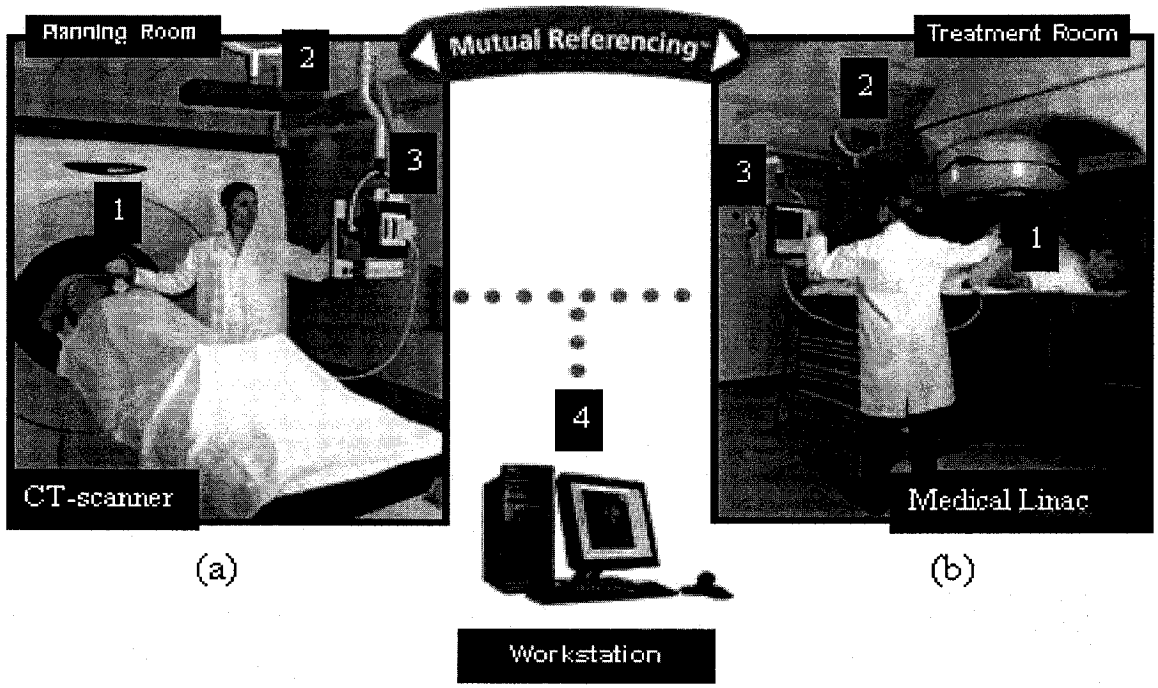

Figure 2.6: RES system located in (a) the CT room and (b) the treatment room. Each system includes its own (1) US probe, (2) motion tracking system and (3) image acquisition system. To visualize and analyze volumetric information acquired in 3D a workstation (4) is shared between the rooms. [Courtesy of Resonant Medical Inc].

Comparing US images at planning and at treatment removes the variation between different imaging modalities, which can be quite significant. In fact, US has been previously reported to yield 47 % smaller prostate volumes than CT [10]. Moreover, in a previous study showing a significant systematic difference between BAT and RES assessment of prostate alignment [4], RES displacements were found to be consistent with bi-weekly CT measurements. RES was concluded from that work to be more accurate than BAT for prostate alignment.

The RES system consists of a conventional 2D US probe (Figure 2.7.a) and a 3D laser tracking camera (Figure 2.7.b). The probe has active markers to emit infrared signals that get detected in space by the tracking system. A dedicated software then reconstructs 3D images from a set of 2D images, typically 640 x 405 or 640 x 473 voxels in size. The images get displayed on a ceiling-mounted screen (Figure 2.7.c).

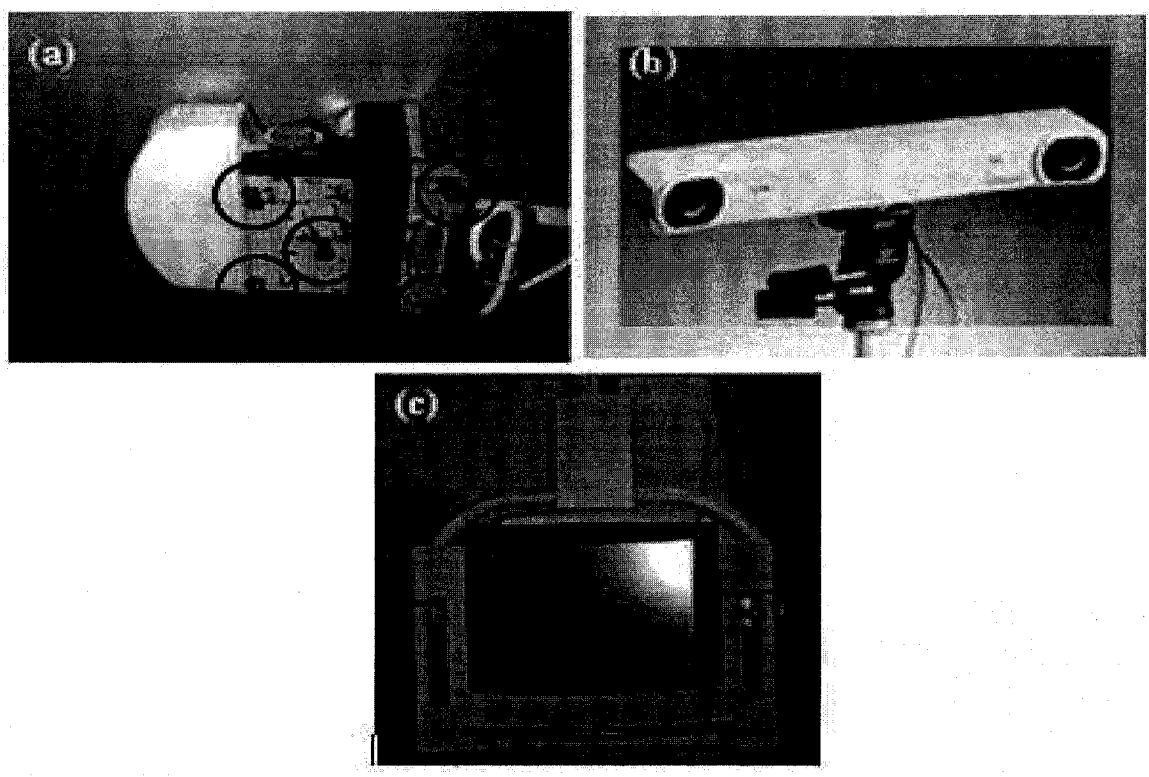

Figure 2.7: RES system components; (a) a 2D US probe with active markers (indicated by circles), (b) a ceiling-mounted infrared laser tracking camera (Polaris) and (c) a touch-screen.

The 3D reconstruction can only occur once the system is properly calibrated; one calibration for the probe and one for the room. Probe calibration relates the position and orientation of the probe sensor array to pixels in 2D US frames. This is performed by inserting the probe into a special phantom with a set of distinctive internal rods and external passive markers (Figure 2.8.a). Knowing the rods and phantom positions in space, the system automatically finds the center of the rods relative to their position in real space. This calibration does not change over time so it is not required at every treatment fraction. The room calibration informs the optical tracker about the coordinate system of the room lasers. It requires another special phantom with passive markers aligned with the room lasers (Figure 2.8.b). To make sure the tracking system has not moved and that the room lasers have not been recalibrated, room calibration is performed before every US scan. Note that although the precision on the shifts is quoted as 1 mm by the manufacturer, the room calibration can only be as accurate as the lasers.

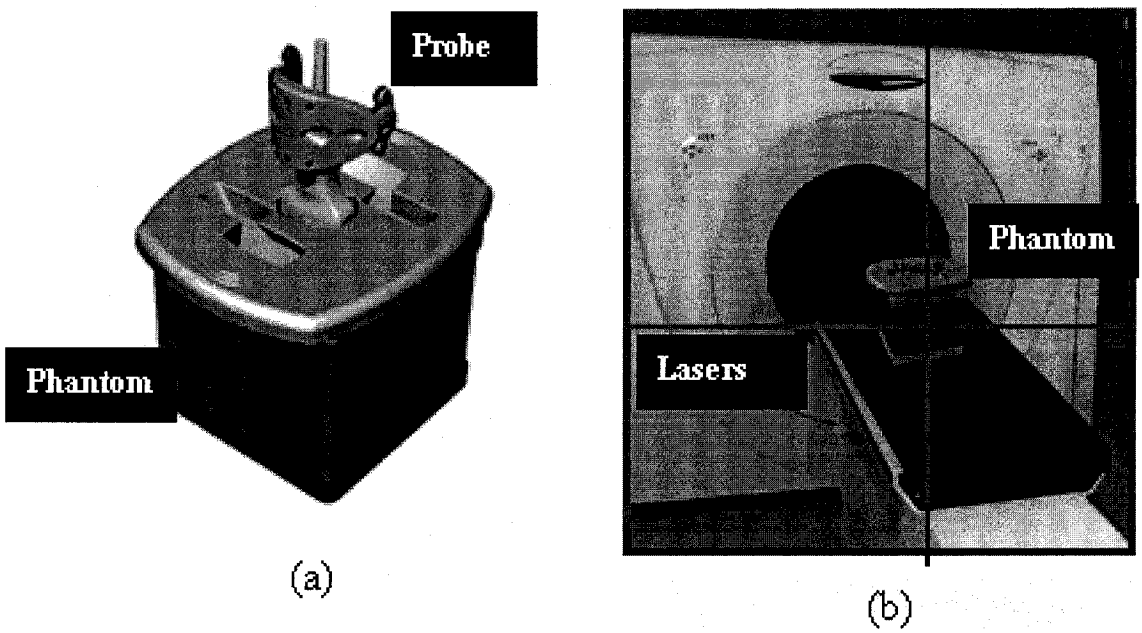

Figure 2.8: (a) Probe calibration and (b) Room calibration. [Courtesy of Resonant Medical Inc].

Once both calibrations have been carried out in both rooms, the RES systems are ready to acquire US images. Patients are initially scanned at TP in the CT room. Once the treatment starts the patient is US scanned every day in the Linac room. An optimized segmentation algorithm is then applied on the US data sets taken at planning and at treatment time to delimit the targeted organs at risk. For example, bladder and prostate US contours are shown in Figure 2.9. Prostate positional and volumetric changes can be quantified by comparing the prostate contour taken at CT (contour 2) to that taken at treatment time (contour 3).

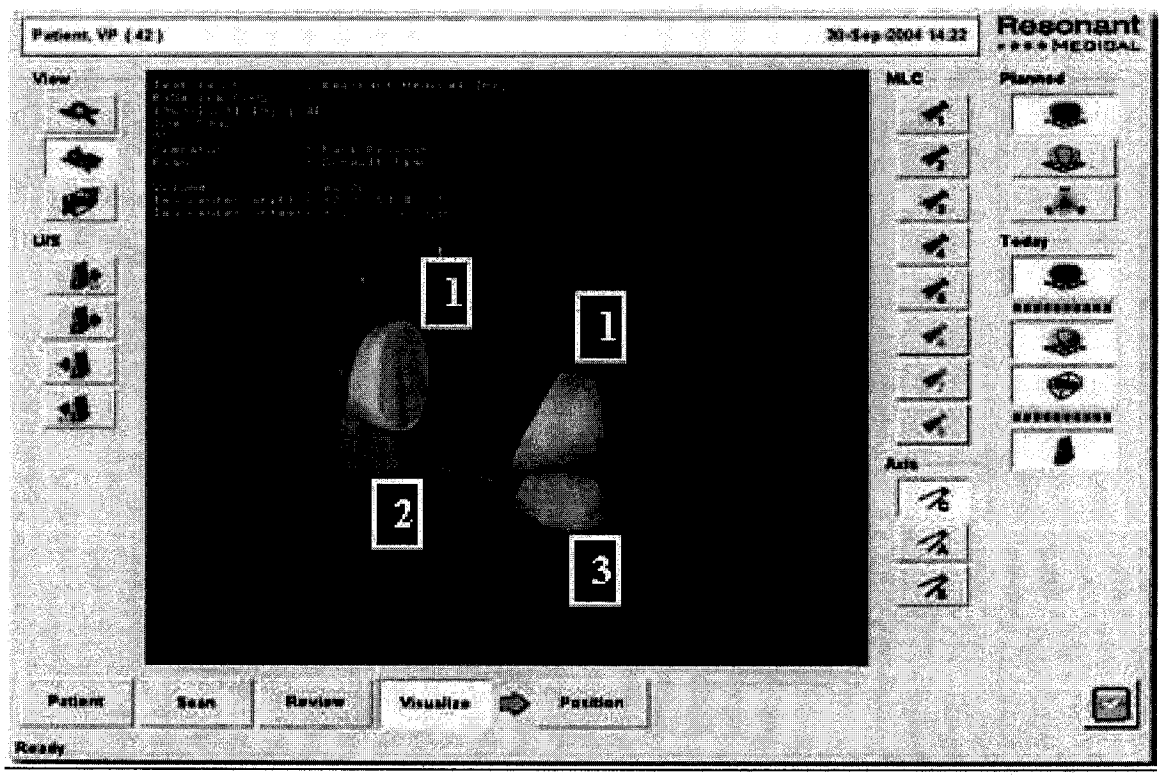

Figure 2.9: 2D slice of a set of 3D US images taken with RES through a pelvic region, with the bladder (contour 1) and the prostate (contour 2) on CT day and on the first treatment day (contour 3). [Courtesy of Resonant Medical Inc].

2.3.3 2003 clinical study

For the clinical study considered herein the procedure was as follows. Each of the 26 prostate patient was scanned at treatment planning with the RES system in the CT room. Then, at treatment time, each patient was scanned with both the RES and the BAT system in the Linac room. Following conventional procedure, the BAT shifts were used to reposition the patient in the treatment fields. Because of equipment difficulties and shortage of staff some treatment days were missed by the RES scans. The data used for analysis is hence a partial time series of 3D US scans.

References

[1] Antolak J.A., Rosen I.I., Childress C.H., Zagars G.K. and Pollack A. "Prostate Target Volume Variations during the course of Radiotherapy", Int. J. Radiat. Oncol. Biol. Phys., 42 (3), pp. 661-672, 1998.

[2] Chander A., Dong L., Huang E., Kuban D.A., O'Neill L., Rosen I. and Pollack A. "Experience of ultrasound-based daily prostate localization". Int. J. Radiat. Oncol. Biol. Phys., 56, pp. 436-447, 2003.

[3] Chesapeake Veterinary Cardiology Associates, http://www.cvcavets.com/showpracfaq.cfm?FAQID=3390&Private=1

[4] Cury F., Shenouda G., Souhami L., Duclos M., Faria S., David M., Corns R. and Falco T. "Comparison of BAT System and a New 3D Trans-abdominal Ultrasound-Based Image-Guided System for Prostate Daily Localization During External Beam Radiotherapy". Depts. Of Radiation Oncology and Medical Physics, McGill University Health Center. Resonant Medical Inc., Research and Development, Montreal, Canada.

[5] Curry III.T.S., Dowdey J.E. and Murry R.C. "Christensens's physics of diagnostic radiology". 4th ed, Philadephia, Lippincott Williams and Wilkinds, 522 pages, 1990.

[6]Department of biomedical Engineering, University of Texas at Austin http://www.bme.utexas.edu/ugrad/UGLab

[7] Dong L. "Development of automated image analysis tools for verification of radiotherapy field accuracy with an electronic portal imaging device" [PhD. thesis]. Houston, TX: The University of Texas Health Science Center at Houston, 1995.

[8] Duck F.A., Baker A.C. and Starritt H.C. "Ultrasound in medicine". Bristol and Philadelphia, Institute of Physics Publishing, Philadephia, 314 pages, 1997.

[9] Fenster A., Downey D.B. and Cardinal H.N. "Three-dimensional ultrasound imaging". Phys. Med. Biol., 46, pp. 67-99, 2001.

[10] Langen, K.M., Pouliot J., Anezinos C., Aubin M., Gottschalk A.R., Hsu I-C., Lowther D., Liu Y-M., Shinohara K., Verhey L.J., Weinberg V. and Roach M. "Evaluation of ultrasound-based prostate localization for image-guided radiotherapy". Int. J. Radiat. Oncol. Biol. Phys., 57(3), pp. 635-44, 2003.

[11] Lattanzi J., McNeeley S., Pinover W., Horwitz E., Das I., Schultheiss T.E. and Hanks G.E. "A comparison of Daily CT localization to a daily Ultrasound-based system in prostate cancer", Int. J. Radiat. Oncol. Biol. Phys., 43 (4), pp. 719-725, 1999.

[12] Ssi Robotics, Medical - Products/Services, http://www.ssirobotics.com

Chapter 3: Methods and Material

Patient Dose Calculation

In order to evaluate the extent to which planned dose distributions are degraded by prostate motion and volume changes, dose distributions are first calculated within a Treatment Planning System (TPS) and then analyzed in our McGill Monte Carlo Treatment Planning system (MMCTP). The different cases considered are listed in Table 3.1.

Case	TPS (CADPLAN or XVMC)	MMCTP		Name	
	Patient	CT contour Position	CT contour Volume	CADPLAN	XVMC
1	Fixed	Fixed	CT	DVH_2	DVH_8
2	Fixed	BAT	CT	DVH_3	DVH_9
3	Fixed	RES	CT	DVH_4	DVH_{10}
4	BAT	BAT	CT	DVH_5	DVH_{11}
5	BAT	RES	CT	DVH_6	DVH_{12}
6	RES	RES	CT	DVH_7	DVH_{13}
7	BAT	RES	RES	DVH_{14}	DVH_{16}
8	RES	RES	RES	DVH_{15}	DVH_{17}

Table 3.1: Cases considered regarding patient positioning and volumes.

Section 3.1 describes the basics of the two TPS used for dose calculations. Section 3.2 lists the steps involved in introducing the US prostate shifts into these TPS. Section 3.3 dives into details concerning the implementation and capabilities of MMCTP used for analysis of prostate motion and volume changes.

3.1 Treatment Planning Systems

3.1.1 CADPLAN

Treatment plans (TP) for External Beam 3D Conformal Radiotherapy (3D-CRT) are generated at the MGH using CADPLAN (Varian Oncology System, CA) based on the segmentations of pelvic organs on CT scans. In the clinical study under consideration, 26 prostate patients treated from May to October 2003 were planned using CADPLAN without heterogeneity correction. Unfortunately, dose accuracy can be compromised by heterogeneities in the prostate region, such as bone in the femurs. Three heterogeneity corrections are hence available in CADPLAN; the Batho Power Law, the Modified Batho Power Law and the Equivalent Tissue-Air Ratio (ETAR). Each correction factor is applied in turn in CADPLAN dose recalculations to evaluate its effectiveness. The original and recalculated plans are transferred from the clinic to our research network for analysis.

Heterogeneity corrections were originally developed for the large fields of conventional treatments. They are not very useful when there is a lack of electronic equilibrium. The Batho Power Law method was introduced in 1964 for doses beyond a single heterogeneity [1] and the Modified Batho Power Law came as a generalization to allow multiple heterogeneities [14]. These methods account for photon attenuation but not electron transport and they tend to overestimate the dose within low dose regions for small field sizes [6]. ETAR is the only correction in CADPLAN to account for scattered photon dose. It calculates the first scatter exactly and the higher order scatters by approximately weighting the already scattered photons [3]. For small heterogeneities, ETAR was found by Du Plessis *et al* [3] to be more accurate than either Batho methods.

3.1.2 Monte Carlo simulations

Even modern TPS that explicitly account for electron transport cannot reproduce the advanced dosimetry offered by MC in heterogeneous regions [7]. Several research groups have hence worked on implementing MC for clinical dose calculations [10,12,13]. MC is capable of calculating accurate dose distributions in complex geometries; using the

BEAMnrc code for Linacs (section 3.1.2.1) and either XVMC or DOSXYZ for patients (section 3.1.2.2).

3.1.2.1 BEAMnrc

BEAMnrc is a MC simulation system used for the first stage of a MC dose calculation involving the accelerator head. It is based on the Electron-Gamma-Shower code (EGSnrc) and uses component modules (CM) to model the different parts of a Linac such as jaws, wedges and MLCs. The code is currently implemented at our institution on a cluster of 20 dual CPU computers. The master server uses a PIII 500 GHz and the slaves include PIII 900 GHz, P4 3.4GHz and AMD 1800.

All prostate patients considered in this study were treated with 18 MV photon beams on Varian Clinac 2300 C/D at the MGH. The accelerator model had previously been validated in our group between measurements and MC calculations. In order to perform a MC simulation, specific information is extracted from CADPLAN: (1) the coordinates of the isocenter, (2) the field sizes, (3) the beam weights, (4) the couch and gantry angles, (5) the wedge angles and positions and (6) the MLC leaf positions. Physical wedges are inserted into a BEAMnrc input file using two parameters: the wedge orientation and the location of the thick end. The MLC leaf positions for each beam are specified in a CADPLAN file. This file is read by an in-house code to calculate and insert the leaf openings into the BEAMnrc input file.

The user code contains a subroutine (HATCH) to read material dependent cross section data generated by PEGS4. A phase space (phsp) file is collected for each beam on a plane 70 cm from the Linac target. The phsp file contains information on the physical characteristics of all particles passing through the plane. A separate BEAM simulation is performed for each beam for each patient. Each simulation uses 20 million primary histories at the target resulting in approximately 3 million particles in the phsp file. This information is then used in XVMC or DOSXYZ to get the dose distributions in patients, as described in the next section.

3.1.2.2 XVMC and DOSXYZ

XVMC and DOSXYZ are dose calculation routines used to propagate individual particles in complex geometries such as patients. Particle interactions are modeled from interaction cross sections, step sizes and production of secondary particles. These MC codes take phsp files generated in BEAMnrc for each beam to calculate the 3D absorbed dose distribution in a patient.

The first step in setting up a simulation is to use in-house codes to generate from a patient CT image set a 3D density matrix in DOSXYZ or electron density matrix in XVMC. The following entries are then filled in the input file,: (1) the isocenter position, (2) the name of the phsp file, (3) the gantry, collimator and couch positions and (4) the number of histories. To select the proper number of histories to use, patient 8 is calculated in MC with both 7 and 35 million histories per beam. Each phsp file contains approximately 2 million particles, each recycled around 3.5 or 10 times, respectively. Each of the 5 beams has its own phsp file, leading to a total of either 35 or 175 million histories. The resulting dose distributions are compared based on dose-volume histograms (DVHs) which display the dose covering a certain percentage of organ volume. DVHs enhance the ability to compare quantitatively different simulations and are commonly used as a tool for TP evaluation. Based on these MC calculations (Figure 3.1), the smaller number of histories is chosen to speed up calculation time while still yielding good statistics.

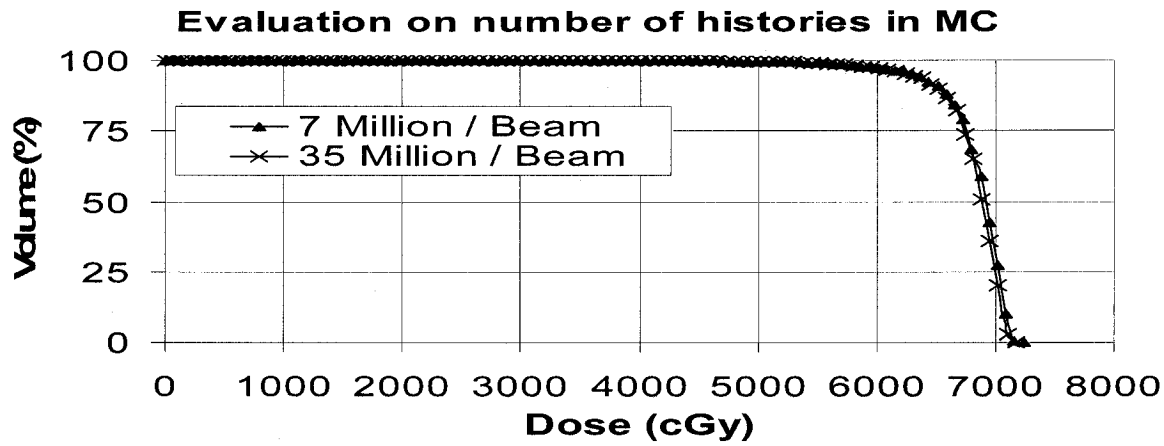

Figure 3.1: Dose-volume histogram (DVH) of the PTV for patient 8 to evaluate the number of histories needed in MC.

Once the simulations are done, dose distributions for each beam are combined and the sum converted to an absolute dose using a normalization factor. This normalization translates dose per particle from MC to a dose in Gray (Gy) by weighting each beam by its prescribed MUs in CADPLAN. The normalization uses the dose per incident particle at d_{max} (3.5 cm for an 18 MV photon beam) obtained from a MC simulation with a 10 x 10 cm^2 reference field at an Source-Surface Distance (SSD) of 100 cm in a water phantom. Finally, dose distributions are displayed in MMCTP and used in DVH analysis (section 3.3).

XVMC is a 3D photon dose calculation MC algorithm based on Voxel Monte Carlo (VMC) originally developed for electron beams [4]. In contrast to DOSXYZ, the conventional MC patient modeling tool of EGS4, XVMC uses several simplifications and approximations to increase computational speed by a factor of 15-20 [4]. The improvement is due to: (1) a fast electron transport algorithm, (2) an omission of bremsstralung photons that contribute less dose than electrons, (3) a fast ray tracing technique and (4) an initial ray tracing method to calculate the number of electrons set in motion by primary photons in each voxel. Due to the time savings, all patients are simulated using XVMC in this project. One patient is also simulated with DOSXYZ under the exact same simulation conditions to compare the dose calculation accuracies of

the two codes. Note that care is taken to introduce the proper isocenter coordinates in the DOSXYZ coordinate system, which differs from that of XVMC. A new c-routine is developed to combine the dose files for each beam, as they are in a different format than in XVMC. The results comparing XVMC and DOSXYZ are presented in chapter 5.

MC considers real patient geometries extracted from CT scans while CADPLAN only considers contours and assumes the material inside to be water. To compare MC and CADPLAN dose distributions, we filled contours in both XVMC and DOSXYZ with water for one patient. In DOSXYZ, every voxel is assigned a material and density based on the CT data sets using a stand alone program (ctcreate). The process goes as follows; (1) read the CT format, (2) read the CT header, (3) read the binary CT data, (4) re-sample the CT data to correspond to voxels, (5) convert the CT data to materials and densities for each voxel and (6) transfer the data to be input to DOSXYZ. Step (5) is based on a ramp function (Figure 3.2). If the CT number of a certain voxel lies below a predefined upper limit, the voxel is assigned that material, which is then read from a material data file (PEGS4) during the simulation. The voxel is also assigned a density using linear interpolation between the materials density limits. We modified ctcreate to read instead a text file containing only air and water materials along with their corresponding densities. The code hence replaces all densities larger than that of air by that of water. The material data file is then used to read air for surrounding voxels and water for patient voxels.

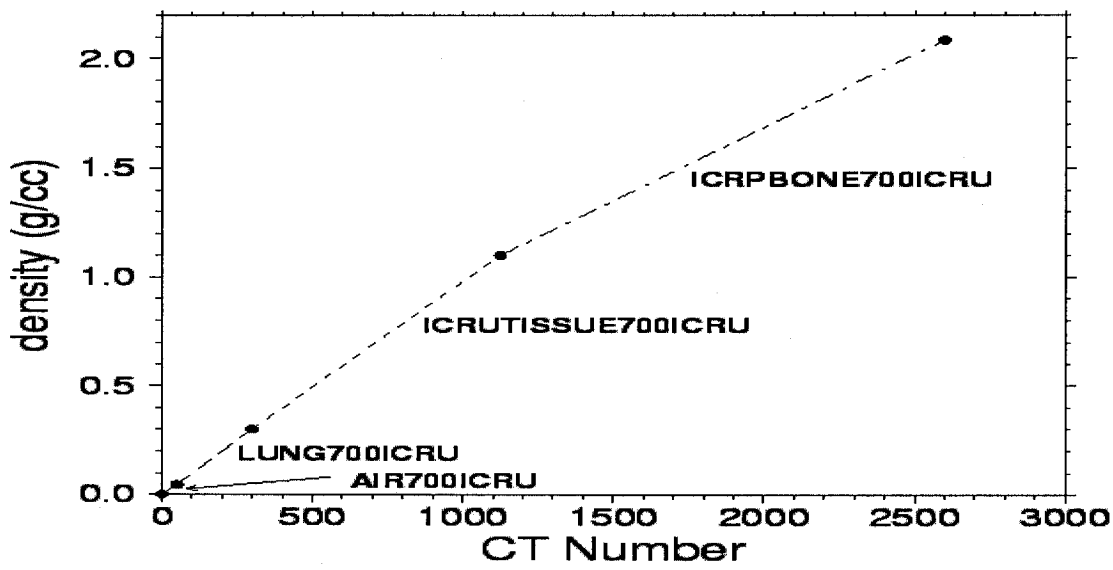

Figure 3.2: Default ramp to convert CT numbers to material and density [7].

In XVMC compton scattering dominates for energies used in RT. The cross sections for photon transport hence mostly depend on the electron density of a material. This is obtained from scaling the electron density of water by the ratio of the material and water densities [8]. For electron transport, the scattering power is scaled by the density of the material obtained from CT numbers. We developed an in-house code that modifies the electron density matrix to sequentially fill all the organ contours with water density. This effectively turns all patient voxels to water material and density, as in DOSXYZ. The results of XVMC and DOSXYZ simulations using water voxels in one patient are given in chapter 5.

3.2 Introducing motion changes in TPS

The previous sections dealt with dose distributions calculated for the ideal situation where the prostate does not move from one day to the next (case 1, Table 3.1, Figure 3.3). The dose distribution can also be calculated for the more realistic clinical situation by simulating the daily prostate displacements measured with both US systems within either CADPLAN (section 3.2.1) or MC (section 3.2.2). Using MMCTP for analysis, we are then able to evaluate the extent to which planned dose distributions are degraded by

prostate motion. This gives an indication of the value of repositioning patients before daily treatments, as shown in Figure 3.3. Of main interest is the comparison between a single dose calculation from CADPLAN in a single CT image from the start of treatment and the fraction-by-fraction MC dose calculations including 2D and 3D US positional information.

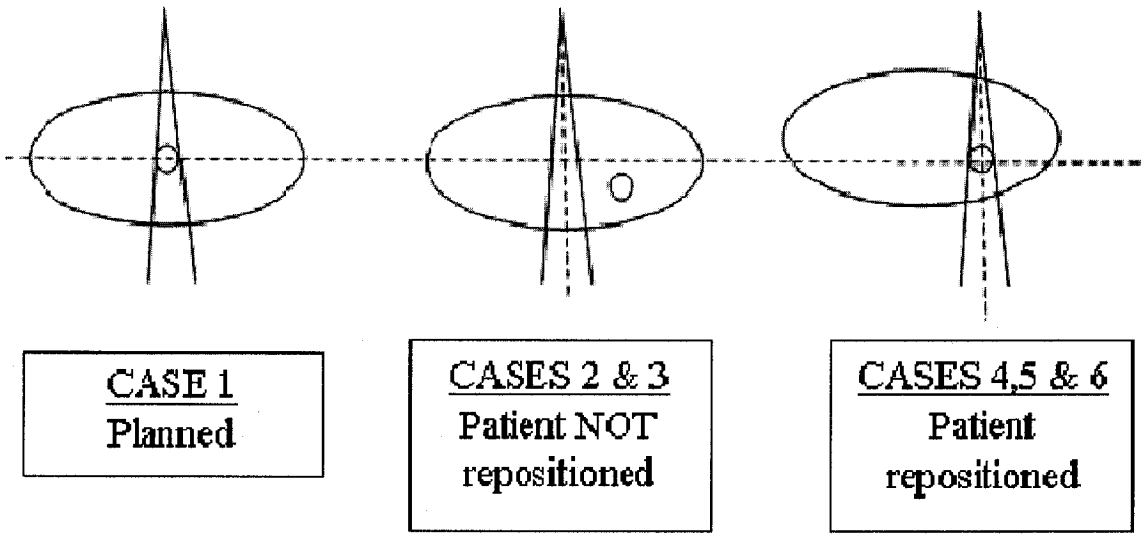

Figure 3.3: Schematic of US shifts introduced in the TPS and in MMCTP. The cases listed refer to Table 3.1.

3.2.1 CADPLAN

Prostate motions measured by both the BAT and RES system, quantified in chapter 4, can be introduced into CADPLAN for every treatment fraction of every patient. CADPLAN allows the user to shift the position of the treatment isocenter in 3D relative to the patient anatomy. Figure 3.4 displays a CADPLAN CT axial slice of a patient, the panel to enter the isocenter position, along with two coordinate system conventions: for CADPLAN (x,y and z) and for the patient anatomy (A/P, RT/LT and SUP/INF).

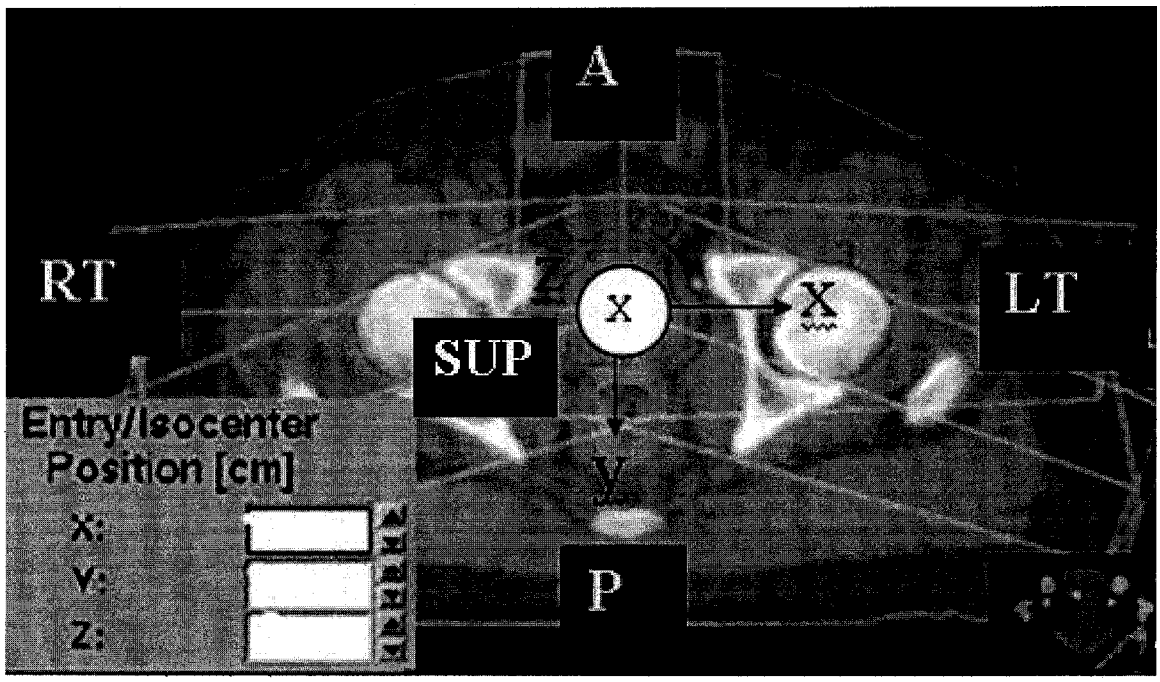

Figure 3.4: CADPLAN CT axial slice of a patient, the panel to enter the isocenter position and two coordinate system conventions: CADPLAN (x,y and z) and patient anatomy (A/P, RT/LT and SUP/INF).

The user can introduce the prostate shifts keeping in mind that the treatment isocenter is relative to the patient anatomy. Hence, the values entered in this panel shift the patient while the beams stay at a fixed position. Of course, this does not represent the clinical situation yet, but it will once the prostate contours are moved to follow the beams in MMCTP (section 3.3). The following equations are used to shift the beam isocenter in the direction and magnitude given by the US measurements $(dx)_{US}$, $(dy)_{US}$ and $(dz)_{US}$.

$$\left(X_{shiftedISO}\right)_{CADPLAN} = \left(X_{ISO}\right)_{CADPLAN} - \left(dx\right)_{US} \tag{3.1.a}$$

$$\left(Y_{shiftedISO}\right)_{CADPLAN} = \left(Y_{ISO}\right)_{CADPLAN} + \left(dy\right)_{US} \tag{3.1.b}$$

$$\left(Z_{shiftedISO}\right)_{CADPLAN} = \left(Z_{ISO}\right)_{CADPLAN} + \left(dz\right)_{US} \tag{3.1.c}$$

The US shifts are measured in the patient anatomical coordinate system following the convention used in Table 2.3. Once the shifts are entered in CADPLAN, the plan is recalculated and transferred to our computer network. This is performed for every treatment fraction using the US data from both systems acquired in the treatment room prior to treatment delivery. Figure 3.5 shows an arbitrary shift introduced in CADPLAN.

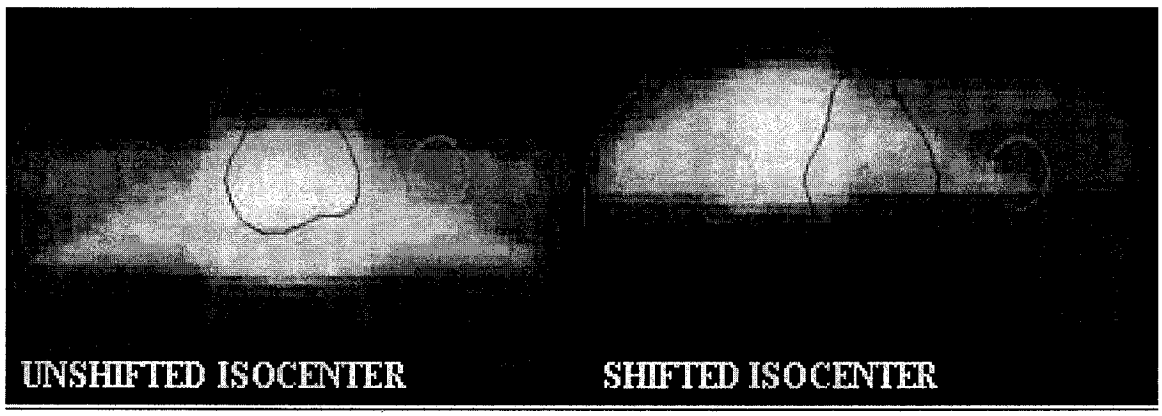

Figure 3.5: Arbitrary shift in CADPLAN calculations for one fraction on patient 8. The shift introduced is: dx = + 5 cm (RT), dy = - 2 cm (A), dz = + 5 cm (SUP).

3.2.2. Monte Carlo

US prostate motion is also introduced into MC simulations for comparison with CADPLAN calculations. This procedure involves shifting the patient relative to the treatment beams by indicating new isocenter coordinates in the XVMC input file (vmc) according to either BAT or RES data, for every beam of every treatment fraction of every patient. This requires around 3 000 XVMC simulations of 20-30 minutes each. The newly generated plans are saved for further analysis with MMCTP. Taking the XVMC and US coordinate systems into account, equation 3.2 is used to shift the isocenter.

$$\left(X_{shiftedISO}\right)_{XVMC} = \left(X_{ISO}\right)_{XVMC} - \left(dx\right)_{US} \tag{3.2.a}$$

$$\left(Y_{shiftedISO}\right)_{XVMC} = \left(Y_{ISO}\right)_{XVMC} + \left(dz\right)_{US} \tag{3.2.b}$$

$$\left(Z_{shiftedISO}\right)_{XVMC} = \left(Z_{ISO}\right)_{XVMC} - \left(dy\right)_{US} \tag{3.2.c}$$

The convention of Table 2.3 is again used for the US patient anatomical coordinate. As was the case in CADPLAN, the shifts move the patient relative to the beams. As described next, the prostate contours are shifted in MMCTP when DVHs are calculated.

3.3 McGill Monte Carlo Treatment Planning system

Over the past few years, the McGill Medical Physics Unit has built and validated a system for clinical patient dose evaluation based on the MC code called the McGill MC Treatment Planning system (MMCTP). This tool needs to be extended to integrate prostate motion and volume changes from US data. Section 3.3.1 states the system capabilities. The next section covers the methods of DVH analysis. The last section describes how the US information is integrated into the existing software.

3.3.1 State of the art system capabilities

This system is developed in *RealBasic* (Real Software Inc., Austin, Texas) as a front end to the EGSnrc and XVMC codes and offers flexible TP visualization tools. It extracts information from the CADPLAN prescribed treatments such as; beam geometries, CT images taken prior to the start of treatment, organ contours as outlined by the physician as well as dose calculations. It offers a visualization of dose distributions using isodose lines superimposed onto CT images. Most importantly, it provides a comparison between MC and conventional dose calculations using DVH analysis.

3.3.2 Methods of DVH analysis

CADPLAN, XVMC and DOSXYZ simulations give isodose distributions, but it is the dose-volume information that enhances the ability to compare quantitatively different simulations. MMCTP calculates DVHs from dose distributions in multiple planes, thereby implementing a 3D dose calculation system. However, DVHs encode the cumulative volumetric information about the dose distribution, not the geometric and topological information. DVHs hence lose spatial information such as the locations of high- and low-dose regions ("hot" and cold" spots) inside the volumes of interest.

DVHs in MMCTP are computed the following way. First the dose values are divided into 100 equally spaced bins representing a normalized dose distribution with the maximum at 100 %. To simplify and speed up DVH calculations, we chose a base volume (V_{base}) equal to 1/3 the voxel size of the CT image. This is different than CADPLAN [5] where a fixed grid size of 1.5 or 2.5 mm is employed in the x/y-plane for structures bigger 5 cm^3 and another grid size is calculated for smaller structures. In the z-plane CADPLAN offers an unlimited resolution. Because the dose matrix is larger than the voxels grid in MMCTP, we interpolate the dose in the x/y-plane and in the z-plane to assign dose values to each voxel in every contoured organ. Each voxel is then evaluated to see in which bin its dose falls. Once the correct bin is found, the element volume in cm^3 is added to this bin. After all voxels have been placed, we display the differential DVH curve by showing the 100 dose bins on the x-axis and the corresponding volume on the y-axis. Dose is then made absolute (cGy) and the volume is normalized to 100 %. To obtain the cumulative DVH used throughout this thesis, we step through all the bins summing all the voxels starting from bin 100 and going towards bin 1. This effectively adds together all voxels that have at least the dose of the current bin, the exact definition of a cumulative DVH.

MMCTP DVH calculation capabilities are first evaluated using a simple CADPLAN dose calculation on a water phantom (40 x 20 x 40 cm) with a cubic contour (10 x 10 x 10 cm). Four 18 MV opposing fields are positioned at the isocenter to create a homogeneous dose distribution over the contour (Figure 3.6).

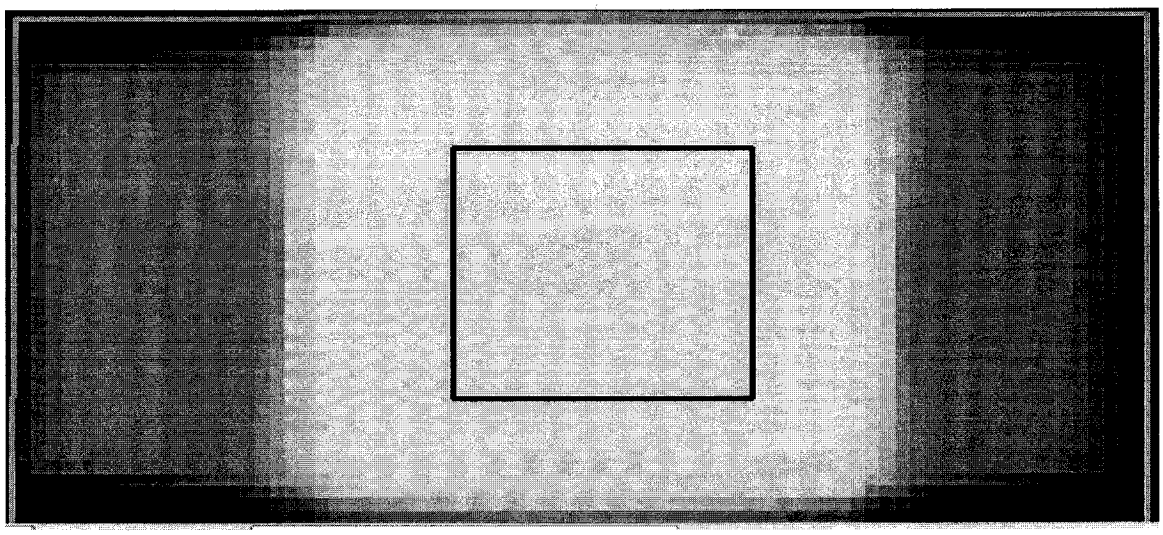

Figure 3.6: Validation of MMCTP DVH algorithm on a water phantom with a single cubic contour (black) and a homogeneous CADPLAN dose distribution.

The resulting DVHs, calculated from both CADLAN and MMCTP, are shown in Figure 3.7. MMCTP is seen to agree with CADPLAN.

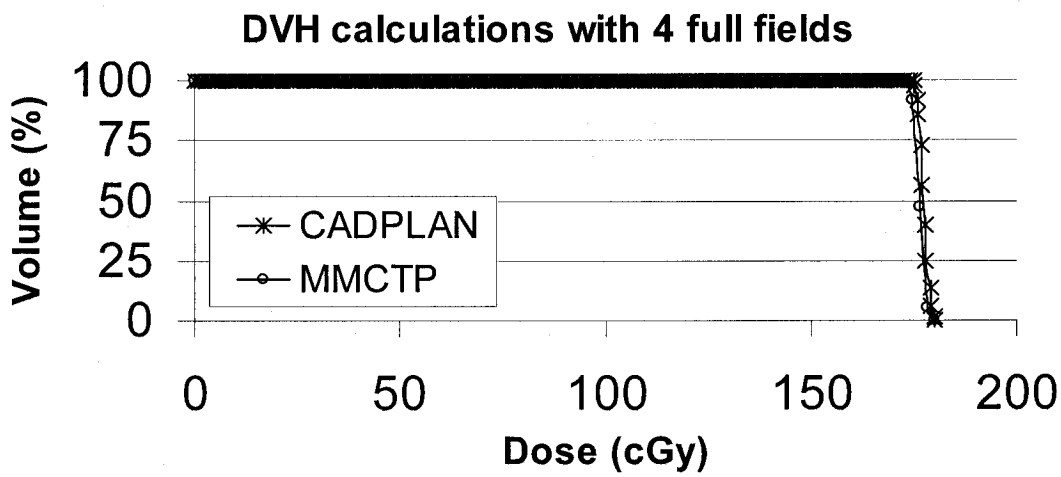

Figure 3.7: CADPLAN and MMCTP DVHs for the water phantom of Figure 3.6.

As mentioned above, the base volume used in CADPLAN for DVH calculations differs from that used in MMCTP. CADPLAN offers an unlimited resolution in the z-plane while MMCTP uses voxel sizes equal to the 1/3 of the distance between CT slices. To evaluate the effect of the CADPLAN implementation on DVH calculations, the four

fields used above are reduced in size to encompass fewer CT slices, as shown in Figure 3.8.

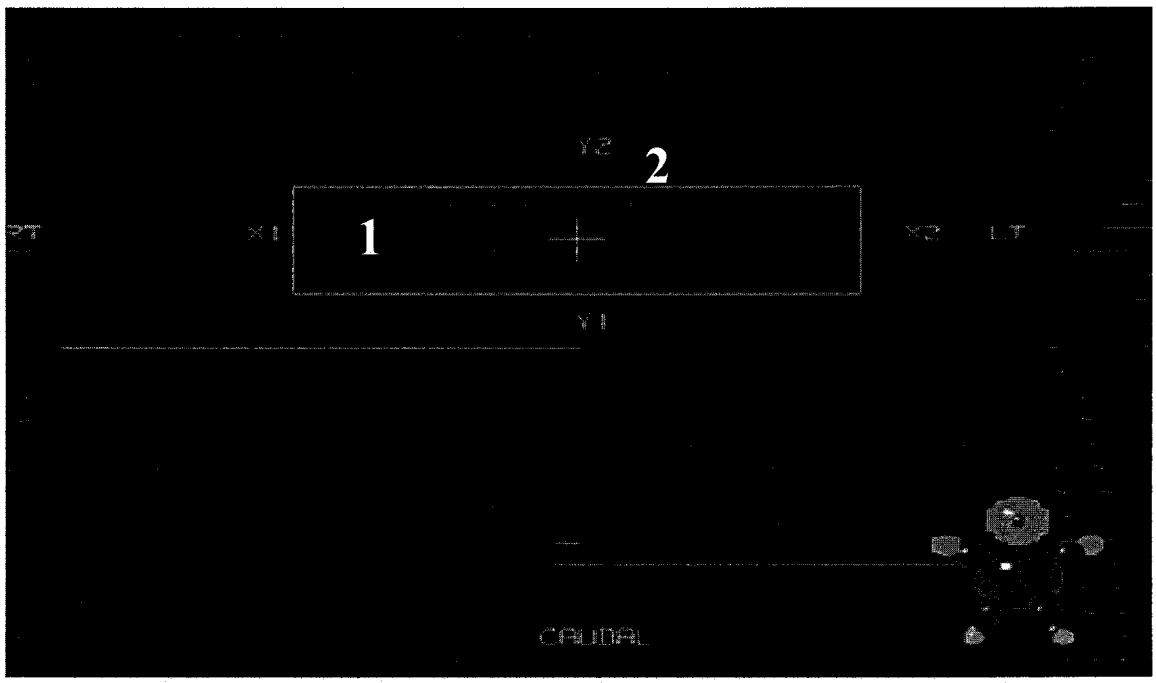

Figure 3.8: Coronal beam eye view of partial fields (1) covering only a few CT slices on which lie the cubic contour (2).

In the resulting DVHs (Figure 3.9) CADPLAN gives smoother DVH curves than MMCTP in the low dose region. The stepwise curve shown with MMCTP represents the real information provided on CT slices. The number of steps equals the number of CT slices included in the fields.

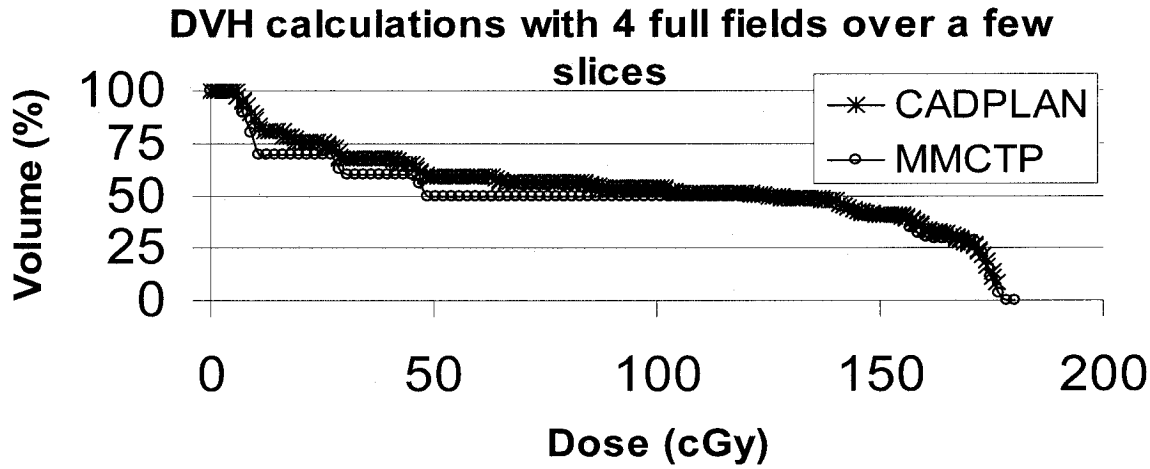

Figure 3.9: DVHs comparing CADPLAN and MMCTP with 4 fields covering only a few CT slices in a water phantom.

Since DVH calculations are based on volumes, we compare the volumes calculated by CADPLAN and MMCTP. Table 3.2 gives the volumes obtained for arbitrary geometrical contours of varying sizes. The calculated volumes are also compared to the real geometrical volumes by quoting the volume error.

$$V_{error}(\%) = \left[\frac{V_{real}(cm^3) - V_x(cm^3)}{V_{real}(cm^3)} \right] X\ 100 \tag{3.3}$$

where x in V_x is either CADPLAN or MMCTP.

V_{real} (cm^3)	$V_{CADPLAN}$ (cm^3)	V_{error} (%)	V_{MMCTP} (cm^3)	V_{error} (%)
1000	906.6	9.3	999.4	0.1
700	612.6	12.5	699.6	0.1
175	156.2	10.8	174.9	0.1
87.5	78.1	10.8	87.4	0.1
14	11.1	21.0	12.3	12.1

Table 3.2: CADPLAN and MMCTP volume calculations on geometrical contours.

MMCTP appears more precise than CADPLAN on the volume calculation. MMCTP calculates the volumes within 0.1 % of their real value while CADPLAN under-estimates them by as much as 12.5 %. The exception is the smallest contour used (14 cm^3). This contour leads to the largest error in both cases due to the very few voxels used to represent it. However, prostate sizes are larger than this contour (section 4.2).

DVHs usually use normalized volumes to remove volume effects. This explains why the differences in volumes between CADPLAN and MMCTP were hard to detect in the results already presented. There is however one effect not removed by normalization. It is the overestimation in dose coverage in CADPLAN compared to MMCTP. For a fixed dose distribution, the smaller CADPLAN volume gets covered by more dose than the MMCTP volume, leading to a higher CADPLAN DVH curve (Figure 3.7, Figure 3.9).

To further evaluate DVH capabilities in MMCTP, the PTV of two patients are used. Patient 2 is a typical case patient and patient 26 is the worst case encountered. Figure 3.10 shows the DVHs for these two patients calculated in CADPLAN and MMCTP based on CADPLAN calculated dose distributions. Generally, MMCTP is seen to agree very well with CADPLAN. Again, the slight overestimation in CADPLAN comes from the smaller volume it calculates.

To quantify the differences in these DVHs, we can extract the percentage difference in dose covering 95 % of the PTV volume ($\triangle_{D95\%PTV}$), following equation 3.4 and reported in Table 3.3.

$$\Delta D_{95\%PTV}(\%) = \left[\frac{(D_{95\%PTV})_{CADPLAN}(cGy) - (D_{95\%PTV})_{MMCTP}(cGy)}{(D_{95\%PTV})_{CADPLAN}(cGy)} \right] X\ 100 \qquad (3.4)$$

Positive values indicate that CADPLAN is overestimating the MMCTP curve. For patient 2, the difference is within 1 % while for patient 26, it is slightly above 3 %.

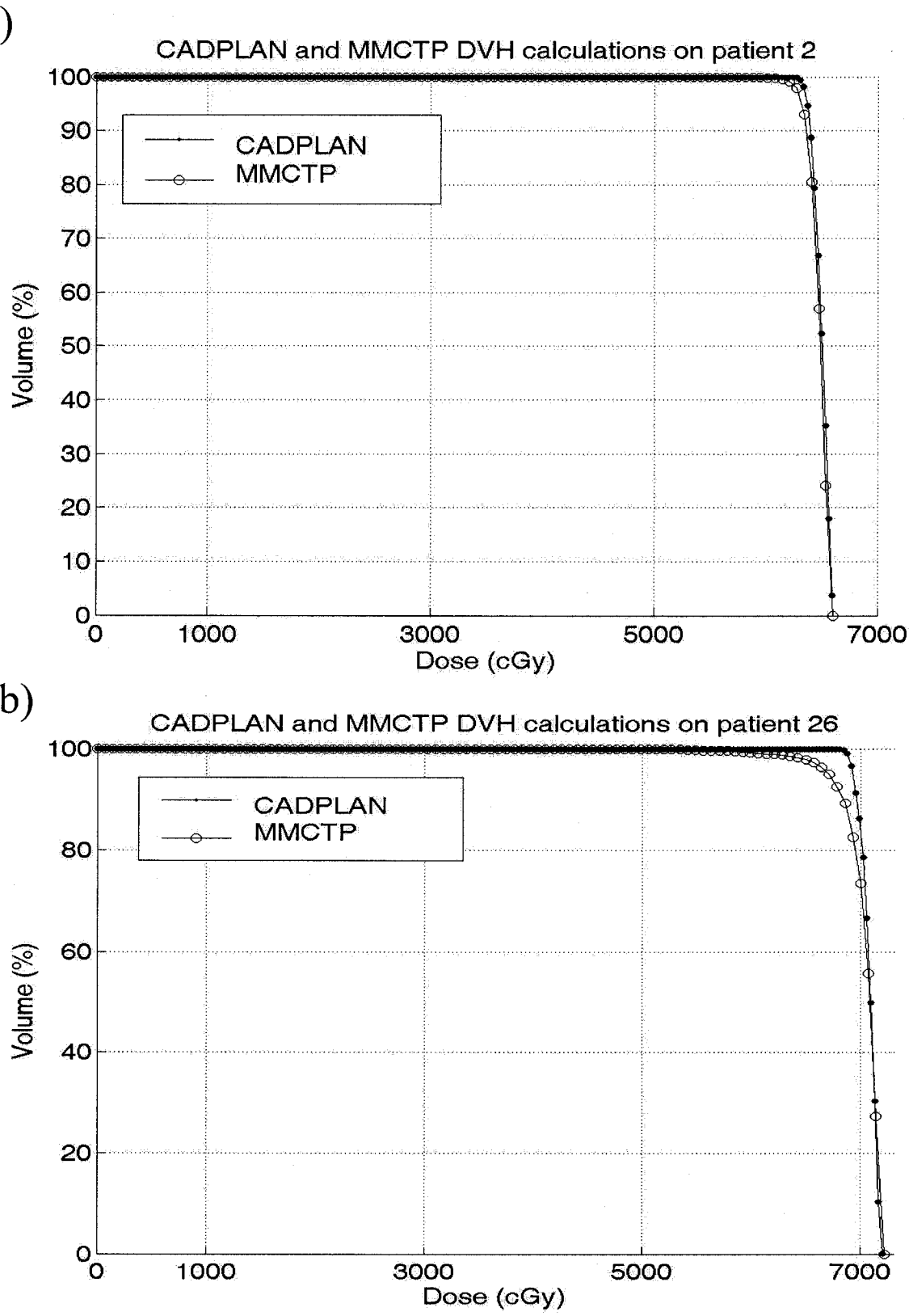

Figure 3.10: CADPLAN and MMCTP DVHs on two patients: (a) patient 2 (typical case) and (b) 26 (worst case).

Patient	$D_{95\%PTV}$ (cGy)		$\triangle D_{95\%PTV}$ (%)
	CAD	MMCTP	
2	6365	6314	**0.8**
26	6923	6711	**3.1**

Table 3.3: CADPLAN and MMCTP DVHs on the dose received by 95 % of the PTV volume ($D_{95\%PTV}$). Data is shown for patients 2 (typical) and 26 (worst).

Figure 3.11 and Table 3.4 report $\triangle D_{95\%PTV}$ for all patients. On average over all patients MMCTP differs from CADPLAN by less than 1 %.

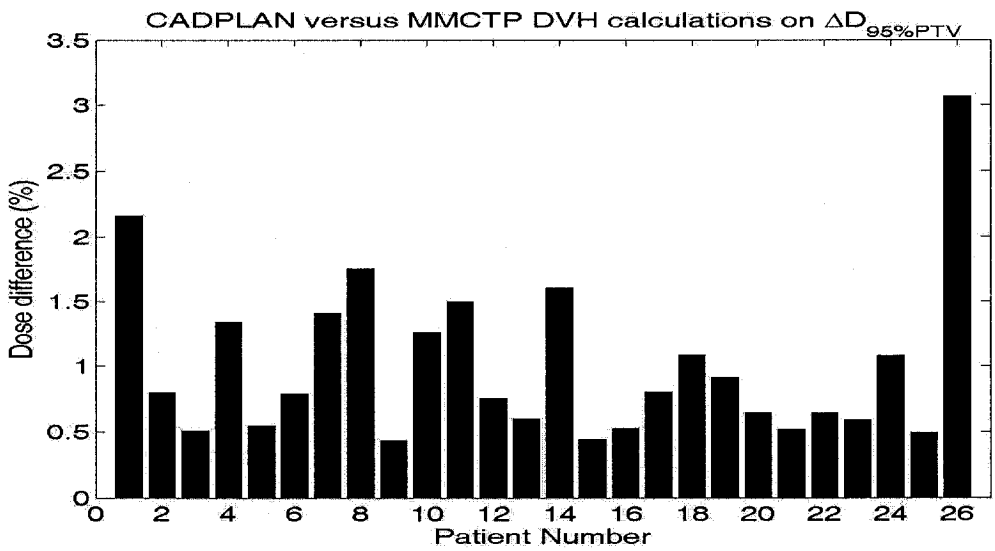

Figure 3.11: Difference in percentage dose covering 95% of the PTV ($\triangle D_{95\%PTV}$) for CADPLAN versus MMCTP DVHs. Data is shown for 26 patients.

	$\triangle D_{95\%PTV}$ (%)
Mean ± SD	0.6 ± 1.9
Range	0.4 to 3.1

Table 3.4: Statistical analysis of the difference in percentage dose covering 95 % of the PTV in CADPLAN versus MMCTP DVHs. Data for 26 patients.

The volumes calculated with both methods for both patients are reported in Table 3.5. Since true prostate volumes cannot be calculated directly as in the geometrical cases, the volume difference between CADPLAN and MMCTP volumes ($\triangle V_{PTV}$) is given instead.

Patient	V_{PTV} (cm^3)		$\triangle V_{PTV}$
	CAD	MMCTP	(%)
2	112.6	115.2	**-2.3**
26	85.9	89.6	**-4.1**

Table 3.5: CADPLAN and MMCTP PTV volume difference (V_{PTV}). Data is shown for patients 2 (typical case) and 26 (worst case).

On even the worst case patient (number 26), CADPLAN and MMCTP PTV volume calculations are seen to differ by less than 5 %. As expected, Figure 3.12 seems to indicate that the largest discrepancies come from the smallest volumes.

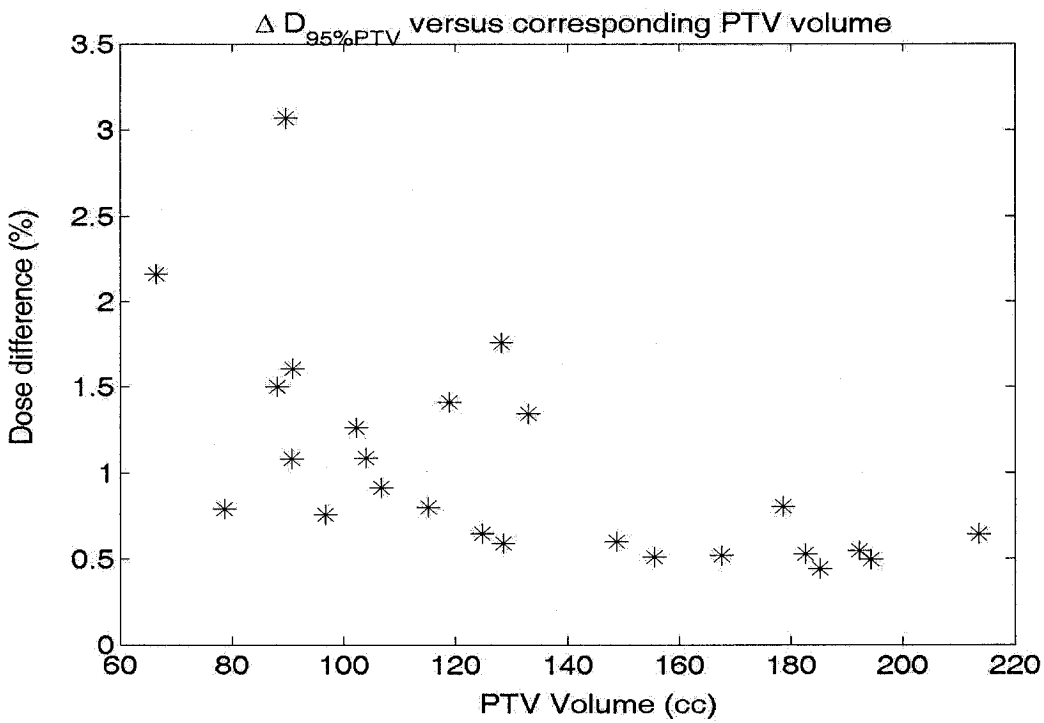

Figure 3.12: Comparison of $\triangle_{D95\%PTV}$ (shown in Figure 3.11) versus corresponding PTV volumes calculated in MMCTP. Data is shown for 26 patients.

3.3.3 System adaptations to introduce ultrasound data

To investigate the effects of prostate inter-fraction variation on clinically planned dose, we modified the MMCTP tool to include US data. The newly developed MMCTP code constitutes a novel technique, which permits MC recalculation of the dose delivered at every treatment fraction, taking into account positional (section 3.3.3.1) and volumetric (section 3.3.3.2) prostate changes. It allows a more accurate assessment of the real dose delivered to organs over a treatment course. Figure 3.13 shows the new graphical user interface (GUI) with the integration of US data.

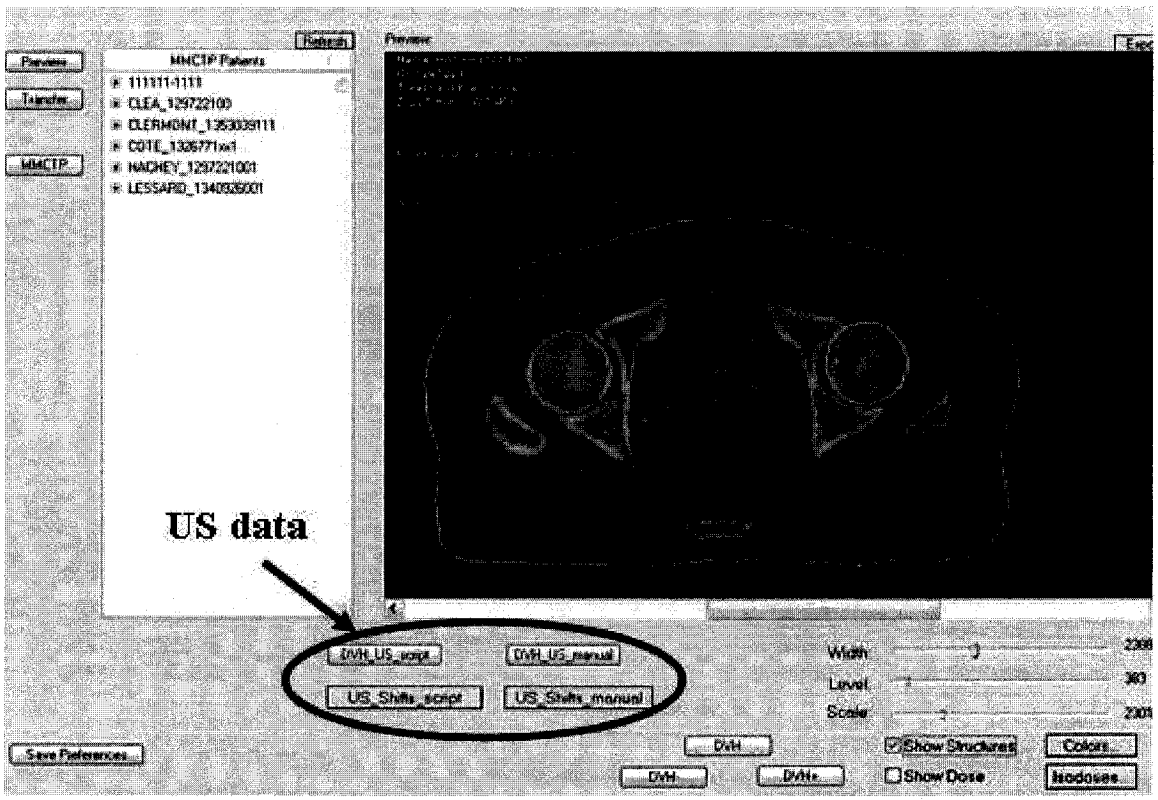

Figure 3.13: Screenshot of the MMCTP GUI showing the US integration.

In preparation for the introduction of fractional US information, the DVH calculation algorithm described in section 3.3.2 needs modifications. Each fraction now requires one MC simulation in order for it to include the US changes in position (cases 1-6, Table 3.1) and volume (cases 7-8, Table 3.1). Since MC simulations are evaluated based on DVHs this leads to one DVH per fraction. To evaluate the overall effect of inter-fraction variation on a treatment the fractional DVHs must be combined in their differential form

and then converted to cumulative. Simple combination cases are evaluated to validate the DVH combination algorithm. For example in Figure 3.14, an almost null DVH is combined to a 100% DVH to yield a 50 % result.

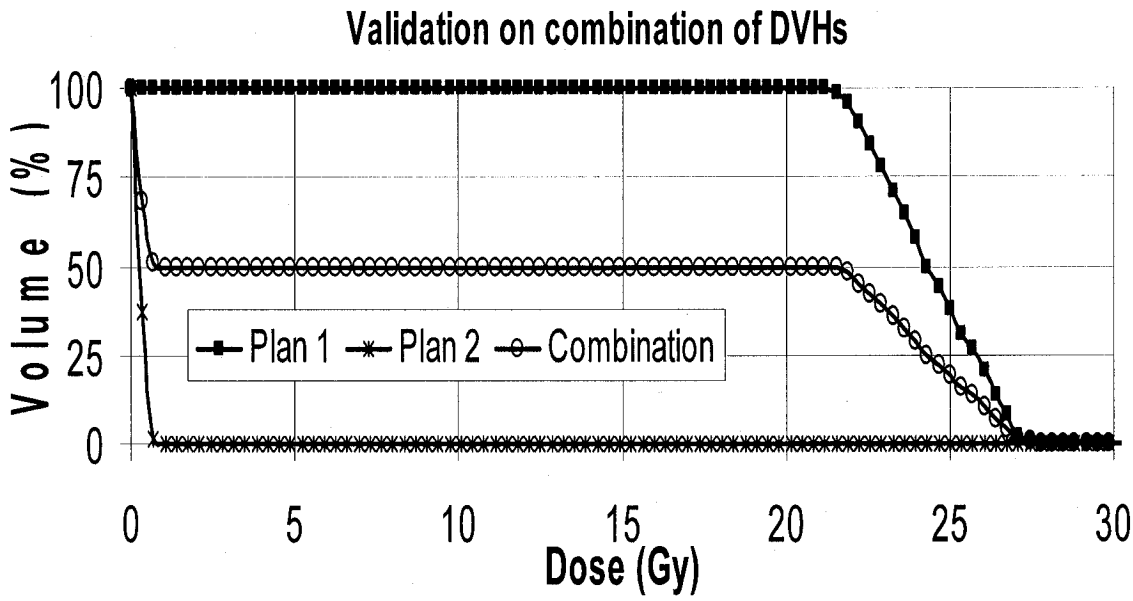

Figure 3.14: Validation on combination of DVHs from different plans in MMCTP.

3.3.3.1 Positional variations

To indicate the value of patient repositioning at every treatment fraction, the initial step of US integration into MMCTP is to include prostate motion alone, keeping the organ volume fixed over time (cases 1-6 in Table 3.1). The prostate PTV contour, taken as the initial CT contour outlined by the physician at TP, is chosen for analysis. This contour is then moved according to the measured US shifts. The new MMCTP GUI allows the user to shift any organ in 3D either by: (1) manually entering the desired shift (Figure 3.15.a), shown on the CT image displayed or (2) automatically loading a series of shifts from a file (Figure 3.15.b), to be applied sequentially on the specified plans. By integrating the time dependency of prostate motion from US data, MMCTP becomes a 4D dose distribution analysis tool for TP.

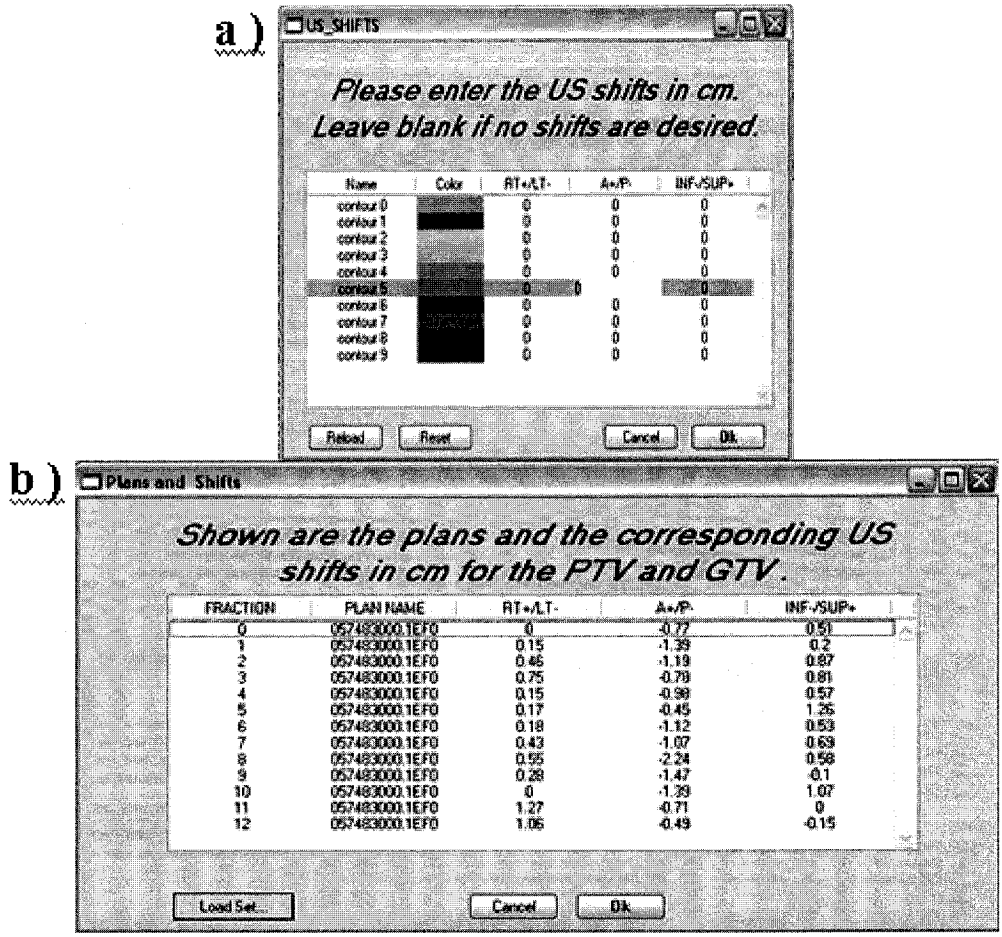

Figure 3.15: New MMCTP GUI for shifts in 3D: (a) manual entry and (b) automatic reading of shifts and plans.

As a validation to this new algorithm, a rectangular water phantom (40 x 20 cm x 40 cm) is designed with a single cubic contour of 5 cm sides. Four CADPLAN dose calculations are performed with a single anterior field: (1) positioned at the isocenter of the cube (Figure 3.16.a), (2) shifted left by 10 cm (LT = - 10 cm) (Figure 3.16.b), (3) shifted 5 cm anteriorly (A = +5 cm) and (4) shifted inferiorly by 10 cm (INF = - 10 cm). The applied shifts follow the convention given in equation 3.1. To evaluate the capabilities of MMCTP to shift organs, Figure 3.16.c displays the cubic contour shifted left by 10 cm, following the convention described in equation 3.5.a. The US shifts refer to the convention of Table 2.3.

$$\left(X_{shifted}\right)_{MMCTP} = \left(X\right)_{MMCTP} - \left(dx\right)_{US} \quad (3.5.a)$$

$$\left(Y_{shifted}\right)_{MMCTP} = \left(Y\right)_{MMCTP} - \left(dy\right)_{US} \quad (3.5.b)$$

$$\left(Z_{shifted}\right)_{MMCTP} = \left(Z\right)_{MMCTP} - \left(dz\right)_{US} \quad (3.5.c)$$

To evaluate the shifts introduced and confirm the conventions used DVHs are calculated in MMCTP for each case. As expected for RT/LT (Figure 3.17.a) and INF/SUP shifts (Figure 3.17.c), the DVH obtained in the isocenter case (*Isocenter*) can be reproduced by moving the contour back under the shifted beams (*Shifted beam and contour*). The particularity of the A/P shift (Figure 3.17.b) is that a smaller dose is delivered to the cubic contour if the beam is shifted anteriorly away from the phantom surface (*Shifted beam*). As expected, once the contour is moved closer to the surface to follow the shifted beam (*Shifted beam and contour*) it receives a larger dose than in the original situation (*Isocenter).*

To further validate the MMCTP shifting algorithm, shifts are introduced on a real prostate in a XVMC simulation with a single anterior field. Three DVHs are calculated for the beam: (1) at the isocenter, (2) shifted by LT = -10 cm and (3) shifted in XVMC and PTV shifted in MMCTP, both by LT = -10 cm. These shifts follow equation 3.5.a. Figure 3.18 displays the dose distributions and DVHs for all three cases. The DVHs show an interesting feature of the patient geometry not observed in the symmetrical phantom. Shifting both the isocenter and the PTV by LT/RT (*Shifted beam and contour*) does not reproduce the DVH obtained initially (*Isocenter*). In the shifted case, the PTV gets closer to the patient skin so it receives a higher dose. This is of course an exaggeration to the results in real prostate patients. The arbitrary shift used as validation is around 100 times larger than average LT/RT measured prostate shifts (Table 4.3). Moreover, prostate TP involve 5 beams which partially compensate each other.

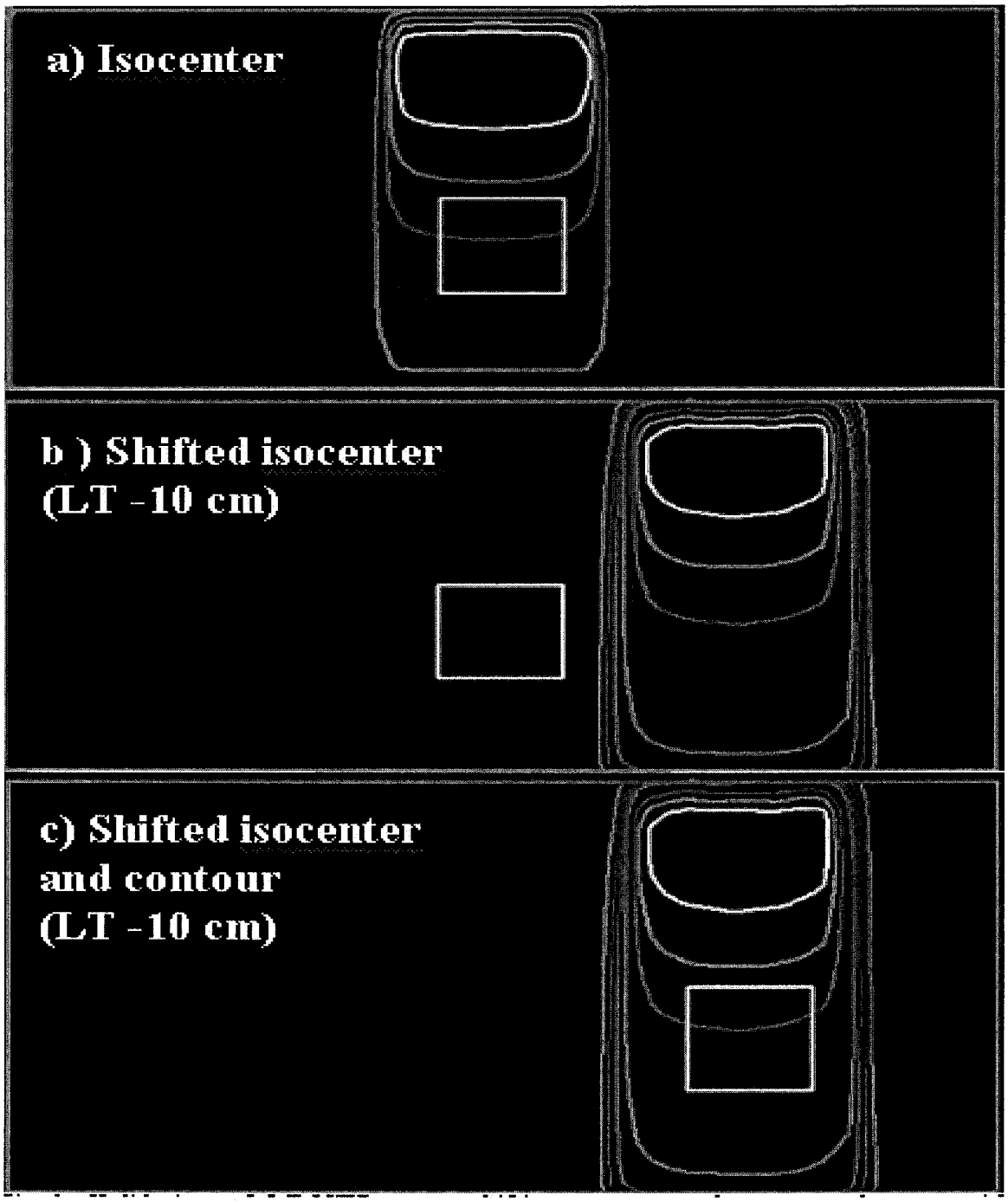

Figure 3.16: Validation of MMCTP organ shifting on a water phantom with CADPLAN dose distributions at (a) isocenter, (b) isocenter shifted by LT = - 10 cm and (c) isocenter shifted in CADPLAN and the contour shifted in MMCTP, both by LT = - 10 cm.

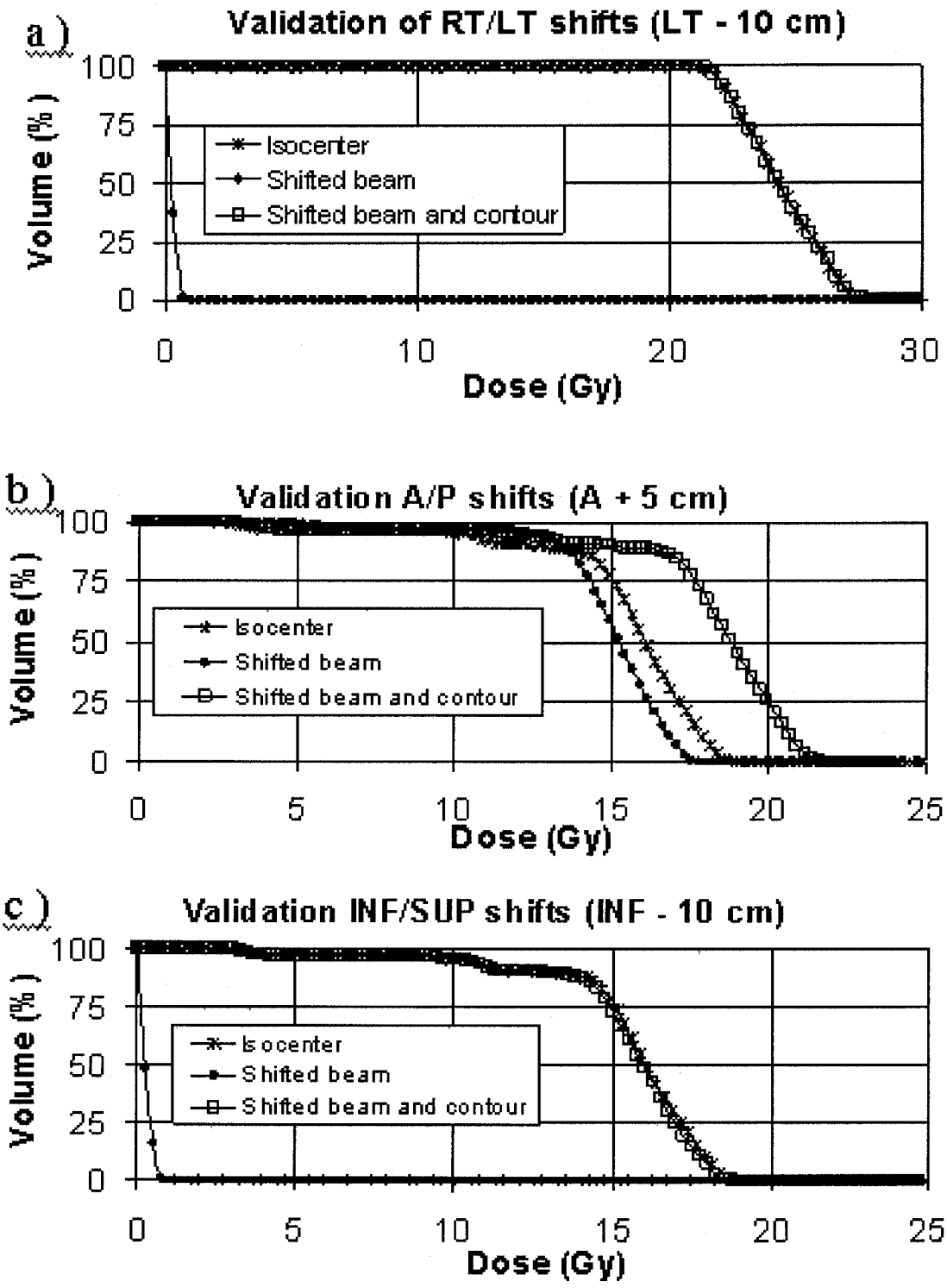

Figure 3.17: MMCTP DVHs for the validation of organ shifting in the: (a) LT/RT, (b) A/P and (c) INF/SUP dimensions.

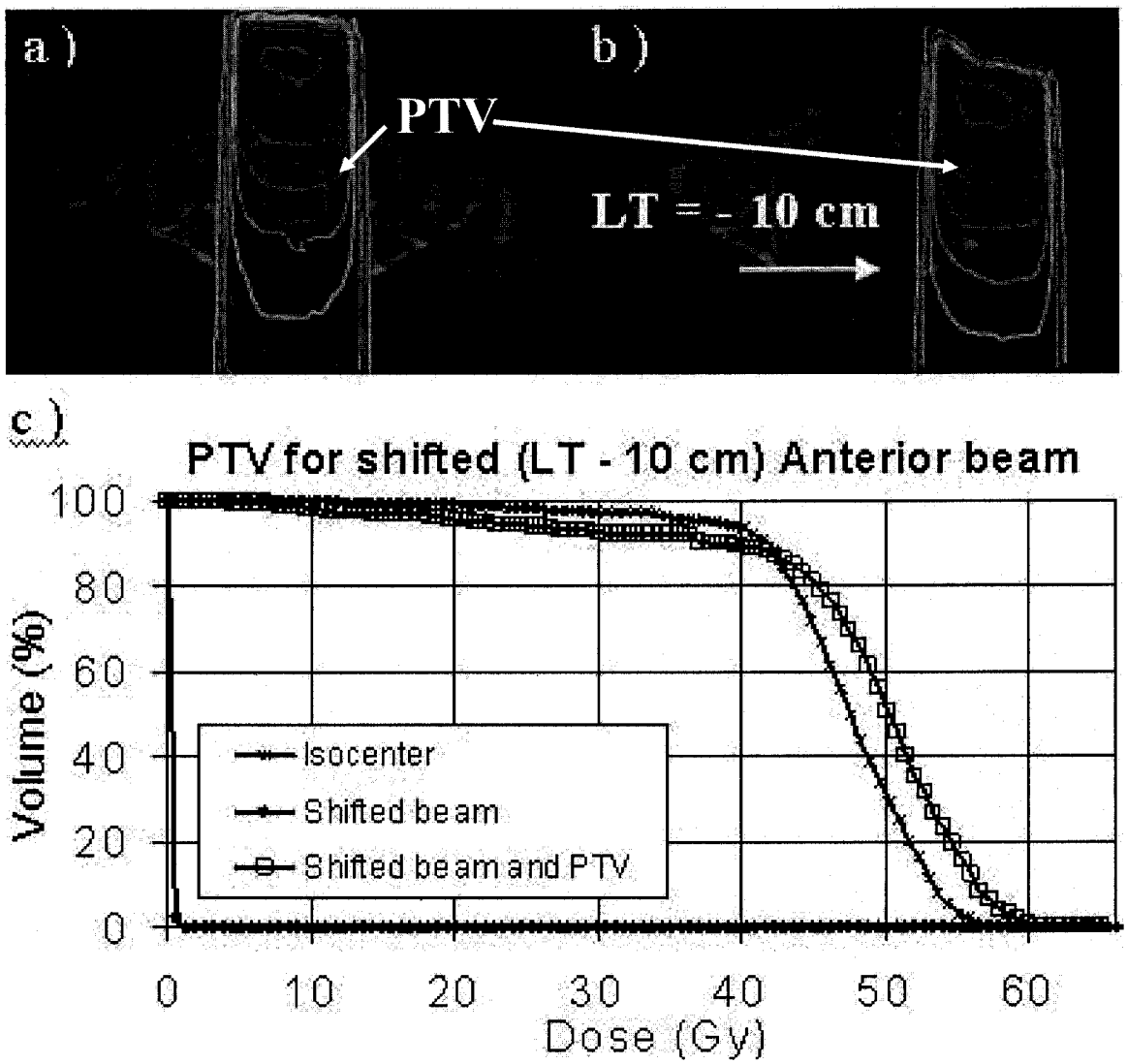

Figure 3.18: Validation of MMCTP organ shifting on a real prostate with one anterior beam in XVMC showing the CT contours for PTV at: (a) isocenter and (b) beam shifted in XVMC and contours shifted in MMCTP. (c) Corresponding DVHs calculated in MMCTP. Data is for patient 7.

The validated MMCTP is used to calculate and combine for each patient fractional DVHs containing US organ motion. The results in chapter 6 serve to evaluate the ability of BAT and RES repositioning to improve the accuracy of dose delivery.

3.3.3.2 Volumetric variations

The final step is to give MMCTP the capability to use the US volumetric information registered on a day-to-day basis (cases 7-8 in Table 3.1). Of course, this is only possible with the 3D RES system. The BAT system used in the clinic only provides positional information. Because RES is a 3D free-hand system, its images must be reconstructed into a regular 3D voxel array as shown in Figure 3.19 [11].

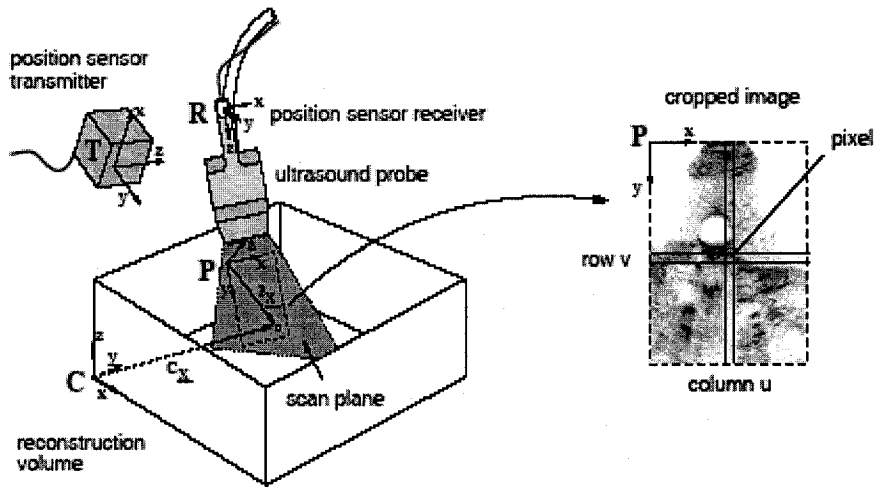

Figure 3.19: The P, R, T and C coordinate systems of the reconstruction process.

The first coordinate system used for reconstruction is the B-scan plane (**P**) with its origin at the top left hand corner of the US image. The x-axis is in the lateral direction, the y-axis follows the beam entering the patient and the z-axis runs through the multiple images acquired over a single scan. Since US images are recorded in pixel values, equation 3.6 converts every pixel in every US image to cm. The column and row indexes of the pixels in the original US image are denoted by u and v, respectively. The scaling factors are given in cm/pixel by s_x and s_y.

$$P_x = \begin{pmatrix} s_x u \\ s_y v \\ 0 \\ 1 \end{pmatrix} \tag{3.6}$$

The next coordinate system (**R**) is where the US probe markers give the position and orientation of each cross-section of the data sequence. **T** is the coordinate system of the Polaris position sensor transmitter. The final coordinate system (**C**) has its origin at the corner of the 3D-matrix of voxels created from the set of acquired US images.

In the reconstruction process, every pixel in every US image ($\mathbf{P_x}$) is transformed to the coordinate system **R**, then **T** and finally **C** to find its location $\mathbf{C_x}$ according to:

$$C_x = \left({}^{C}T_{T}\right)\left({}^{T}T_{R}\right)\left({}^{R}T_{P}\right)P_x \tag{3.7}$$

Where $\left({}^{i}T_{j}\right)$ indicates a transformation from coordinate systems *j* to *i*.

Knowing $\mathbf{C_x}$ each US image can be inserted into a reconstruction volume that allows any-plane slicing, volume and surface rendering. Unfortunately, in the study under consideration, none of the calibration files were recorded at the time of scanning. A complete reconstruction cannot be performed without the information on the Polaris coordinate system (**T**) with respect to the room laser coordinate system (**C**). As a result, the US contours drawn on US images cannot be integrated into the MMCTP system. All one can do in this case is to obtain the correct orientation and position of the US images with respect to one another. The US volumes can then calculated and used indirectly in MMCTP to resize the CT prostate contours. Neglecting shape changes appears to be a valid approach from the work by Deurloo *et al* [2]. After quantification of prostate shape variations of 19 patients with CT-scans during EBRT, prostate deformation was found to be small compared to motion.

To calculate US volumes each pixel must be transformed from the original image ($\mathbf{P_x}$) to a location with respect to the fixed transmitter ($\mathbf{T_x}$).

$$T_x = \left({}^{T}T_{P}\right)P_x \tag{3.8}$$

The transformation between **P** and **T** has six degrees of freedom which must be applied in the right order: three rotations and three translations. This is implemented in a 3D US viewer in *RealBasic*. For each patient fraction the US information is given as binary image pixels and sizes (*sxi*), segmentation contour points (*sxg*) and rotations and translations for individual images (*sx*). A visual example is given in Figure 3.20 for a single fraction of patient 13. Figure 3.20.a shows the original US contours and one original US image as given in the raw data files. For 3D visualization an arbitrary distance is chosen between the 2D images. Figure 3.20.b shows the resulting fan-beam after transformation of both images and contours. This represents the true physical scan performed on the patient with the correct orientation relative to Polaris and the true prostate shape in 3D. The prostate volume to be introduced in MMCTP for DVH calculations can be obtained from the transformed contours.

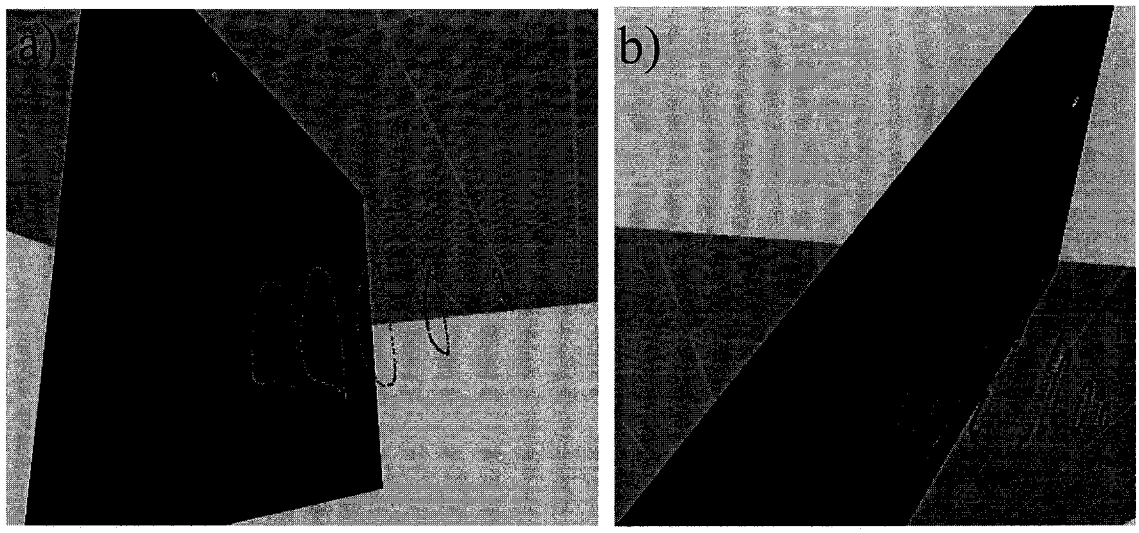

Figure 3.20: 3D US viewer screen-shot of (a) the original US images and contours and (b) the transformed US images and contours in the T coordinate system. For clarity, only 1 of 39 images is shown.

There are probably better ways to calculate volumes than the one described hereafter. However, the chosen method offers good approximations on the prostate volumes given the coarseness of the drawn contours. We perform five steps to calculate volumes from contour points: (1) we find the center of mass of each contour, (2) we compute the

distance between the center of mass of consecutive contours, (3) we calculate the area of each contour, (4) we multiply the contour area by the distance to the next contour and (5) we sum the contribution of each contour. The center of mass is calculated because the contours are arranged in a fan-beam fashion. The distances separating adjacent contours vary along the length of the contours and are different for different pairs of contours. The center of mass of a contour (CM) defined by n points (equation 3.9.a) is used to calculate the distance (d) between two consecutive contours (C1 and C2 in equation 3.9.b).

$$CM = (X_c, Y_c, Z_c) \quad Where \quad X_C = \frac{\sum_{i=0}^{n-1} X_i}{n}, \quad Y_C = \frac{\sum_{i=0}^{n-1} Y_i}{n}, \quad Z_C = \frac{\sum_{i=0}^{n-1} Z_i}{n} \tag{3.9.a}$$

$$d_{C1,C2} = \sqrt{(X_{C1} - X_{C2})^2 + (Y_{C1} - Y_{C2})^2 + (Z_{C1} - Z_{C2})^2} \tag{3.9.b}$$

Finding the area (A) of each contour (C) comes down to computing the area of a planar polygon. The basic geometry calculation is described by equation 3.10 where each of the polygon n vertices V_i has coordinates (x_i, y_i).

$$A(C) = \frac{1}{2} \sum_{i=0}^{n-1} (x_i y_{i+1} - x_{i+1} y_i) \tag{3.10}$$

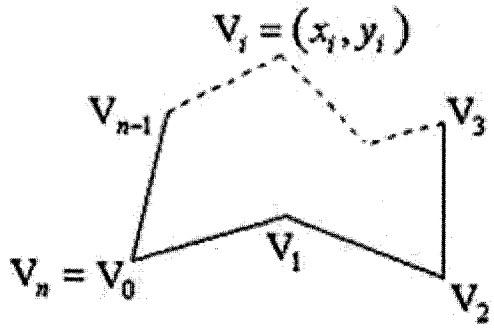

Figure 3.21: 2D polygon with n vertices $V_i = (x_i, y_i)$.

This formulism gives a signed area, which is positive when the vertices (V_i) are oriented counterclockwise around the polygon and negative otherwise. The absolute value of each

contour area is used to compute the final volume given by N contours according to equation 3.11. The volume results for 7 patients are summarized in chapter 4.

$$V(cm^3) = \sum_{j=0}^{N-1} \left[d_{j,j+1} \right] \; X \left[A(C_j) \right] \tag{3.11}$$

To introduce these US volumes into MMCTP, the US scans acquired at planning time (V_{US_sim}) and at treatment time *i* ($V_{US\_treatmenti}$) are used. It is then possible to calculate the change of US volumes at each treatment with respect to the planning US volume. This ratio is used to scale the CT PTV volume (V_{CT_PTV}) according to equation 3.12 to yield the CT PTV volume at each fraction ($V_{CT\_treatmenti}$).

$$V_{CT\_treatment_i}(cm^3) = \left(\frac{V_{US\_treatment_i}}{V_{US\_sim}} \right) \; X \; V_{CT\_PTV} \tag{3.12}$$

Volume scaling performed this way avoids two issues; (1) that of US measuring 47 % smaller prostate volumes than CT [9] and (2) the fact that the US contours are derived from prostate anatomy rather than PTV definition which includes planning margins.

The final step is for the MMCTP DVH calculation routine to replace the fixed CT volumes by time-evolving volumes for each fraction ($V_{CT\_treatmenti}$). This is implemented by reading a list of US volumes and corresponding RES shifts. The CT volumes are then scaled by adding or subtracting layers of pixels around each contour until the best fit is found. The algorithm starts from the middle contour, removes or adds one layer and evaluates the new volume. If more scaling is required, the first contour to the left is modified, then the first contour to the right, and so on until the best fit is found. For all patients the resulting volumes in MMCTP fall within 1.2 % of the volumes calculated in equation 3.12. While the ideal situation might be to replace the CT volumes in MMCTP by the US volumes, none of the calibration files were recorded in the present study.

Hence, the US contours cannot be superimposed onto CT images and we can only estimate the effects of prostate volume changes by scaling the CT volumes.

Figure 3.22 shows a water phantom used to test the newly implemented MMCTP volume change algorithm. Two cubic contours are drawn, a large one of 1000 cm^3 (white) and a small one of 100 cm^3 (black). The CADPLAN dose distribution is seen to only partly cover the large cube while the small cube fits entirely inside the maximum dose region. The resulting DVH is displayed in Figure 3.23. Using the new MMCTP code to scale down the large cube to a size of 100 cm^3, the resulting contour falls onto the initial small cube (Figure 3.22 in black) with the same DVH (Figure 3.23).

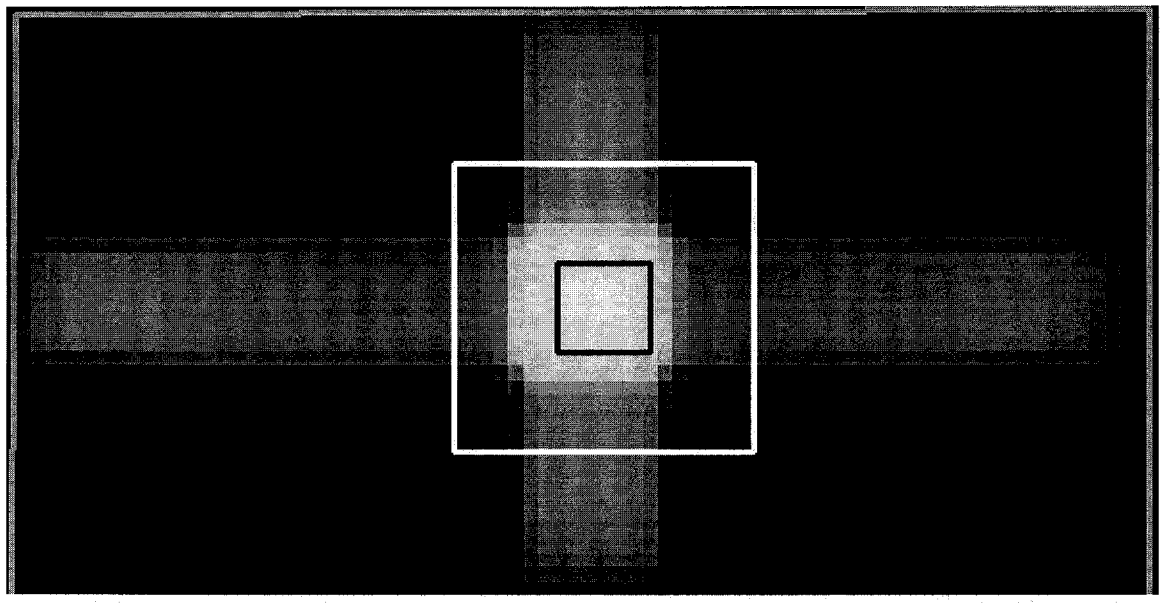

Figure 3.22: Validation of MMCTP volume change algorithm on a CADPLAN dose distribution of a water phantom with two cubic contours (white = large cube, black = small cube and reduced cube).

The MMCTP algorithm is then extended to allow DVH calculation to include not only US shifts but also volumes for multiple fractions (Table 4.6). These fractional DVHs are then combined and the volume normalized to 100 %. A validation test is shown in Figure 3.24 where the DVHs for a cube of 100 cm^3 and a cube of 200 cm^3 are combined to yield a DVH that lies in between the individual curves.

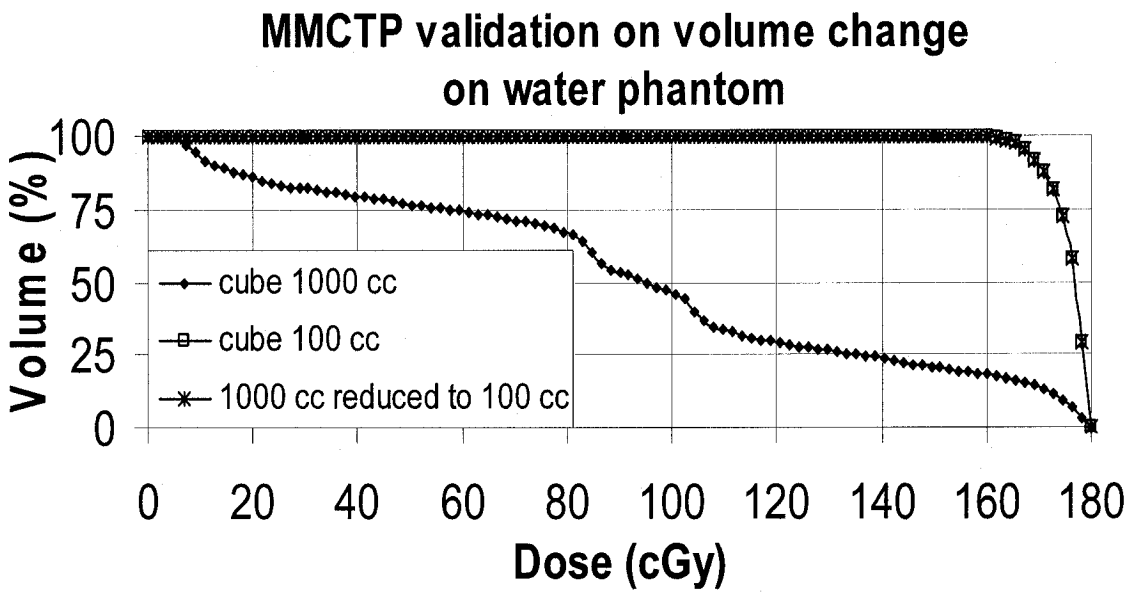

Figure 3.23: DVH for the validation of the volume change algorithm in MMCTP.

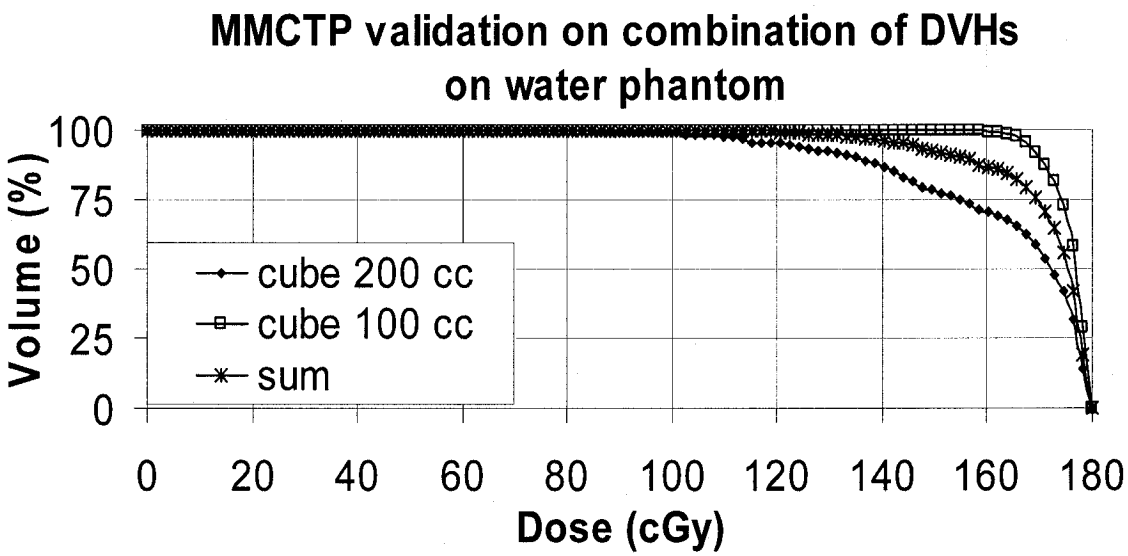

Figure 3.24: DVH for the validation of DVH combination in MMCTP.

The treatment outcome of prostate volume changes can be quantified using this new MMCTP tool to compare 3D dose distributions in tumors obtained using fixed or varying CT volumes. The results are shown in chapter 6.

References

[1] Batho H.F. "Lung corrections in Cobalt 60 beam therapy", J. Can. Assoc. Radiol., 15, pp. 79-83, 1964.

[2] Deurloo K.E.I., Steenbakkers R.J.H.M., Zijp L.J., De Bois J.A., Nowak P.J.C.M., Rasch C.R.N. and Van Herk M. "Quantification of shape variation of prostate and seminal vesicles during external beam radiotherapy". Int. J. Radiat. Oncol. Biol. Phys., 61 (1), pp. 228-238, 2005.

[3] Du Plessis F.C.P., Willemse C.A. and Lotter M.G. "Comparison of the Batho, ETAR and Monte Carlo dose calculation methods in CT based patient models". Med. Phys., 28 (4), pp. 582-589, 2001.

[4] Fippel M. "Fast Monte Carlo dose calculation for photon beams based on the VMC electron algorithm". Med. Phys., 26 (8), pp. 1466-1475, 1999.

[5] Herman G.T., Zheng J. and Bucholtz C.A. "Shape-Based interpolation". IEEE Computer Graphics and Applications, 12, pp.69-79, 1992.

[6] Jones A.O. and Das I.J. "Comparison of inhomogeneity correction algorithm in small photon fields". Med. Phys., 32 (3), pp. 766-776, 2005.

[7] Kappas C. and Rosenwald J.-C. "Quality control in inhomogeneity corrections algorithms used in treatment planning systems". Int. J. Radiat. Oncol. Biol. Phys., 32 (3), pp. 854-858, 1995.

[8] Kawrakow I., Fippel M. and Friedrich K. "3D Electron Dose Calculation using a Voxel based Monte Carlo Algorithm". Med. Phys., (23) pp. 445-457, 1996.

[9] Langen, K.M. and Pouliot J., Anezinos C., Aubin M., Gottschalk A.R., Hsu I.-C., Lowther D., Liu Y.-M., Shinohara K., Verhey L.J., Weinberg V. and Roach M. "Evaluation of ultrasound-based prostate localization for image-guided radiotherapy". Int. J. Radiat. Oncol. Biol. Phys., 57(3), pp. 635-44, 2003.

[10] McDermott P., He T. and DeYoung A. "Dose calculation accuracy of lung planning with a commercial IMRT treatment planning system", J. Appl. Clini. Med. Phys., 4, pp. 341-351, 2004.

[11] Prager R.W., Rohling R.N., Gee A.H. and Berman L. "Automatic calibration for 3-D free-hand ultrasound", Technical report CUED/F-INFENG/TR 303, Cambridge University of Engineering, pp. 2-5, 1997.

[12] Pawlicki T. and Ma C.M. "Monte Carlo simulation for MLC-based intensity modulated radiotherapy", Med. Dosim., 26, pp. 157-168, 2001.

[13] Seco, J. Adams E., Bidmead M., Partridge M. and Verhaegen F. "Head-and-neck IMRT treatments assessed with a Monte Carlo dose calculation engine", Phys. Med. Biol., 50 (5), 2005.

[14] Webb S. and Fox. R.A. "The direct use of CT data for inhomogeniety corrections in radiotherapy planning". Br. J. Radiol. Suppl., 15, 1979.

Chapter 4: Results and discussion
2D versus 3D Ultrasound

This chapter presents the quantification of the measured US positional and volumetric changes over the course of RT for 26 patients treated with EBRT at the MGH from May to October 2003.

4.1 Quantification of daily positional measurements

Table 4.1 gives the details on the RT treatments and US scans (2D BAT and 3D RES) for each patient. Each patient got planned only once and the single plan was used throughout the course of treatment. All fractions were delivered without incidents. At the MGH, prostate patients considered as low risk are generally prescribed a lower dose (50 cGy), while the ones considered as high risk receive a higher dose (72 cGy). Doctors may have different opinions on this matter because several clinical factors must be taken into account. The general belief is that the higher the dose the better the tumor control rate.

Figure 4.1 shows an example of BAT prostate motion for the 36 fractional treatments of patient 11. These displacements were written down by the technologists in the couch coordinate system. They are translated here into the patient anatomical coordinate system to represent true prostate motion. RT/LT stands for Right-/Left-Transverse, A/P for Anterior/Posterior and Sup/Inf for Superior/Inferior. These values represent shifts from the CT planned isocenter. They were calculated as the displacement of the center-of-mass (CM) of the prostate contour on treatment day relative to that on planning day. This sample data is symmetrical in the RT/LT direction (mean = -0.09 ± 0.29 cm), biased towards the posterior (mean = - 0.41 ± 0.43 cm) and biased slightly towards the inferior (mean = -0.16 ± 0.39 cm). The range is -1.10 to 0.73 cm in RT/LT, -1.56 to 0.35 cm in A/P, and -0.17 to 0.60 cm in Sup/Inf.

Patient number	Total prescribed dose (Gy)	Number of fractions	Number of US Scans	
			BAT	RES
1	66	22	22	1
2	66	22	21	3
3	50	20	20	6
4	66	22	22	6
5	66	22	22	15
6	66	22	24*	9
7	66	22	22	17
8	72	36	36	26
9	72	36	35	0
10	66	22	22	17
11	72	36	36	23
12	72	36	35	30
13	72	36	36	27
14	72	36	36	0
15	70	35	34	0
16	66	22	4	0
17	66	22	4	0
18	66	22	5	0
19	66	22	6	0
20	66	22	6	0
21	66	22	18	0
22	66	22	19	2
23	66	22	19	2
24	66	22	19	11
25	66	22	16	11
26	72	36	30	2

Table 4.1: Details on patient treatment and US scans. * Two extra BAT shifts were recorded for this patient due to a malfunction of the BAT on one treatment day.

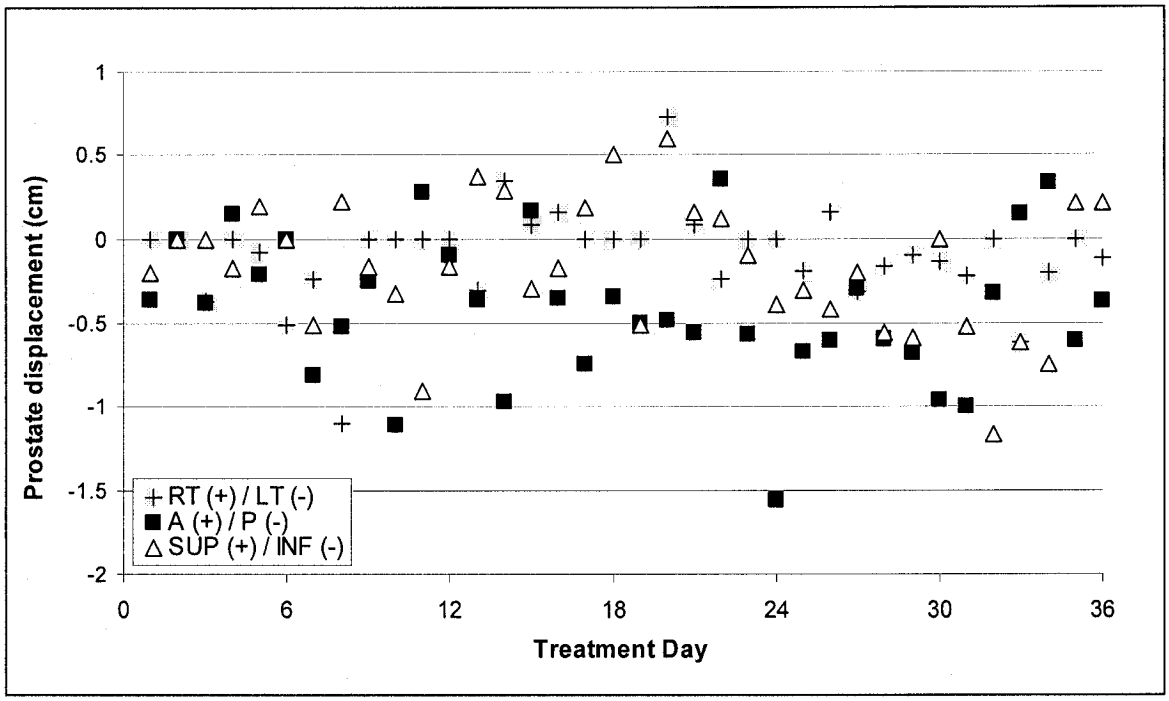

Figure 4.1: BAT daily prostate motion from the treatment isocenter in 3 dimensions for patient 11 over the full course of treatment consisting of 36 fractions.

Figure 4.2 shows the distribution of prostate BAT and RES shifts for all patients averaged over their corresponding treatment duration. To show the difference in prostate alignment assessment between the US systems, a Wilcoxon signed-ranks test is performed on 201 BAT and RES measurements. Patients with less than 3 RES scans (Table 4.1, light gray) are removed from the statistics, leading to a total of 13 usable patients. This test detects differences between measurements in similar way to the Sign-test. Wilcoxon is however more powerful for measurements that can be quantified because it utilizes both the signs and the magnitudes of differences [16]. Table 4.2 shows the statistics obtained in each dimension. The difference between paired measurements is quoted in terms of the median as it is a more robust estimator than the mean for the central tendency.

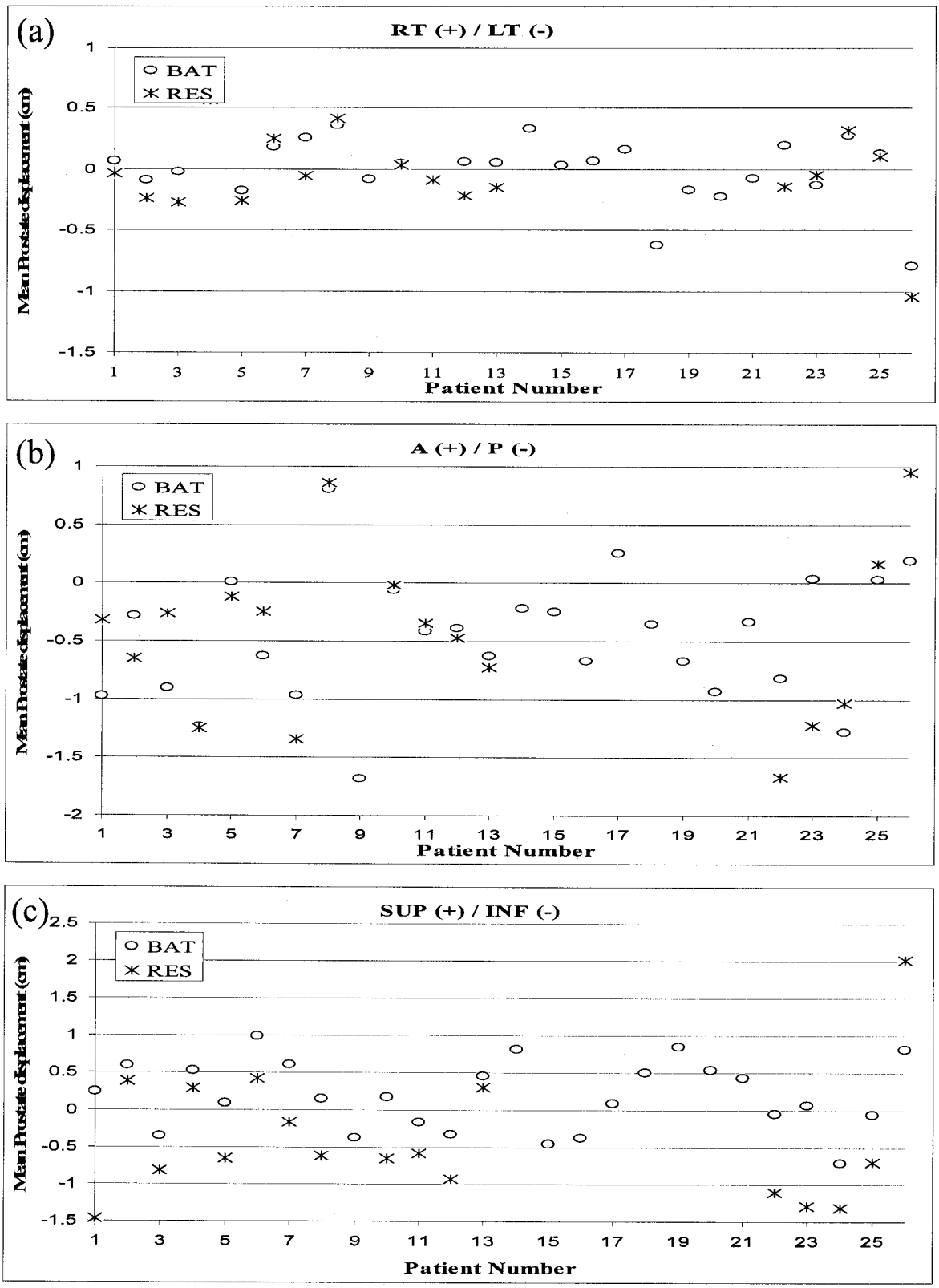

Figure 4.2: Distribution of prostate shifts for all patients averaged over their treatment duration in the (a) RT/LT, (b) A/P and (c) Sup/Inf dimension.

Direction	Difference between medians (cm)	95 % Confidence Interval (cm)	2-tailed p values
RT (+) / LT (-)	0.10	0.05 to 0.15	< 0.0001
A (+) / P (-)	0.02	-0.04 to 0.07	0.5033
Sup (+) / Inf (-)	0.60	0.53 to 0.66	<0.0001

Table 4.2: Difference in 201 daily BAT and RES paired displacements.

The p-values serve to accept or reject the null hypothesis of a zero difference between the measurements. With a confidence interval of 95 %, p-values lower than the significance level ($p < 0.05$) indicate that one must reject the null hypothesis while p-values higher than the significance level ($p > 0.05$) indicate that one must accept the null hypothesis. From Table 4.2, the null hypothesis is rejected in two out of three dimensions. This indicates that a significant systematic difference exists between BAT and RES assessments of prostate alignment in the RT/LT and Sup/Inf dimensions. This result agrees with previous unpublished analysis made on the same data set by Cury *et al* [3]. They also found RES prostate displacements to be consistent with CT-scan measurements, taken 3 times at bi-weekly intervals on 10 patients during treatment. They concluded RES to be more accurate than BAT for prostate alignment.

The significant systematic difference between BAT and RES in the RT/LT and Sup/Inf dimensions cannot be seen from Figure 4.2. This figure shows the averaged BAT and RES shifts over the treatment duration. On the other hand, the Wilcoxon signed-ranks test considers BAT-RES pairs independently as it does not average them over patient treatment fractions. As a consequence, even if on average BAT and RES seem to agree over the whole treatment, the measurements might differ significantly at each fraction. For example, Figure 4.2.a shows excellent agreement (0.01 cm difference) between the average BAT and RES RT/LT measurements for patient 10. However, these measurements deviate significantly from each other (up to 0.54 cm) on individual fractions (Figure 4.3).

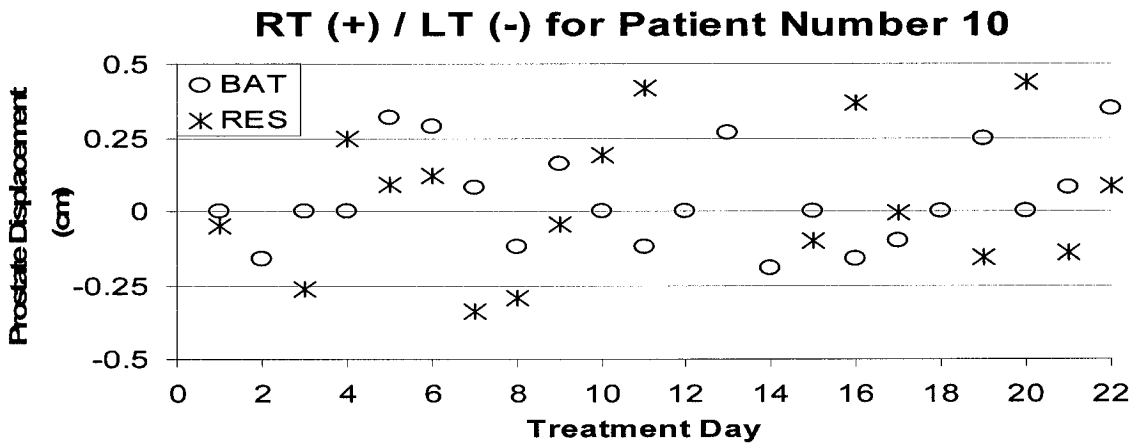

Figure 4.3: Distribution of prostate RT/LT shifts for patient 10 at each fraction.

Table 4.3 summarizes prostate motion for the same 13 patients. The maximum prostate displacement measured in any dimension with the BAT system lies between 0.81 cm and 2.49 cm, while this range is 1.17 cm to 2.44 cm with the RES system. Figure 4.4 shows the extent of these maximum US shifts on an axial CT-slice through patient 11. Such displacements are quite significant for typical prostates of dimensions 3-5 cm [6].

	Prostate displacement from planned isocenter (cm)			
Direction	**BAT**		**RES**	
	Mean ± SD	**Range**	**Mean ± SD**	**Range**
RT (+) / LT (-)	0.11 ± 0.37	-0.81 to 1.60	0.01 ± 0.43	-1.17 to 1.52
A (+) / P (-)	-0.33 ± 0.73	-2.26 to 2.49	-0.33 ± 0.76	-2.19 to 2.44
Sup (+) / Inf (-)	0.11 ± 0.57	-1.43 to 1.77	-0.47 ± 0.69	-2.05 to 1.35

Table 4.3: Prostate motion in 3D for 13 patients scanned with both US systems. A total of 402 daily prostate displacements are used.

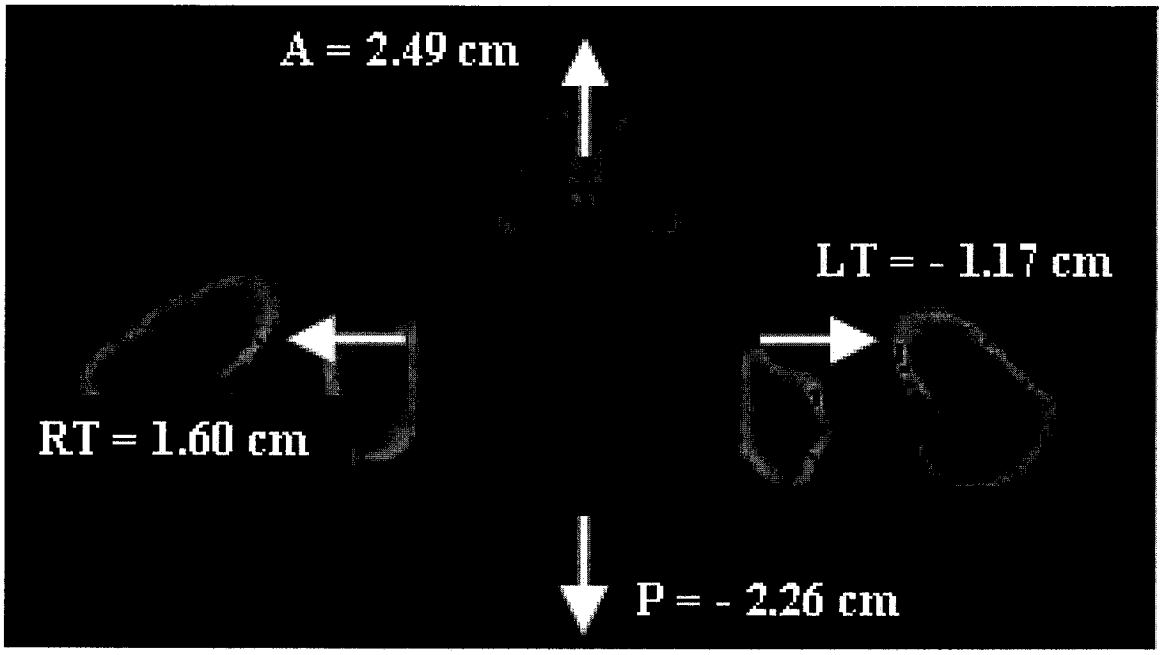

Figure 4.4: Maximum prostate PTV shifts on an axial CT-slice through patient 11. Shown are the PTV at the isocenter (heavy line) and shifted (lighter lines).

Table 4.3 shows a standard deviation (SD) around 0.4 cm in the RT/LT dimension while it is 0.6-0.8 cm in the A/P and Sup/Inf dimensions. This smaller SD indicates that bladder and rectal fills have less effect on prostate motion in the lateral dimension. From Table 4.3, BAT and RES agree only on the A/P shifts (BAT: -0.33 cm and RES: -0.33 cm). However, within the precision of the systems the RT/LT difference in the mean shifts is not statistically significant (BAT: 0.11 cm and RES: 0.01 cm). However, in the Sup/Inf direction the difference is significant. While BAT displays an average superior shift of 0.11 cm, RES gives an average inferior shift of 0.47 cm, for a total difference of 0.58 cm. This trend is also found in the RES Sup/Inf ranges (-2.05 to 1.35 cm) shifted to the inferior direction compared to the BAT ranges (-1.43 to 1.77 cm).

Since RES was found to be more accurate than BAT by Cury *et al* [3], the inferior RES shift is believed to represent the real prostate movement. There might also be a bias introduced by the different pressure applied on the patient by the different probes. As explained in chapter 1, BAT only requires the acquisition of two transverse images. In fact, a previous study showed that the prostate shifts by less than 1 mm in the Sup/Inf

directions due to the pressure applied by the probe [18]. On the other hand, RES typically involves sweeping the probe over the prostate region in the SUP to INF direction while pressing down for good contact. It is possible although not proven that the pressure applied with the RES probe mechanically shifts the prostate inferiorly. No other publications on this issue are available at this time on the research RES prototype. Moreover, the uncertainty in patient marking can significantly bias the mean displacement on a small pool of data. This is indicated by a 2002 study performed in this department on 4 patients with the BAT system [4]. The authors found that an error in patient isocenter skin marking can lead to an inferior displacement of as much as 2 cm

Many researchers have investigated prostate localization accuracy using a variety of imaging modalities. Several studies performed with BAT on patients undergoing EBRT are summarized in Table 4.4. A large variability is seen to exist between the published data.

Reference	BAT mean ± SD prostate displacement (cm)		
	RT (+) / LT (-)	**A (+) / P (-)**	**Sup (+) / Inf (-)**
[2]	-0.05 ± 0.19	-0.06 ± 0.34	0.09 ± 0.32
[5]	0.04 ± 0.22	0.04 ± 0.40	-0.15 ± 0.33
[7]	0.18 ± 0.39	-0.07 ± 0.52	0.27 ± 0.45
[8]	0.01 ± 0.34	0.02 ± 0.46	0.0 ± 0.57
[10]	-0.08 ± 0.20	-0.13 ± 0.41	-0.17 ± 0.41
[11]	0.26 ± 0.21	0.47 ± 0.27	0.42 ± 0.28
[12]	0.22 ± 0.39	-	0.58 ± 0.52
[15]	0.03 ± 0.25	-0.13 ± 0.47	0.1 ± 0.51

Table 4.4: Prostate motion in 3D in several publications.

The results obtained by Langen *et al* [7], when evaluating prostate motion in 10 patients with BAT and radiopaque markers, agree more or less with the results presented in this thesis (Table 4.3). However, these studies are hard to compare as their statistical

uncertainty differs. Only 24 US scans were considered in the published results by Lattanzi *et al* [8] while Chandra *et al* [2] analyzed 3509 BAT alignments. Moreover, Trichter *et al* [18] noted that a discrepancy exists in the BAT shifts of the studies they compared [5,8,10,11,12,15]. They concluded the variation between the presented data might come from inherent problems or uncertainties in BAT, differences in bladder or bowel preparation, differences in patient immobilization or even differences in BAT users. One noticeable trend amongst the publications presented in Table 4.4 has been reproduced in this thesis; the variance is smaller in the RT/LT dimension than in the two other dimensions.

4.2 Quantification of daily volumetric measurements

Based on RES images, the US prostate contours of 7 patients were reconstructed in 3D and their volumes were calculated (section 3.3.3.2). Table 4.5 lists for each patient the US prostate volumes at planning (V_{US_SIM}) and the PTV and GTV volumes defined on CT images and calculated by MMCTP (V_{CT_PTV} and V_{CT_GTV}, respectively). The ratio of GTV CT to US volumes (V_{CT_GTV} / V_{US_SIM}) clearly illustrates the potential variations in prostate volumes from different imaging modalities. In the literature, prostates have been found to appear significantly larger on CT than on 3D US [17]. The US volumes calculated here are on average 1.6 times smaller than the CT volumes. These results fall within the 1.3 ratio found by Smith *et al* [17] and the 2.1 ratio found by Langen *et al* [7]. From Table 4.5, on CT the PTV is on average 2.4 times larger than the GTV (V_{CT_PTV} / V_{CT_GTV}). Since US contours represent the true anatomical prostate volume, they are more closely related to GTV than PTV. Following equation 4.1 with V_{CT_PTV} / V_{CT_GTV} = 4 and V_{CT_GTV} / V_{US_SIM} = 1.6, the US volumes at treatment time are scaled on average by a factor of around 4 to yield the new PTV CT volume.

$$V_{CT\_treatment_i}(cm^3) = \left(\frac{V_{CT\_PTV}}{V_{CT\_GTV}}\right)\left(\frac{V_{CT\_GTV}}{V_{US\_sim}}\right) X \; V_{US\_treatment_i} \qquad (4.1)$$

Patient	V_{CT_PTV} (cm^3)	V_{CT_GTV} (cm^3)	V_{US_SIM} (cm^3)	V_{CT_GTV} / V_{US_SIM}	V_{CT_PTV} / V_{CT_GTV}
2	115.2	51.3	40.5	1.3	2.2
3	155.5	45.8	53.9	0.8	3.4
4	133.0	63.4	23.3	2.7	2.1
5	192.2	83.5	28.8	2.9	2.3
7	119.0	47.3	32.6	1.5	2.5
10	102.3	42.1	28.7	1.5	2.4
13	148.4	69.9	97.0	0.7	2.1
Average	**137.9**	**57.6**	**43.5**	**1.6**	**2.4**

Table 4.5: Prostate volumes from US and CT images. Data is shown for 7 patients.

A summary of the volumes taken at several fractions for 7 patients is presented in Table 4.6. Listed is the number of fractions for which US image and contour data is available, the average volume (Vmean) and standard deviation (SD) as well as the volume range (Vmin to Vmax). Vmean represents the US volume averaged over the fractions. The SD is given as a percentage of V_{US_SIM} (Table 4.5). Vmin and Vmax are the minimum and maximum prostate volumes over all fractions.

Patient Number	Number of fractions	Vmean ± SD (cm^3) (%)	Vmin to Vmax (cm^3)
2	3	50.7 (32.1)	39.4 to 64.9
3	4	47.0 (20.6)	34.9 to 57.6
4	4	35.5 (54.9)	22.1 to 51.4
5	8	44.8 (43.3)	28.4 to 57.6
7	13	41.2 (30.8)	26.1 to 58.0
10	14	46.3 (31.2)	30.0 to 60.7
13	17	69.4 (15.1)	48.6 to 97.3
Average	**9**	**47.8 (32.6)**	**32.8 to 63.9**

Table 4.6: Summary of US volumes for 7 patients over all treatment fractions.

As seen in Table 4.6 the US prostate volumes among this group of patients ranged from 36 to 70 cm^3 with an average of 48 cm^3. Knowing that US prostate volumes are smaller than CT volumes [8], these values are in the right range compared to a CT study that documented the size of 10 prostates to a maximum of 115 cm^3 and an average of 56 cm^3 [14]. For most patients the range of volumes varies by a factor of almost 2, in agreement with previous studies on prostate volume variations over the course of RT [1,13]. Since a typical treatment lasts 4-8 weeks, this also agrees with the 20 % variation over 2 weeks quoted in Table 1.1. As found in previous studies, no trend was observed in the change of prostate volumes over the course of RT [14].

Such variability in measuring prostate volumes has been found to be a limitation to 3D-CRT [9]. Debates exist over the accuracy achievable in image-based prostate volumes without which it is not possible to obtain close conformity of dose escalation. Some differences in prostate volumes are of course attributable to real changes in the gland but there are other factors that contribute to the variations: (1) intra-fraction patient and organ motion, (2) the pressure applied by the free-hand US probe which can deform organs during the acquisition process and (3) the variability of the observer in defining volumes. For 3D US, a difference of up to 53 % has been found between repeated volume measurements for the same patient by the same observer [17]. The explanation lies in a varying contrast or signal to noise ratio between US images, leading to an uncertainty in the delineation of critical organs.

References

[1] Antolak J.A., Rosen I.I, Childress C.H., Zagars G.K and Pollack A. "Prostate Target Volume Variations during the course of Radiotherapy", Int. J. Radiat. Oncol. Biol. Phys., 42 (3), pp. 661-672, 1998.

[2] Chandra A., Dong L., Huang E., Kuban D.A., O'Neil L., Rosen I. and Pollack A. "Experience of ultrasound-based daily prostate localization". Int. J. Radiat. Oncol. Biol. Phys., 56, pp. 436-447, 2003.

[3] Cury F., Shenouda G., Souhami L., Duclos M., Faria S., David M., Corns R. and Falco T. "Comparison of BAT System and a New 3D Trans-abdominal Ultrasound-Based Image-Guided System for Prostate Daily Localization During External Beam Radiotherapy". Depts. Of Radiation Oncology and Medical Physics, McGill University Health Center. Resonant Medical Inc., Research and Development, Montreal, Canada.

[4] Falco T., Shenouda G., Kaufmann C., Belanger I., Procaccini C., Charrois C. and Evans M. "Ultrasound imaging for external-beam prostate treatment setup and dosimetric verification". Medical Dosimetry, 27 (4), pp. 271-273, 2002.

[5] Huang E., Dong L., Chandra A., Kuban D.A., Rosen I.I., Evans A. and Pollack A. "Intrafraction prostate motion during IMRT for prostate cancer". Int. J. Radiat. Oncol. Biol. Phys., 53 (2), pp. 261-268, 2002.

[6] Jin B., Turner L., Walters W. A. W. and Handelsman D.J. "The effects of Chronic High Dose Androgen or Estrogen Treatment on Human Prostate", Medical/hormonal library, 1996. http://www.transgendercare.com/medical/HighDoseTx-prostate.htm

[7] Langen, K.M, Pouliot J., Anezinos C., Aubin M., Gottschalk A.R., Hsu I-C., Lowther D., Liu Y-M., Shinohara K., Verhey L.J., Weinberg V. and Roach M. "Evaluation of ultrasound-based prostate localization for image-guided radiotherapy". Int. J. Radiat. Oncol. Biol. Phys., 57(3), pp. 635-44, 2003.

[8] Lattanzi, J., McNeeley S., Pinover W., Horwitz E., Das I., Schultheiss T.E. and Hanks G.E. "A comparison of Daily CT localization to a daily Ultrasound-based system in prostate cancer", Int. J. Radiat. Oncol. Biol. Phys., 43 (4), pp. 719-725, 1999.

[9] Levitt S.H. and Khan F.M. "The rush to judgment: Does the evidence support the enthusiasm over three-dimensional conformal radiation therapy and dose escalation in the treatment of prostate cancer ?". Int. J. Radiat. Oncol. Biol. Phys., 51(4), pp. 871-879, 2001.

[10] Little D.J., Dong L., Levy B. and Kuban D.A. "Comparison of portal imaging and BAT for patient setup and prostate localization for IMRT [Abstract]". Int. J. Radiat. Oncol. Biol. Phys., 54 (2), pp. 12-13, 2002.

[11] Morr J., DiPetrillo T., Tsai J.-S., Engler M. and Wazer D.E. "Implementation and utility of a daily ultrasound-based localization system with intensity-modulated radiotherapy for prostate cancer". Int. J. Radiat. Oncol. Biol. Phys., 53 (5), pp. 1124-1129, 2002.

[12] Powell T.M., Van den Heuvel F., Kahn M. and Forman J.D. "Independent prostate motion as measured by daily BAT ultrasound and electronic portal imaging [Abstract]". Int. J. Radiat. Oncol. Biol. Phys., 51 (3), p. 215, 2001.

[13] Roach M., Faillace-Akazawa P. and Malfatti C. "Prostate volumes and organ movement defined by serial computerized tomographic scans during three-dimensional conformal radiotherapy". Radiat. Oncol. Invest., 5, pp.187-194, 1997.

[14] Roeske J.C., Forman J.D. Mesina C.F., He T., Pelizzari C.A., Fontenla E., Vijayakumar S. and Chen G.T.Y. "Evaluation of changes in the size and location of the prostate, seminal vesicles, bladder, and rectum during a course of external beam radiation therapy". Int. J. Radiat. Oncol. Biol. Phys., 33 (5), pp. 1321-1329, 1995.

[15] Serago C.F., Chungbin S.J., Buskirk S.J., Ezzell G.A., Collie A.C. and Vora S.A. "Initial experience with ultrasound localization for positioning prostate cancer patients for external beam radiotherapy". Int. J. Radiat. Oncol. Biol. Phys., 53 (5), pp. 1130-1138, 2002.

[16] Siegel S. and Castellan Jr. "Non-parametric Statistics for the Behavioral Sciences". 2nd ed, N.J, pp. 80-87, 1988.

[17] Smith W., Lewis C., Bauman G., Rodrigues G., D'Souza D., Ash R. Venkatesan V., Downey D. and Fenster A. "3D US, MRI and CT prostate volume definition: 3D evaluation of intra- and inter-modality and observer variability". Med. Phys, 32(6), p. 2083, 2005.

[18] Trichter F. and Ennis R.D. "Prostate localization using transabdominal ultrasound imaging". Int. J. Radiat. Oncol. Biol. Phys., 56, pp. 1225-1233, 2003.

Chapter 5: Results and discussion
Monte Carlo dose calculations

5.1 XVMC versus CADPLAN

As described in chapter 3, the CADPLAN commercial TPS offers the option to use heterogeneity correction to calculate patient dose distributions. However, TP currently devised for prostate cancer patients are usually obtained without heterogeneity correction for several reasons: (1) the prostate is surrounded by soft tissues, (2) contrast agents sometimes used in the bladder for imaging can change the CT numbers and (3) gas pockets can occasionally appear in the rectum. Phenomena (2) and (3) can adversely affect dose calculations if heterogeneity correction is applied. Moreover, CADPLAN correction factors only offer an approximation to MC based calculations, where patient heterogeneities are taken into account more accurately. Section 5.1.1.1 compares dose recalculations in XVMC to original CADPLAN calculations without heterogeneity correction. Section 5.1.1.2 looks at recalculations in CADPLAN using heterogeneity correction versus XVMC.

5.1.1 CADPLAN without heterogeneity correction

This section analyzes the original CADPLAN calculations used as clinical TP for all patients by comparing them to recalculated dose distributions in XVMC. The patient with the biggest discrepancy between the two calculation methods is shown in Figure 5.1. For clarity, the only isodose lines shown are the ones representing 80 % and 95 % of the maximum dose. The 95 % isodose line seems to indicate that near tissue heterogeneities CADPLAN (Figure 5.1.a) is unable to calculate absorbed dose distributions with the accuracy offered by XVMC (Figure 5.1.b). Electron scattering effects and attenuation of treatment beams through the femurs are both modeled in XVMC but not in CADPLAN. To see the extent by which the two calculation methods differ, their dose ratio (equation 5.1) is shown in Figure 5.1.c.

$$D_{ratio}(\%) = \left[\frac{D_{CADPLAN}(cGy) - D_{XVMC}(cGy)}{D_{CADPLAN}(cGy)} \right] X\ 100 \qquad (5.1)$$

A positive D_{ratio} indicates that XVMC predicts a cold spot relative to CADPLAN. On the single CT slice shown, CADPLAN original calculations and XVMC recalculations differ by approximately 10 % inside the PTV due to the femoral heads.

To quantitatively differentiate CADPLAN and XVMC dose distributions dose-volume histograms (DVHs) are used. DVHs calculated in MMCTP for the PTV and OAR are compared for the same worst case patient (Figure 5.2.a) and for a more typical patient (Figure 5.2.b). The 10 % D_{ratio} shown on only one CT slice in Figure 5.1.c averages to a difference of 5.7 % for the whole prostate. This value is obtained from equation 5.1 by extracting from Figure 5.2.a the dose to 95 % of the PTV in CADPLAN (6274 cGy) and in XVMC (5918 cGy).

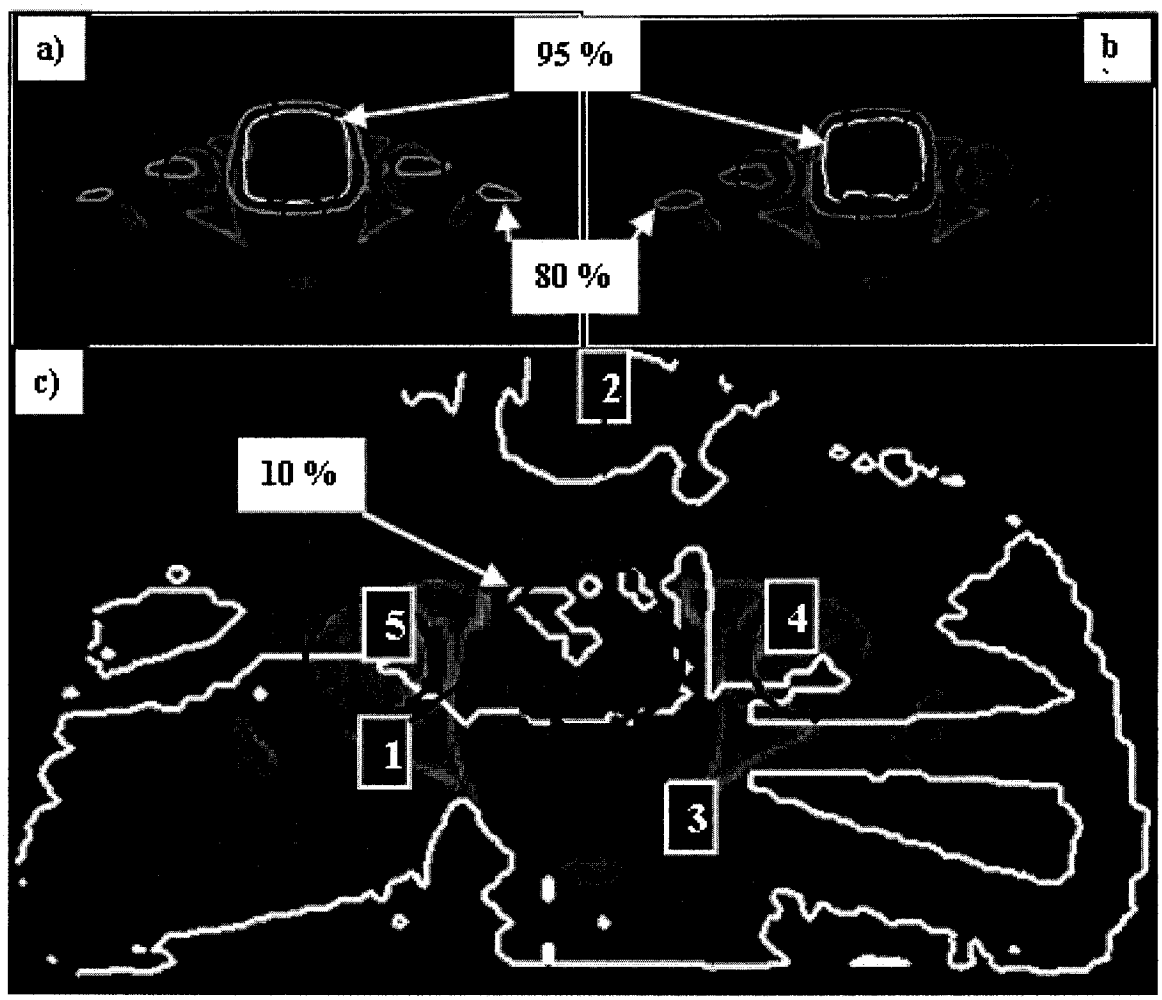

Figure 5.1: Axial CT slice showing the dose distributions for patient 4 (worst case) from (a) CADPLAN without corrections and (b) XVMC. (c) The dose ratio with organ contours; (1) prostate, (2) bladder, (3) rectum, (4) left femur and (5) right femur.

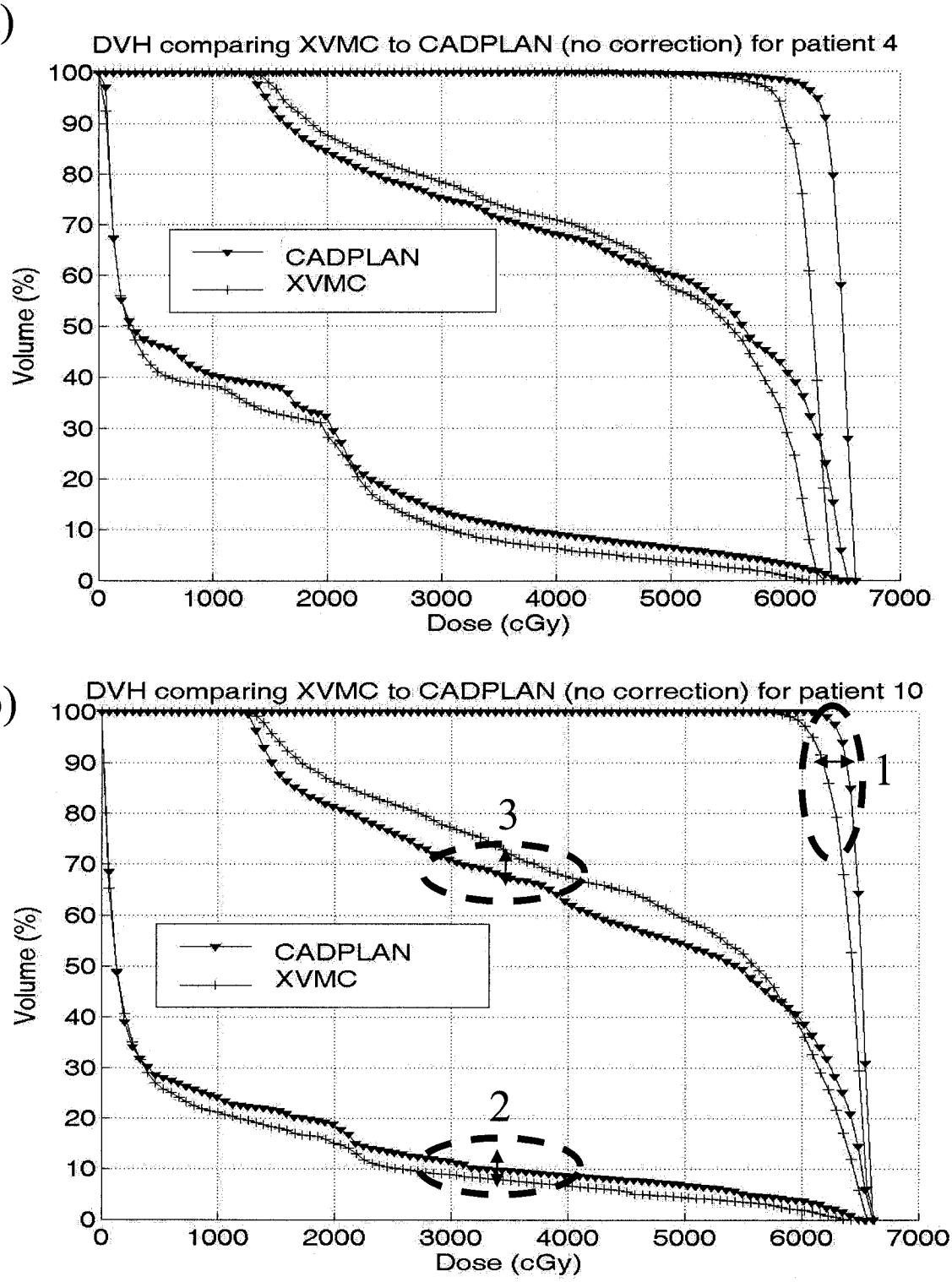

Figure 5.2: DVHs comparing CADPLAN original calculations without heterogeneity correction (triangles) to XVMC recalculations (plus signs) for (1) the PTV, (2) the bladder and (3) the rectum. (a) patient 4 (worst case) and (b) patient 10 (typical case).

One way to read DVHs is to quote the percentage dose difference received by a certain percentage of the volume of interest as seen already in equation 3.4 (*dose-difference method*). Another way is to quote, for a given organ, the difference in percentage volume receiving a certain percentage of the prescribed dose (PD) (*volume-difference method*). DVH comparisons are herein conducted using either method depending on whether the region of interest has steep or shallow dose gradients. Steep dose gradient regions (region 1, Figure 5.2.b) are compared based on the dose-difference method. In such regions, very large volume differences would result from even relatively small dose differences and lead to wrong assessments of calculation accuracies. On the other hand, the dose-difference method is too sensitive in shallow dose gradient regions (regions 2-3, Figure 5.2.b), where the usefulness of the volume-difference method is the strongest.

PTVs are typically compared using the dose-difference method while OAR rely on the volume-difference method. This analysis technique is similar to the composite analysis of Harms *et al* [4,5] based on the simultaneous use of a dose-difference and a distance-to-agreement method. Our technique is also based in part on the gamma index used by Low *et al* [10,11] to define dose and distance criteria to determine calculation quality. These methods are used for commissioning TPS based on specific clinical acceptance criteria. On the other hand, we are firstly interested in the magnitudes of dose and volume differences between calculations and secondly in the dosimetric effects of organ variations.

According to CADPLAN calculations on the typical patient 10 (Figure 5.2.b) 95 % of the PTV volume receives a dose of 6330 cGy while XVMC predicts a dose of 6093 cGy. Hence, most of the PTV will be treated to a dose 3.9 % lower than the intended planned dose. Such a cold spot could adversely affect a RT treatment. Figure 5.3.a compares CADPLAN to XVMC for all patients by reporting the percentage difference in dose covering 95 % of the PTV volume ($\triangle D_{95\%PTV}$).

$$\Delta D_{95\%PTV}(\%) = \left[\frac{(D_{95\%PTV})_{CADPLAN}(cGy) - (D_{95\%PTV})_{XVMC}(cGy)}{(D_{95\%PTV})_{XVMC}(cGy)} \right] X\ 100 \qquad (5.2)$$

A positive $\triangle D_{95\%PTV}$ represents a cold spot while a negative value indicates a hot spot with possible health complications. Figure 5.3.a indicates that XVMC almost always predicts cold spots to the PTV when compared to CADPLAN.

Calculations methods are also compared based on the OAR such as bladder and rectum (Figure 5.3.b) using the volume-difference method. To represent a shallow dose gradient region on the OAR DVHs (regions 2-3, Figure 5.2.b) we chose to use the volumes that receive 50 % of the prescribed dose ($\triangle V_{50\%PD}$).

$$\Delta V_{50\%PD}(\%) = \left[\frac{(V_{50\%PD})_{CADPLAN}(cm^3) - (V_{50\%PD})_{XVMC}(cm^3)}{(V_{50\%PD})_{XVMC}(cm^3)} \right] X\ 100 \qquad (5.3)$$

A negative $\triangle V_{50\%PD}$ indicates that for a certain fixed dose, XVMC predicts coverage of a larger volume than CADPLAN, which could be detrimental to sensitive OAR. This seems to occur on the rectum for nearly all patients (Figure 5.3.b) in the shallow dose gradient region (region 3, Figure 5.2.b). Hence the dose lost in the PTV seems to lead to a dose increase in the rectum.

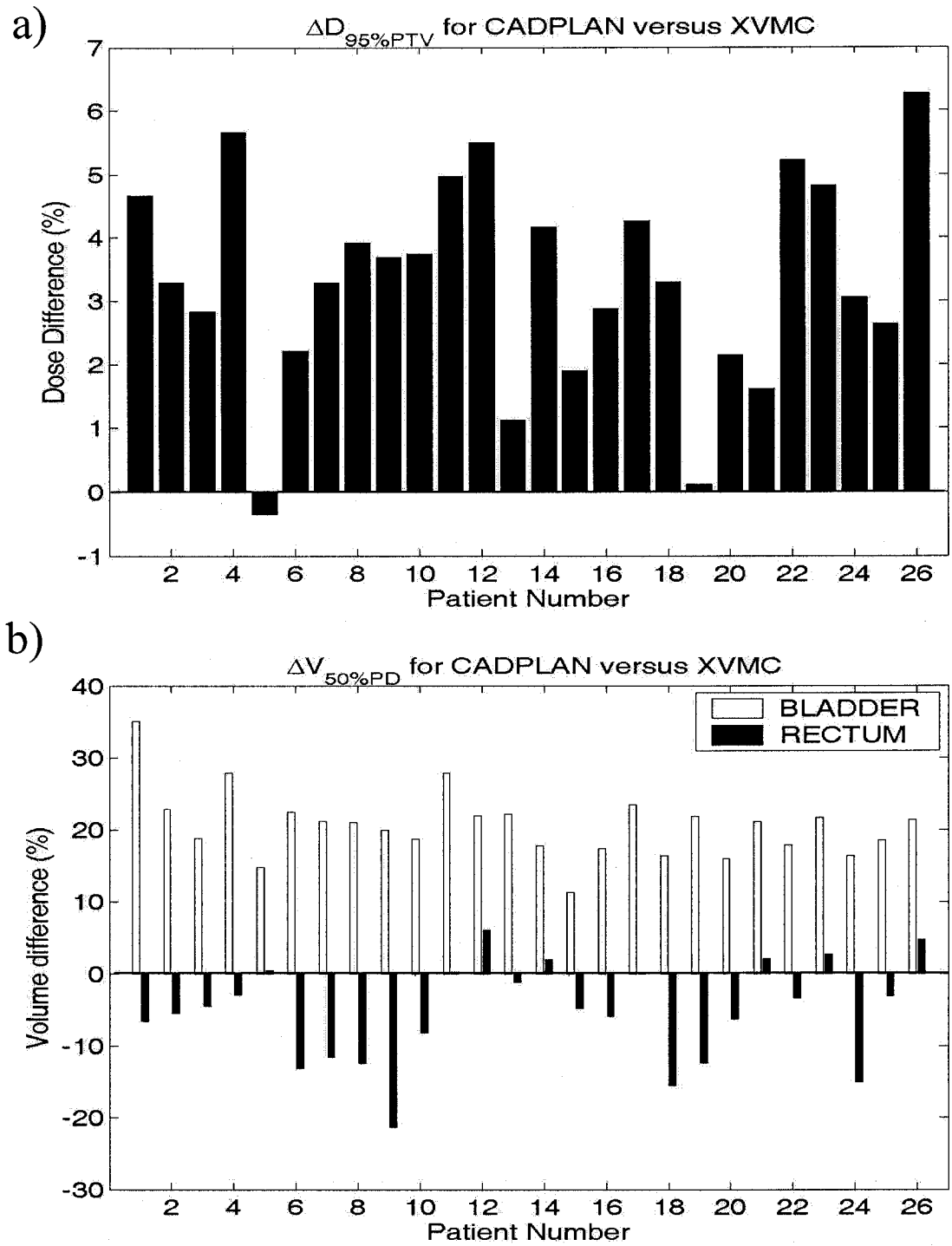

Figure 5.3: Percentage difference of (a) dose covering 95% of the PTV ($\triangle D_{95\%PTV}$) and (b) OAR volumes (bladder and rectum) covered by 50 % of the PD ($\triangle V_{50\%PD}$) for CADPLAN (no heterogeneity correction) versus XVMC. Data is shown for 26 patients.

Table 5.1 compiles the data shown in Figure 5.3 by listing the percentage differences in dose and volume for all patients. On average XVMC seems to predict cold spots of 1.6-5.0 % in dose to 95 % of the PTV when compared to CADPLAN. XVMC also seems to indicate that a dose equal to 50 % of the PD is delivered on average to 15.9-25.3 % less of the bladder volume but to up to 12.2 % more of the rectum. This might indicate less complication to the bladder but possibly more to the rectum, the most radio-sensitive organ of the pelvic region. About 2/3 of patients appear to have an increase of over 2 % in rectal volume (Figure 5.3), the minimum being considered clinically significant [7].

	PTV	Bladder	Rectum
	$\triangle D_{95\%PTV}$ (%)	$\triangle V_{50\%PD}$ (%)	
Mean ± SD	3.3 ± 1.7	20.6 ± 4.7	-5.2 ± 7.0
Range	-0.3 to 6.3	11.3 to 35.1	-21.4 to 6.1

Table 5.1: Statistical analysis of the difference in percentage dose covering 95 % of the PTV and the difference in percentage volume of OAR covered by 50 % of the PD in CADPLAN (no heterogeneity correction) versus XVMC dose calculations. Data for 26 patients.

For prostate RT treatment the couch angle is often set to zero to obtain a coplanar beam arrangement with all beam axes lying in the axial plane. To get the optimum beam orientation to spare normal tissues, the beams can be made to lie in different planes in a non-coplanar arrangement. Price *et al* [14] have found an approximate 30 % increase in dose to the femurs when comparing non-coplanar to coplanar plans. They concluded that beam attenuation in bony structures is more important in non-coplanar plans. Yang *et al* [16] compared TP calculated using MC and the Corvus commercial inverse TPS (Nomos Corp., PA) on 30 prostate patients treated with IMRT. For coplanar cases, they reported an average difference of less than 2 % on the dose received by 98 % of the CTV. They quote this difference as clinically insignificant and not improved by the use of heterogeneity correction in Corvus. For non-coplanar plans, Yang *et al* found dose

differences of up to 9 % when no heterogeneity correction is applied. When heterogeneity correction is used, the differences are seen to be reduced significantly. Their explanation lies in the attenuation of the non-coplanar beams passing thought the femoral heads (4 out of 7 beams for some patients). All patients considered in our study were treated with a co-planar arrangement (Figure 1.1). However, the particularity of the 5 beams used at the MGH is that 4 of them pass through the femurs, hence suffering excessive attenuation by bony structures, much like in the non-coplanar cases described above. Hence, the results we obtain on the PTV (average of 3.3 % $D_{95\%PTV}$) are comparable to, although not as bad as, the non-coplanar arrangements Yang *et al* quote (maximum of 9 % $D_{98\%CTV}$). On a more general note, our results for the PTV appear slightly better than the dose differences larger than 5 % found in other studies in the presence of heterogeneities between MC and analytical calculations of commercial systems [12,13].

5.1.2 CADPLAN with heterogeneity correction

This section analyzes the recalculated CADPLAN dose distributions for all patients including the different heterogeneity correction factors available in CADPLAN. Figure 5.4 compares these CADPLAN corrections to original CADPLAN calculations and to XVMC for a sample patient. Based on the 95 % isodose line, XVMC (Figure 5.4.a) seems to indicate the lateral scatter in the rectum and the attenuation in the femurs. This is not found in the original CADPLAN isodose line (Figure 5.4.b). The Batho Power Law method (Figure 5.4.c) and the Modified Batho Power Law method (Figure 5.4.e) give similar results to the case when no correction is used. The Batho methods are known not to model longitudinal or lateral electron transport in large heterogeneities [8]. On the other hand, the Equivalent Tissue-Air ratio method (ETAR) takes into account lateral scatter [9]. For small heterogeneities, the ETAR method has been found by Du Plessis *et al* [2] to be more accurate than the Batho methods. Our results seem to agree in that the ETAR method (Figure 5.4.d) approximates XVMC results by exaggerating the attenuation in the femoral bones of this patient. The ETAR correction factor hence seems to predict, like XVMC, cold spots in the PTV volume.

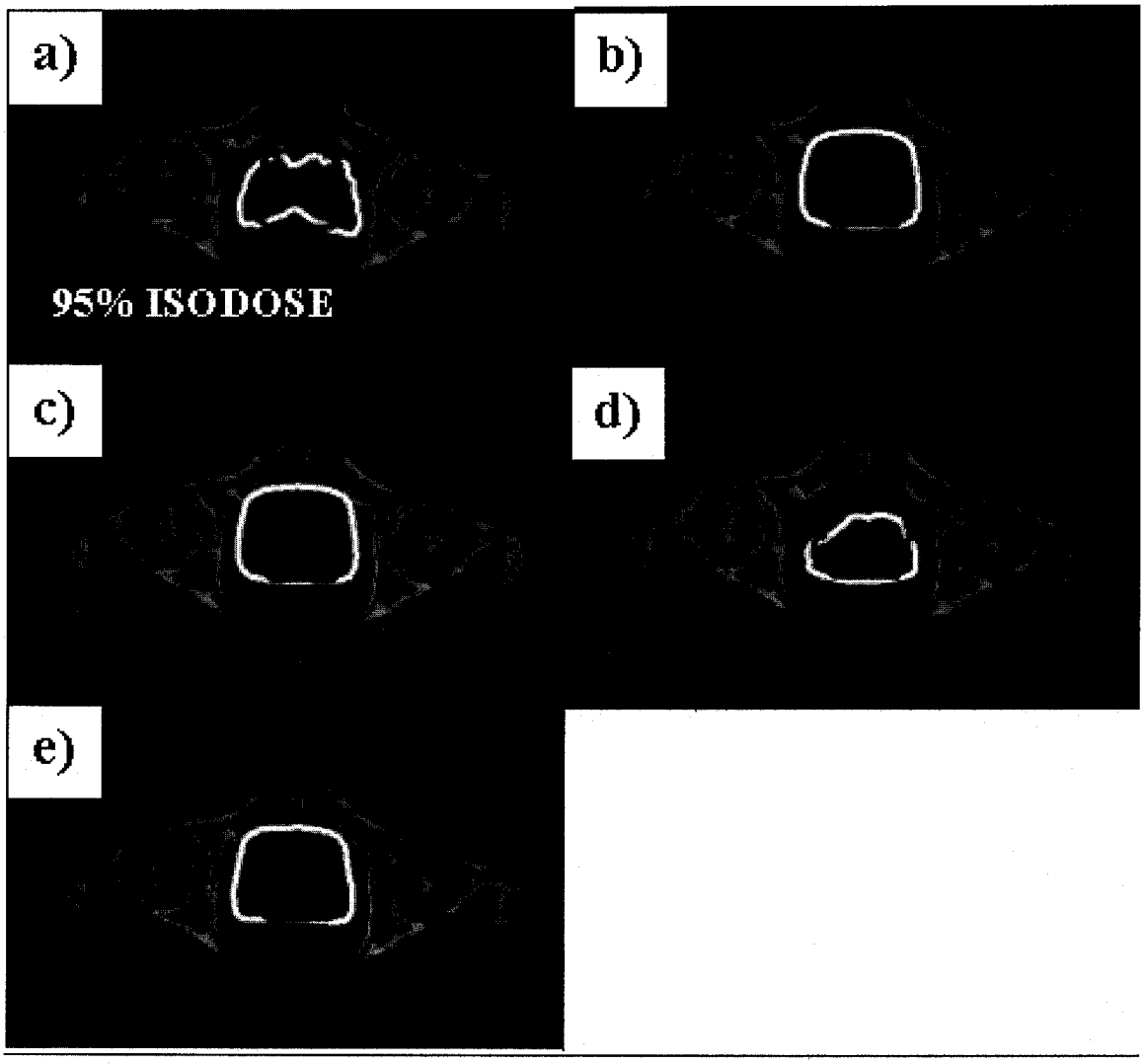

Figure 5.4: Comparison of the 95 % isodose line (white) covering the PTV (black) for patient 7 from: (a) XVMC, (b) CADPLAN without heterogeneity corrections, (c) CADPLAN with Batho Power Law, (d) CADPLAN with ETAR and (e) CADPLAN with Modified Batho Power Law.

Figure 5.5 shows for the same patient the corresponding DVHs obtained in MMCTP. Clearly, the PTV coverage with ETAR (circles) gets closer to XVMC (plus signs) than any other CADPLAN calculation. On the other hand, none of the CADPLAN correction factors seem to improve the dose calculations in the OAR.

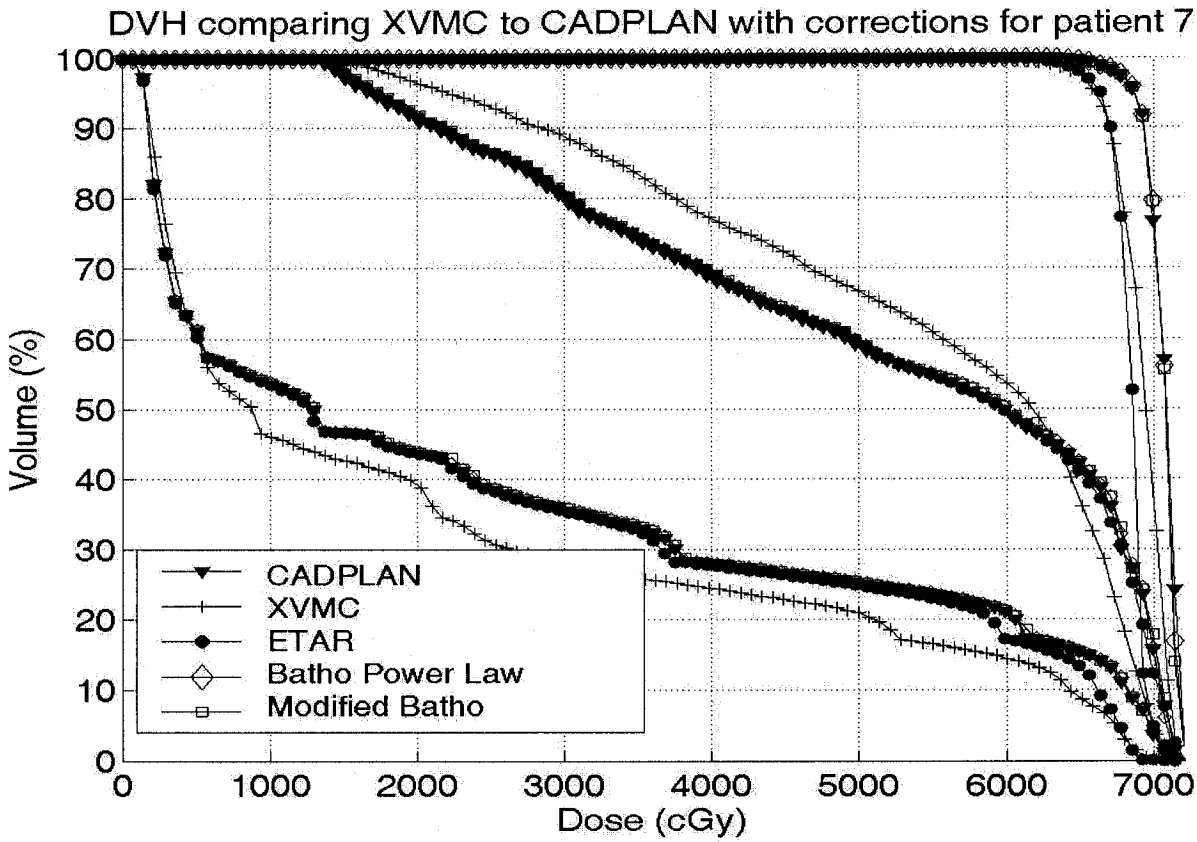

Figure 5.5: DVHs calculated in MMCTP of the PTV, the bladder and the rectum for patient 7, comparing the CADPLAN correction factors to XVMC recalculations.

Table 5.2.a lists the PTV and OAR dose and volume differences, respectively, for this patient. XVMC is seen (as in Table 5.1) to reduce the bladder volume and increase the rectum volume receiving 50 % of the PD. Amongst all CADPLAN corrections, ETAR appears to give the best approximation to XVMC on the dose to 95 % of the PTV. None of the correction factors significant affect bladder or rectum results.

a)		PTV	Bladder	Rectum
		$D_{95\%PTV}$ (cGy)	$V_{50\%PD}$ (cm^3)	
XVMC		6599	94.6	83.8
CADPLAN	No corrections	6867	119.8	74.5
	Batho Power Law	6868	120.6	75.1
	ETAR	6635	115.6	75.1
	Modified Batho	6866	120.7	75.1

b)		PTV	Bladder	Rectum
		$\triangle D_{95\%PTV}$ (%)	$\triangle V_{50\%PD}$ (%)	
XVMC versus CADPLAN	No corrections	4.1	26.7	-11.0
	Batho Power Law	4.1	27.6	-10.3
	ETAR	0.6	22.3	-10.4
	Modified Batho	4.0	27.6	-10.4

Table 5.2: (a) Dose received by 95 % of the PTV and OAR volumes covered by 50 % of the PD (5000 cGy) in CADPLAN including heterogeneity corrections. (b) Percentage difference in dose and volume. Data shown for patient 7.

Table 5.2.b gives for this patient the accuracy of CADPLAN corrections with respect to XVMC, as calculated from:

$$\Delta D_{95\%PTV}(\%) = \left[\frac{(D_{95\%PTV})_{CORR}(cGy) - (D_{95\%PTV})_{XVMC}(cGy)}{(D_{95\%PTV})_{XVMC}(cGy)} \right] X100 \qquad (5.4)$$

$$\Delta V_{50\%PD}(\%) = \left[\frac{(V_{50\%PD})_{CORR}(cm^3) - (V_{50\%PD})_{XVMC}(cm^3)}{(V_{50\%PD})_{XVMC}(cm^3)} \right] X\ 100 \qquad (5.5)$$

Where $(D_{95\%PTV})_{CORR}$ and $(V_{50\%PD})_{CORR}$ stand for the correction factor being considered. For patient 7, the cold spot given by XVMC on the PTV is around 4 % when compared to CADPLAN calculations, except with ETAR where the cold spot is less than 1 %.

Table 5.3 and Figure 5.6 compile the results for 20 patients on which heterogeneity corrections have been applied in CADPLAN dose recalculations. For about ¼ of the patients, using ETAR might get the dose on the PTV closer to that predicted by XVMC (Figure 5.6.a).

XVMC versus		PTV	Bladder	Rectum
		$\triangle D_{95\%PTV}$ (%)	$\triangle V_{50\%PD}$ (%)	
CAD Batho Power Law	Mean ± SD (%)	3.4 ± 1.9	27.4 ± 9.2	-5.1 ± 6.2
	Range (%)	-0.6 to 6.4	12.9 to 53.7	-17.2 to 6.5
CAD ETAR	Mean ± SD (%)	2.9 ± 2.3	27.4 ± 9.7	-4.6 ± 6.1
	Range (%)	-1.2 to 6.6	12.4 to 54.1	-16.3 to 6.5
CAD Modified Batho	Mean ± SD (%)	3.5 ± 2.0	27.7 ± 9.4	-5.0 ± 6.3
	Range (%)	-1.1 to 6.6	13.0 to 53.7	-17.5 to 6.5

Table 5.3: Statistical analysis of the difference in percentage dose and volume of PTV and OAR in CADPLAN (with heterogeneity correction) versus XVMC recalculations. Data for 20 patients.

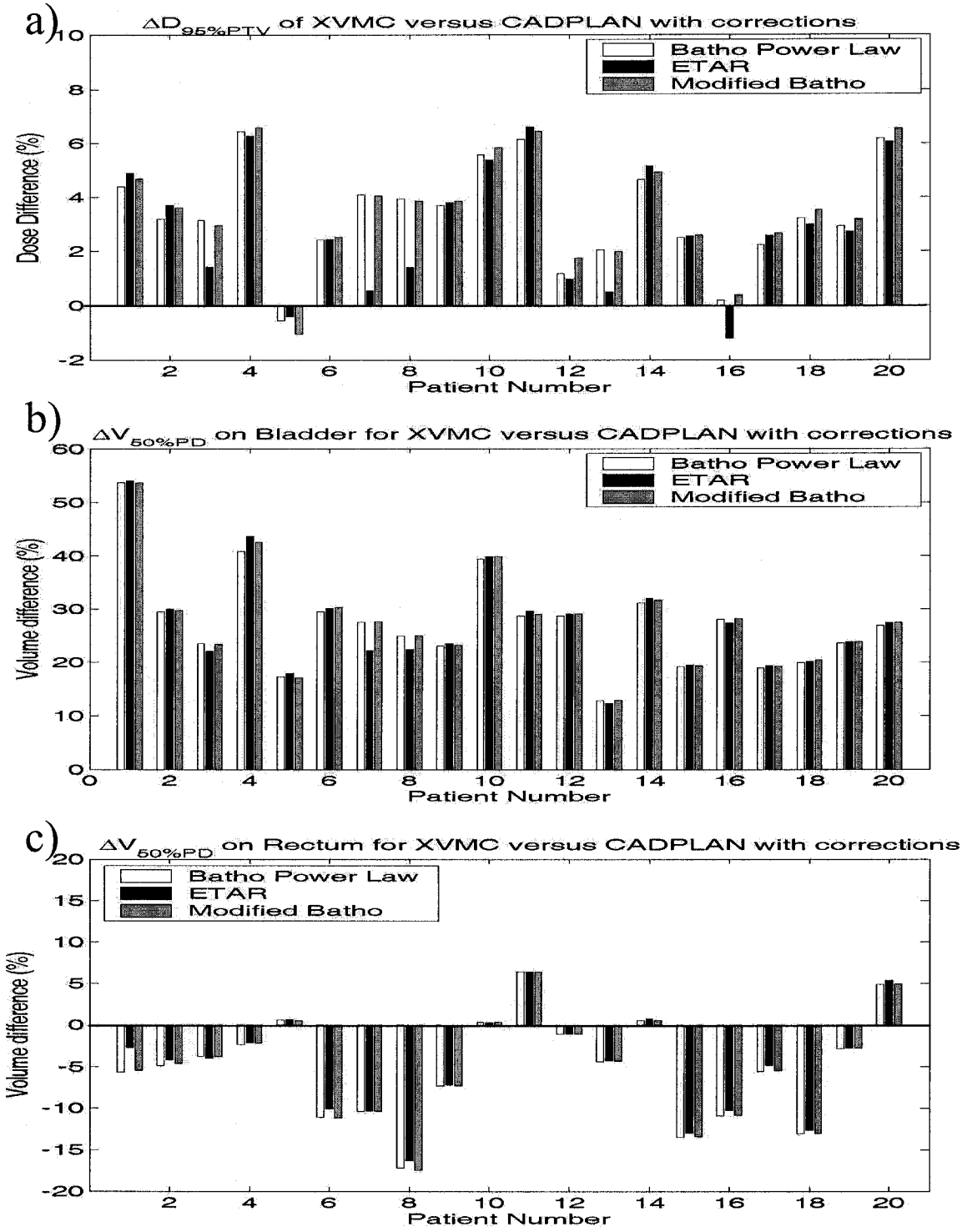

Figure 5.6: Comparison of the (a) percentage of dose difference covering 95 % of the PTV volume for CADPLAN (with heterogeneity corrections) versus XVMC and the percentage volume difference of bladder (b) and rectum (c) covered by 50 % of the prescription dose. Data shown for 20 patients.

On this pool of patients, when compared to original CADPLAN calculations (Table 5.3), XVMC predicts 17.7-37.1 % less of the bladder volume will receive 50 % of the PD, leading to less complication. On the contrary, XVMC predicts this dose will be delivered to up to 11.3 % more of the rectum. This is considered clinically significant for half of the patients, as they have an increase in rectal volume of over 2 % [7]. Such hot spots on the rectum could adversely affect a RT treatment.

When comparing PTV coverage, $\triangle D_{95\%PTV}$ is seen to be 1.5-5.5 %. This is similar to original CADPLAN calculations without heterogeneity correction (Table 5.1). ETAR appears to be the only method to slightly better approximate XVMC, with an average $\triangle D_{95\%PTV}$ of 0.6-5.2 %. Out of 20 patients, around 16 patients with either Batho method have dose differences larger than 2 % to 95 % of the PTV. With ETAR, there are 13 patients with such differences, but 9 are now in better agreements with XVMC. Following the discussion in section 5.1.1.1 on the work by Yang *et al* [16], our results seem to indicate an important attenuation by bony structures in the co-planar beams used at the MGH for prostate cancer. This seems to imply the need to use MC simulations to get accurate dosimetry.

5.1.3 Conclusion

Comparing recalculations in XVMC and CADPLAN with heterogeneity corrections, MC seems to be the only technique that accurately models attenuation and scatter in prostate patient heterogeneities. Our results tend to agree with the significant errors reported previously by our research team in CADPLAN [1,6,15]. The analytical technique seems to approximate MC only slightly better on the PTV if it takes into account lateral scatter using the ETAR method.

When compared to original CADPLAN calculations, XVMC predicts cold spots to the PTV for most patients and hot spots to the rectum for half of them. Hence, as simulations become faster there will be a need to integrate MC as a clinical TPS. Section 5.2 investigates two patient MC modeling tools, XVMC and DOSXYZ.

5.2 XVMC versus DOSXYZ

XVMC and DOSXYZ calculation accuracies are compared for patient 4, chosen because it is the worst case patient based on the differences found between XVMC and CADPLAN (section 5.1.1).

5.2.1 CT density and materials

XVMC and DOSXYZ are used to simulate the patient geometry obtained from a conversion of CT number to electron density and mass density material based on a piecewise linear ramp. Figure 5.7 shows the DVHs for this patient, where the coverage on all organs seem to agree between XVMC (dots) and DOSXYZ (crosses). On this patient, XVMC appears to be a good approximation to DOSXYZ. Note that the latter predicts even greater cold spots to the PTV when compared to CADPLAN.

Table 5.4 gives the dose and volume percentage differences between the MC methods. XVMC for this patient agrees with DOSXYZ to within 1 % on both $D_{95\%PTV}$ and $V_{50\%PD}$. This is in agreement with results reported previously on a 3D bone phantom with a 10 MV input, where XVMC and DOSXYZ agreed to within the 1 % statistical uncertainty limited by the number of particles in the phase space file [3].

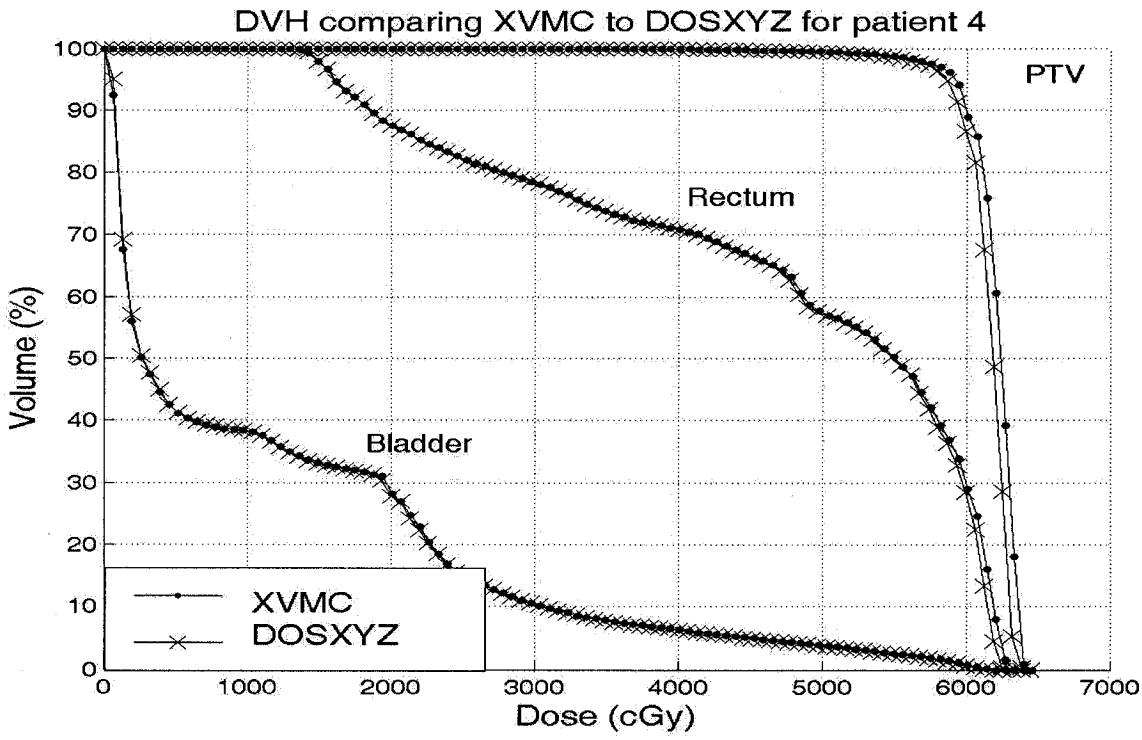

Figure 5.7: DVHs calculated in MMCTP of the PTV, the bladder and the rectum for patient 4, comparing XVMC and DOSXYZ calculations.

a)	PTV	Bladder	Rectum
	$D_{95\%PTV}$ (cGy)	$V_{50\%PD}$ (cm^3)	
XVMC	5918	21.5	52.9
DOSXYZ	5857	21.4	52.8

b)	PTV	Bladder	Rectum
	$\Delta D_{95\%PTV}$ (%)	$\Delta V_{50\%PD}$ (%)	
$\frac{XVMC - DOSXYZ}{DOSXYZ} X\ 100$	1.0	0.5	0.2

Table 5.4: (a) Doses covered by 95 % of the PTV and volume of OAR receiving 50% of the PD (6600cGy) in XVMC and DOSXYZ. (b) Percentage dose and volume differences between XVMC and DOSXYZ. Data shown for patient 4.

Table 5.5 compares the maximum dose (D_{max}) calculated with either XVMC or DOSXYZ. This patient shows a percentage difference in D_{max} of only 0.3 %.

D_{max} (cGy)	XVMC	DOSXYZ
	6466	6447
$\triangle D_{max}$ (%)	0.3	

Table 5.5: Difference in maximum dose in XVMC versus DOSXYZ for patient 4.

5.2.2 Water density and material

To evaluate the extent to which MC models heterogeneity, XVMC and DOSXYZ are recalculated with every voxel in patient 4 replaced by water material with density 1.0 g/cm^3. This resembles CADPLAN simulations in which patients are assumed to entirely consist of water. In Figure 5.8, both XVMC and DOSXYZ are seen to get closer to CADPLAN PTV curves (plus signs) when they are used on water voxels (empty circles and squares) rather than CT voxels (full circles and squares). The remaining discrepancy might be specific to this patient and be explained by the exactness of the MC MLC geometrical models, scattered photons or inter-leaf leakage.

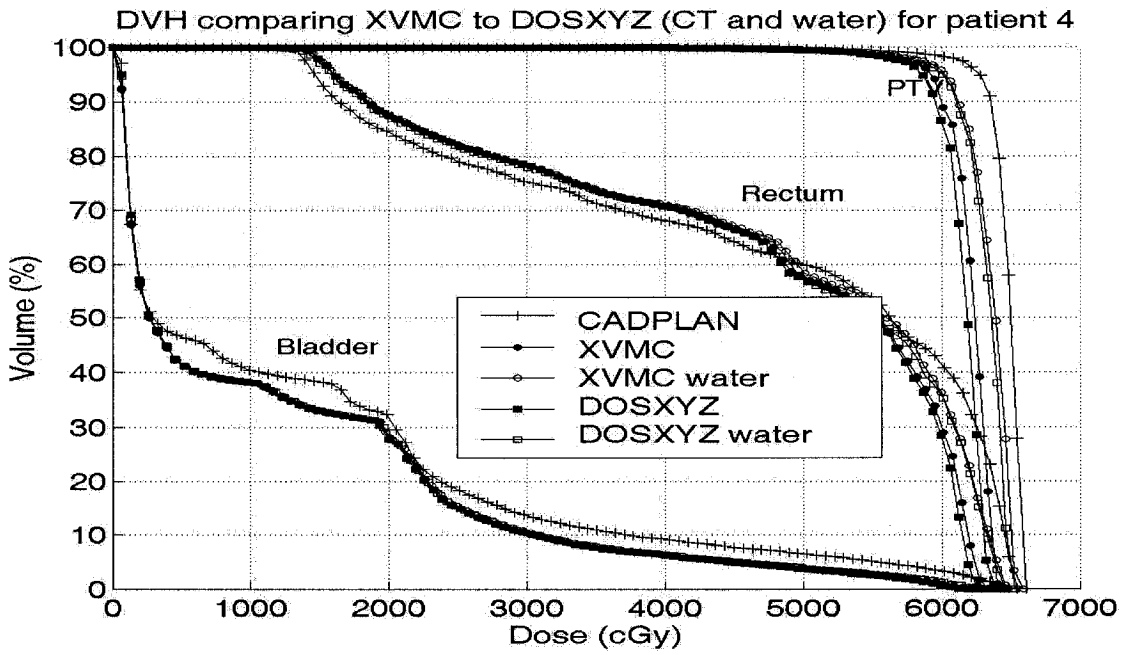

Figure 5.8: DVHs for patient 4 comparing CADPLAN (no heterogeneity correction) to XVMC and DOSXYZ (CT and water voxels).

The numerical values extracted from the DVHs are reported in Table 5.6. a and the percentage difference in dose and volume in Table 5.6. b. The above-mentioned trend is clearly seen; the difference on the PTV between CADPLAN is reduced from 5.7 % to 4.1 % in XVMC and from 6.6 % to 4.3 % in DOSXYZ. The MC dose gets slightly closer to that of CADPLAN on the bladder but no change is seen on the rectum.

On a general note, the accuracy on $\triangle D_{95\%PTV}$ between XVMC and DOSXYZ with water voxels is within 0.5 % (XVMC water = 6020 cGy and DOSXYZ water = 6001 cGy in Table 5.6.a). This agrees with results comparing XVMC and DOSXYZ calculations previously reported on a 3D water phantom [3].

a)	PTV	Bladder	Rectum
	$D_{95\%PTV}$ (cGy)	$V_{50\%PD}$ (cm^3)	
CADPLAN	6274	29.9	51.5
XVMC	5918	21.5	52.9
XVMC water	6020	22.2	53.1
DOSXYZ	5857	21.4	52.8
DOSXYZ water	6001	21.8	52.9

b)	PTV	Bladder	Rectum
CADPLAN versus	$\triangle D_{95\%PTV}$ (%)	$\triangle V_{50\%PD}$ (%)	
XVMC	5.7	27.9	-2.8
XVMC water	4.1	25.7	-3.0
DOSXYZ	6.6	28.2	-2.6
DOSXYZ water	4.3	26.9	-2.7

Table 5.6: (a) Dose to 95 % of the PTV and OAR volumes covered by 50 % of the PD (6600 cGy) in CADPLAN, XVMC and DOSXYZ (CT and water). (b) Percentage dose and volume differences between CADPLAN and MC. Data for patient 4.

The maximum dose is also a good comparison ground (Table 5.7). Using water voxels in MC simulations brings the MC maximum dose closer to that in CADPLAN; from 2.2 % to 0.3 % in XVMC and from 2.5 % to 1.3 % in DOSXYZ.

D_{max} (cGy)	CADPLAN	XVMC	XVMC water	DOSXYZ	DOSXYZ water
	6613	6466	6591	6447	6531
$\triangle D_{max}$ (%) vs CADPLAN		2.2	0.3	2.5	1.3

Table 5.7: Percentage difference in maximum planned dose ($\triangle D_{max}$) in CADPLAN versus XVMC and DOSXYZ (CT and water) for patient 4.

5.2.3 Conclusion

On the patient with the largest discrepancy between XVMC and CADPLAN, the simplifications used in XVMC compared to DOSXYZ do not seem to significantly affect calculation accuracies. When comparing the two MC codes on the CT patient geometry, DOSXYZ and XVMC are within 1 % on the dose to 95 % of the PTV and within 0.3 % on the maximum dose.

References

[1] Doucet R., Olivares M., DeBlois F., Podgorsak E.B., Kawrakow I. and Seuntjens J. "Comparison of measured and Monte Carlo calculated dose distributions in inhomogeneous phantoms in clinical electron beams". Phys. Med. Biol., 48, pp. 2339-2354, 2003.

[2] Du Plessis F.C.P., Willemse C.A. and Lotter M.G. "Comparison of the Batho, and Monte Carlo dose calculation methods in CT based patient models". Med. Phys., 28 (4), pp. 582-589, 2001.

[3] Fippel M. "Fast Monte Carlo dose calculation for photon beams based on the VMC electron algorithm". Med. Phys., 26 (8), pp. 1466-1475, 1999.

[4] Harms W.B., Low D.A., Purdy J.A. and Wong J.W. "A quantitative software analysis tool for verifying 3D dose-calculation programs". Int. J. Radiat. Oncol. Biol. Phys., 30, pp.187, 1994.

[5] Harms W.B., Low D.A, Purdy J.A. and Wong J.W. "A software tool to quantitatively evaluate 3D dose calculation algorithms", Med. Phys. 25 (10), pp. 1830-1836, 1998.

[6] Heath E., Parker W., Curran B. and Seuntjens J.P. "Clinical Evaluation of the PEREGRINE Monte Carlo Dose Calculation System for 6MV photon Beams". World Congress on Medical Physics, Sydney, Australia, August 24-29, [paper No. 1800], 2003.

[7] ICRU "Determination of absorbed dose in patient irradiated by beams of X or gamma rays in radiotherapy procedure". International Commission on Radiation Units and Measurements, 1976, Report #24, Washington, D.C.

[8] Jones A.O. and Das I.J. "Comparison of inhomogeneity correction algorithmg in small photon fields". Med. Phys. 32 (3), pp. 766-776, 2005.

[9] Kappas C. and Rosenwald J.-C. "Quality control in inhomogeneity corrections algorithms used in treatment planning systems". Int. J. Radiat. Oncol. Biol. Phys., 32 (3), pp. 854-858, 1995.

[10] Low D.A, Harms W.B., Mutic S. and Purdy J.A. "A technique for the quantitative evaluation of dose distribtutions", Med. Phys, 25 (5), pp. 656-661, 1998.

[11] Low D.A. and Dempsey J.F. "Evaluation of the gamma dose distribution comparison method", Med. Phys. 30 (9), pp. 2455-2464, 2003.

[12] Ma C.-M., Mok E., Kapur A., Pawlicki T.A, Findley D., Brain S., Forster K. and Boyer A. "Clinical Implementation of a Monte Carlo treatment planning system", Med. Phys. 26, pp. 2133-2143, 1999.

[13] Mohan R. "Why Monte Carlo ?". Proc. 12th Int. Conf. on the Use of Computers in Radiation Therapy. Salt Lake city, UT. pp. 16-18, 1997.

[14] Price R.A., Hanks G.E., McNeeley S.W., Horwitz E.M. and Pinover W.H. "Advantages of using noncoplanar versus axial beam arrangements when treating prostate cancer with intensity-modulated radiation therapy and the step-and-shoot delivery method". Int. J. Radiat. Oncol. Biol. Phys., 53 (1), pp. 236-243, 2002.

[15] Seco J., Verhaegen F. and Bidmead M. "Development and commissioning of a Monte Carlo dose calculation engine for clinical IMRT beams". World congress on Medical Physics, Sydney Australia, August 24-29, 2003.

[16] Yang J., Li J., Chen L, Price R., McNeeley S., Qin L., Wang L, Xiong W. and Ma C.-M. "Dosimetric verification of IMRT treatment planning using Monte Carlo simulations for prostate cancer", Phys. Med. Biol., 50, pp. 869-978, 2005.

Chapter 6: Results and discussion
Introducing ultrasound information

To assess changes in dose coverage due to prostate motion, Falco *et al* [3] included daily BAT shifts into a TPS for 4 prostate patients. Prostate displacement was found to adversely affect dosimetric coverage, justifying the use of a US system to reposition patients during RT. Following this train of thought, we incorporate BAT and RES daily displacements into MMCTP to quantify and compare their dosimetric impact. Section 6.1.1 covers CADPLAN results while section 6.1.2 deals with XVMC results. These calculations assume fixed prostate volumes as defined on CT-scans. Actual prostate volumes derived from US data are later introduced in section 6.2.

6.1 Introducing positional variations

6.1.1 CADPLAN

The PTV is chosen for the dose-volume comparison. Patient 8, presented as an example in Figure 6.1, is one of the patients affected the most by uncorrected prostate shifts. The DVH curves shown represent different beam and prostate arrangements as described in Table 3. 1.

DVH_2 is the ideal situation where the prostate is positioned correctly with respect to the treatment isocenter at every fraction. MMCTP calculates this DVH by keeping the PTV contour in this ideal position. DVH_3 and DVH_4 is when the beams in XVMC are shifted from the isocenter at every fraction according to the US BAT or RES data, respectively. However, MMCTP calculates the DVHs still keeping the ideal PTV prostate position. As such, these cases represent the dose coverage if no repositioning is performed by technicians. We call these results *Uncorrected BAT* and *Uncorrected RES*. DVH_5 is called *Corrected BAT with BAT*, where BAT shifts are used both in XVMC, to shift the beams, and in MMCTP, to move the PTV back under the beams. DVH_6 is called *Corrected BAT with RES*, where BAT shifts are applied in XVMC and then corrected by

RES shifts in MMCTP. According to the conclusion that RES is more accurate than BAT for prostate alignment [1], DVH_6 represents the real clinical scenario. At present BAT shifts are used for patient repositioning while the prostate actually moves by the RES measured displacements. DVH_7 is the *Corrected RES with RES* case, using RES data in both XVMC and MMCTP.

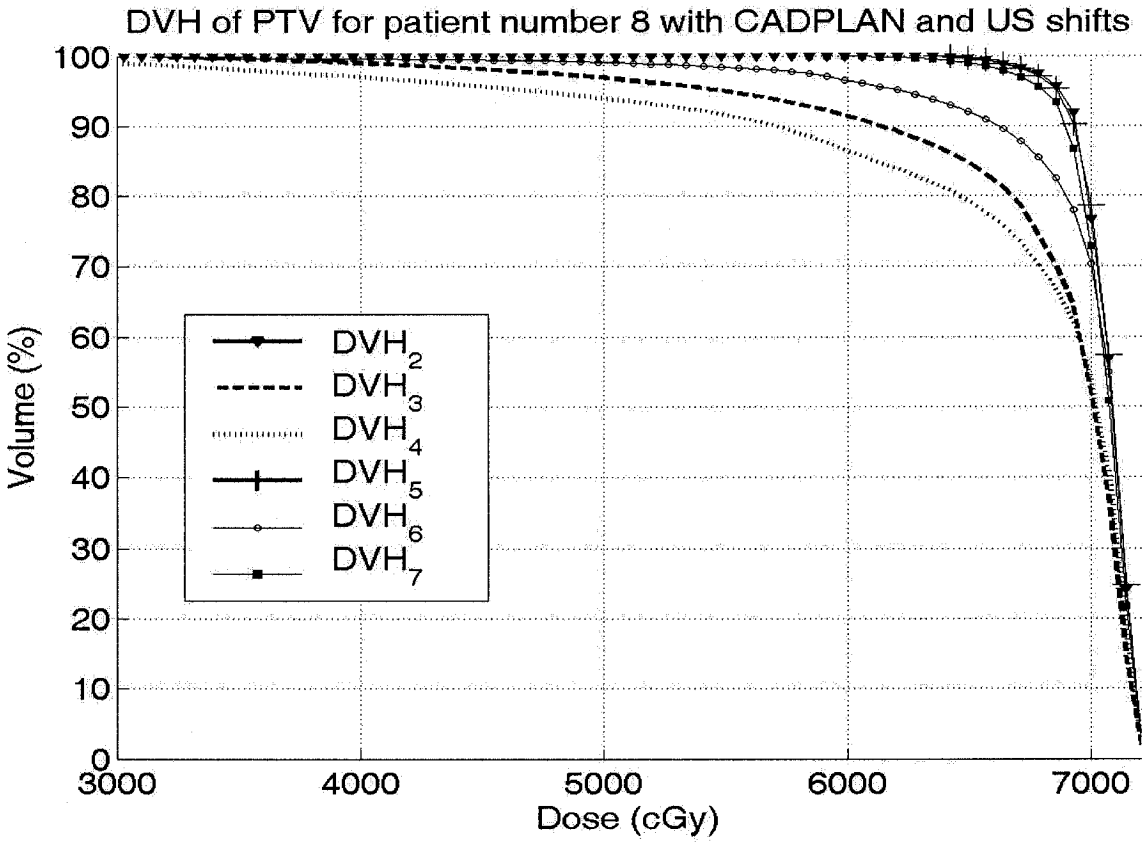

Figure 6.1: US shifts in CADPLAN for patient 8 (worst case): Ideal position (DVH_2), Uncorrected BAT (DVH_3) and RES (DVH_4), Corrected BAT with BAT (DVH_5), Corrected BAT with RES (DVH_6) and Corrected RES with RES (DVH_7).

From Figure 6.1, a prostate that undergoes displacement from its intended treatment position (DVH_3 as measured by BAT or DVH_4 by RES) seems to be treated to a much smaller dose than the ideal fixed prostate (DVH_2). Such major cold spots could have a deleterious impact on the expected local control. Hence, shifting a patient each day to follow prostate motion based on US measurements (DVH_5, DVH_6 or DVH_7) is likely to improve treatment outcome as well as spare normal tissues. This was evaluated by Orton

et al in 2004 [4] on 5 patients treated with IMRT plans with 7 evenly spaced beams. They used an optically guided 3D US localization system to shift patients, resulting in nearly identical dose to the target as in the ideal planned case. They also found that if no shifts were made, the dose distributions were degraded. To analyze potential impact on tumor control Orton *et al* calculated Equivalent-Uniform-Doses (EUD) and Tumor-Control-Probability (TCP) for all patients. Both were found to be degraded when no patient repositioning was made; EUD by 5% and TCP by 7%. The authors mentioned that the remaining cold spots could possibly be totally eliminated by periodically readjusting the plan to follow prostate positions based on US data.

From the numerical values extracted for the DVHs of patient 8 (Table 6.1), daily repositioning prostate patients appears to be a necessity. If no repositioning is performed, the dose delivered to 95 % of the PTV is 20-31 % lower than planned while if it is, the dose is within 1-10 % of the prescribed value. For this patient, using the BAT system alone for repositioning reduces the error on the PTV dose from 20 % to 0.2 %. However, since RES is believed to be more accurate than BAT, true prostate motion is given by the RES data. The reduction from BAT repositioning is then really only from 20 % to 10 %. Table 6.1 seems to indicate that using the RES system alone for repositioning could reduce the error from 31 % down to 1.0 % on this worst case patient.

CADPLAN on patient 8		$D_{95\%PTV}$ **(cGy)**	$\triangle D_{95\%PTV}$ **(%)**
Ideal (DVH_2)		6867	-
Uncorrected	**BAT** (DVH_3)	5499	19.9
	RES (DVH_4)	4713	31.4
Corrected	**BAT with BAT** (DVH_5)	6857	0.2
	BAT with RES (DVH_6)	6216	9.5
	RES with RES (DVH_7)	6801	1.0

Table 6.1: Dose and dose difference covering 95 % of the PTV for patient 8 in CADPLAN dose calculations including both sets of US shifts.

Figure 6.2 summarizes for all 26 patients the PTV dose difference when introducing US shifts in CADPLAN compared to the ideal planned dose. It seems that most patients, if not realigned daily, would suffer from an underdosage likely to cause a substantial reduction in tumor control. Table 6.2 lists the statistics for all patients. Uncorrected BAT shifts appear to yield a PTV dose around 9 % lower than planned. The situation is even worse for uncorrected RES shifts; the dose to the prostate is then reduced by almost 20 %. Performing realignment with RES could get the dose to the PTV back to within 1 % of the planned treatment, while currently with the BAT system it is only within 14 %.

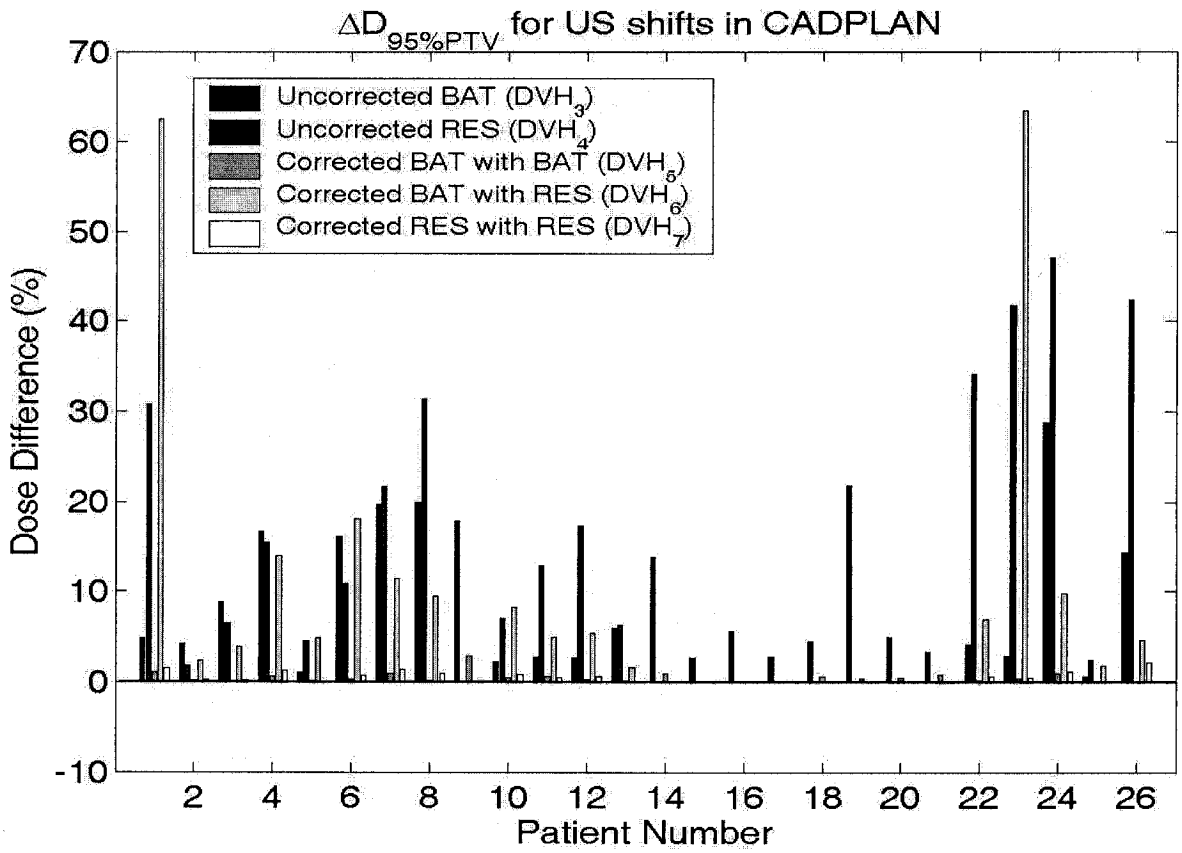

Figure 6.2: Percentage dose to 95 % of the PTV for a series of CADPLAN dose calculations including US shifts. Data is shown for 26 patients.

CADPLAN		$\triangle D_{95\%PTV}$	
		Mean ± SD (%)	Range (%)
Uncorrected	BAT (DVH_3)	9.0 ± 7.9	0.6 to 28.8
	RES (DVH_4) *	19.7 ± 15.3	1.9 to 47.1
Corrected	BAT with BAT (DVH_5)	0.5 ± 0.6	-0.1to 2.9
	BAT with RES (DVH_6) *	13.7 ± 19.0	1.6 to 63.4
	RES with RES (DVH_7) *	0.8 ± 0.6	0.1 to 2.1

Table 6.2: Statistical analysis of the dose and percentage dose difference in PTV in CADPLAN. The data is shown for 26 patients, except cases indicated by (*), where patients without RES shifts were removed from the statistics.

6.1.2 XVMC

To compare the effects of US shifts in CADPLAN and XVMC, patient number 8 is again used as the sample patient in XVMC calculations. Figure 6.3 shows the DVHs obtained with and without positional correction, as described in Table 3. 1. As was the case in CADPLAN (Figure 6.1), XVMC indicates that without daily repositioning (DVH_9 and DVH_{10}) a major cold spot can be seen in the PTV compared to the ideal case (DVH_8). If the patient is shifted back into position using BAT or RES (DVH_{11} and DVH_{13}, respectively) the dose seems to get closer to the ideal case. Once again, a cold spot is seen to remain in the real clinical scenario, *Corrected BAT with RES*, shown by the DVH_{12} curve.

The numerical values extracted for this patient (Table 6.3) seem to indicate that daily repositioning prostate patients is of the utmost importance in RT. XVMC predicts an even worse scenario than CADPLAN, by calculating a PTV dose reduced by 31-39 % without positional correction. On the other hand, if correction is carried out, the dose could be brought back to within 1-10 % of the planned value. Once again, since the true prostate motion is given by the RES data, the reduction actually obtained from BAT repositioning is only from 31 % to 10 % and not 1 %. It appears that using only the RES system could reduce the error from 39 % down to around 1 %.

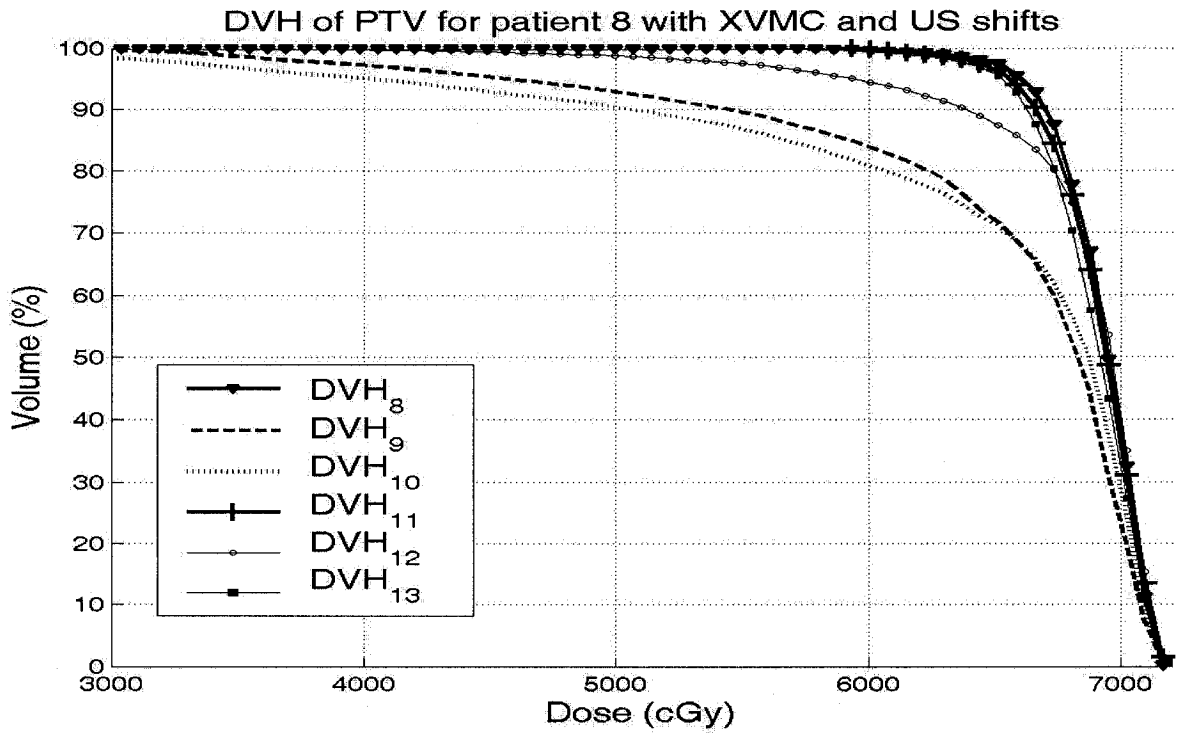

Figure 6.3: US shifts in XVMC for patient 8: Ideal position (DVH_8), Uncorrected BAT (DVH_9) and RES (DVH_{10}), Corrected BAT with BAT (DVH_{11}), Corrected BAT with RES (DVH_{12}) and Corrected RES with RES (DVH_{13}).

XVMC on patient 8		$D_{95\%PTV}$ (cGy)	$\triangle D_{95\%PTV}$ (%)
Ideal (DVH_8)		6599	-
Uncorrected	**BAT** (DVH_9)	4554	31.0
	RES (DVH_{10})	4010	39.2
Corrected	**BAT with BAT** (DVH_{11})	6553	0.7
	BAT with RES (DVH_{12})	5929	10.1
	RES with RES (DVH_{13})	6525	1.1

Table 6.3: Dose and dose difference covering 95 % of the PTV for patient 8 in XVMC dose calculations including US shifts.

Figure 6.4 summarizes the dose difference to the PTV for all patients using XVMC with US shifts and Table 6.4 lists the statistics.

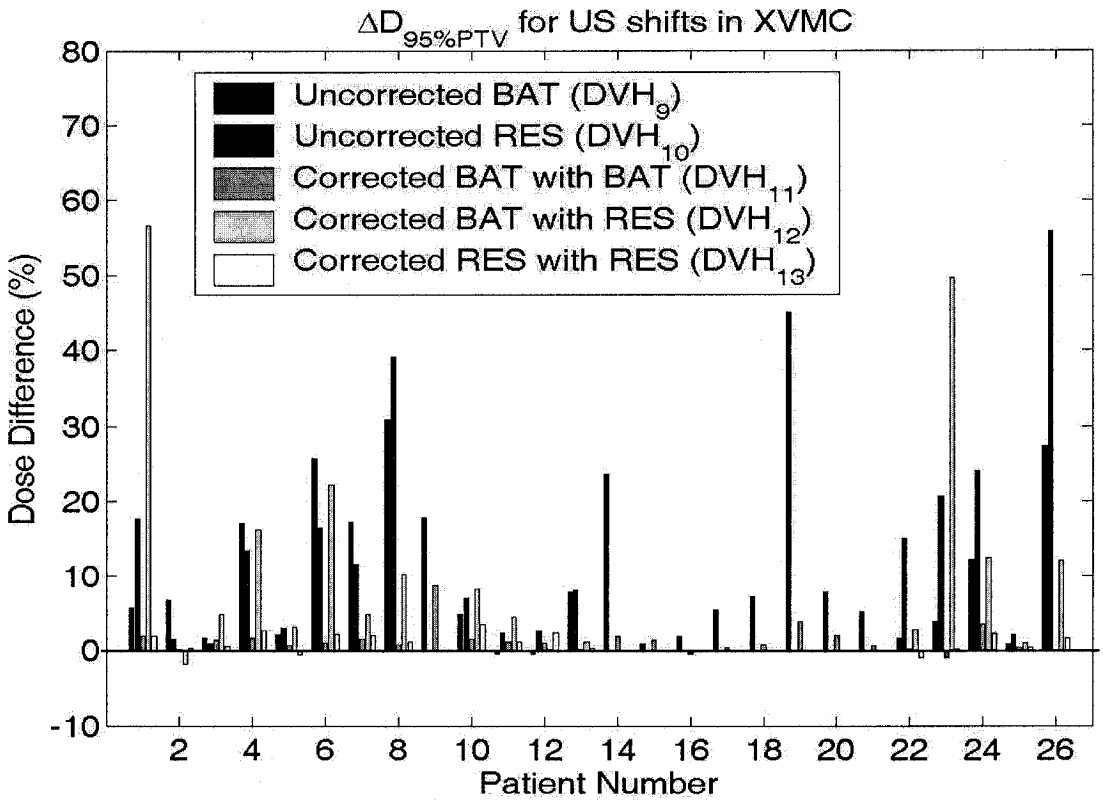

Figure 6.4: Comparison of the percentage dose to 95 % of the PTV for a series of XVMC dose calculations including US shifts. Data shown for 26 patients.

XVMC		$\Delta D_{95\%PTV}$	
		Mean ± SD (%)	**Range (%)**
Uncorrected	**BAT** (DVH_9)	10.8 ± 11.6	-0.5 to 45.0
	RES (DVH_{10}) *	14.2 ± 14.8	0.9 to 55.9
Corrected	**BAT with BAT** (DVH_{11})	1.3 ± 1.8	-0.9 to 8.7
	BAT with RES (DVH_{12})*	12.2 ± 16.7	-1.9 to 56.6
	RES with RES (DVH_{13})*	1.2 ± 1.2	-1.0 to 3.4

Table 6.4: Statistical analysis of the dose and percentage dose difference in PTV in XVMC. The data is shown for 26 patients, except cases indicated by (*), where patients without RES shifts were removed from these statistics.

The situation when no realignment is performed in XVMC is similar to that seen with CADPLAN. If the shifts measured by the BAT system are not corrected for the dose delivered to the PTV falls by 11 % of the planned value (9 % in CADPLAN) while with RES it falls by 14 % (20 % in CADPLAN). Performing realignment with RES could get the PTV dose back to around 1 % of the TP (1 % in CADPLAN) while it is currently 12 % with the BAT system (14 % in CADPLAN).

6.1.3 Conclusion

A US-based system seems to be required to deliver higher radiation doses with less damage to normal organs because prostate inter-fraction movement can adversely affect dosimetric coverage. This conclusion is drawn from 5 beam 3D-CRT plans that have a symmetrical beam arrangement. We hypothesize that prostate motion might affect to a greater extent patients treated with (1) less symmetrical arrangements and (2) IMRT. Because of symmetry, opposing beams in our arrangements largely offset differences in SSD and depth of individual beams. This self-compensating effect might not occur with less symmetrical beam geometries, as mentioned by Orton *et al* [4]. While it is true that 3D-CRT needs high localization accuracy, IMRT which uses steeper dose gradients, is likely to be even more affected by small geometrical misses.

Our results seem to indicate that replacing the clinical BAT system by the RES could improve the dosimetric coverage for prostate patients. Moreover, the cold spots that remain after correcting for patient alignment, due to the new prostate and beam position relative to the patient, could possibly be eliminated by readjusting the plan an optimized number of times. This could account for the US prostate displacements for a few selected fractions throughout the treatment duration. The results should be an improved dosimetry with reduced morbidity to the OAR.

6.2 Introducing volumetric variations

Although no trend is observed in the change of prostate volumes over the course of therapy (section 4.2), the range of volumes in most patients is found to vary by a factor of almost 2. Therefore, to assess changes in dose coverage resulting from such variations, DVHs are calculated in MMCTP by scaling the PTV CT volumes by the US volumes (section 3.3.3.2). For comparison purposes, this is performed on 7 patients with the CADPLAN and XVMC dose calculations, with US shifts, used in section 6.1.

6.2.1 CADPLAN

Figure 6.5 is a typical example on one patient of the effects of PTV volume changes on the DVH in CADPLAN. DVH_2, DVH_6 and DVH_7 are the cases already considered with fixed CT volumes: DVH_2 is the ideal situation, DVH_6 is the *Corrected BAT with RES* and DVH_7 is the *Corrected RES with RES* case.

The new curves in Figure 6.5 are DVH_{14} and DVH_{15}, the *Corrected BAT with RES + V* and the *Corrected RES with RES + V*, respectively. These take the varying fractional volumes into account. The result closest to reality is the one given by DVH_{14}, where the prostate moves and varies in volume as measured by RES but repositioning is performed with BAT.

Table 6.5 reports the values for this typical patient. These seem to indicate that if the BAT system were replaced with the RES, the dosimetric impact of prostate variation might be reduced by half, from 26 % to 13 %.

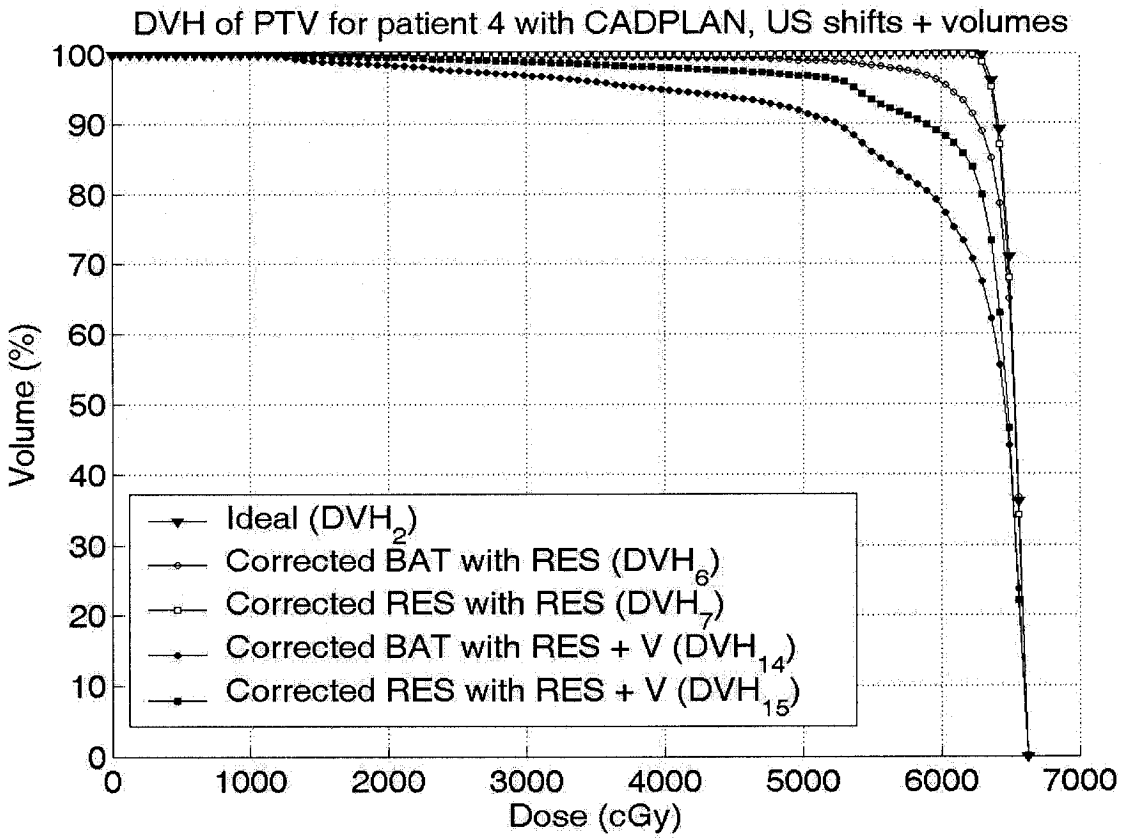

Figure 6.5: US shifts and volumes in CADPLAN for patient 4: Ideal position (DVH_2), Corrected BAT with RES (DVH_6), Corrected RES with RES (DVH_7), Corrected BAT with RES + V (DVH_{14}) and Corrected RES with RES + V (DVH_{15}).

CADPLAN on patient 4		$D_{95\%PTV}$ (cGy)	$\triangle D_{95\%PTV}$ (%)
Ideal (DVH_2)		6372	-
Corrected	**BAT with RES** (DVH_6)	6061	4.9
	RES with RES (DVH_7)	6363	0.1
Corrected (+ US volumes)	**BAT with RES** (DVH_{14})	4722	25.9
	RES with RES (DVH_{15})	5531	13.2

Table 6.5: Dose and dose difference covering 95 % of the PTV for patient 4 in CADPLAN calculations including US shifts and volumes.

Figure 6.6 and Table 6.6 summarize the effects of volume variations for all patients. The values displayed for DVH_6 and DVH_7 differ from the values in Table 6.2 because the number of patients in the statistics is now 7 rather than 26. Currently in the clinic, the 7 % degradation believed to remain in the dose covering most of the PTV (DVH_6) is in reality 17 % (DVH_{14}) due to changes in volume. This situation might be improved to 8 % by using only the RES system. This remaining degradation is due to different patient and beam positions as well as prostate volume. Replanning patients periodically using not only the US shifts but also the varying prostate volume could improve the dosimetry further.

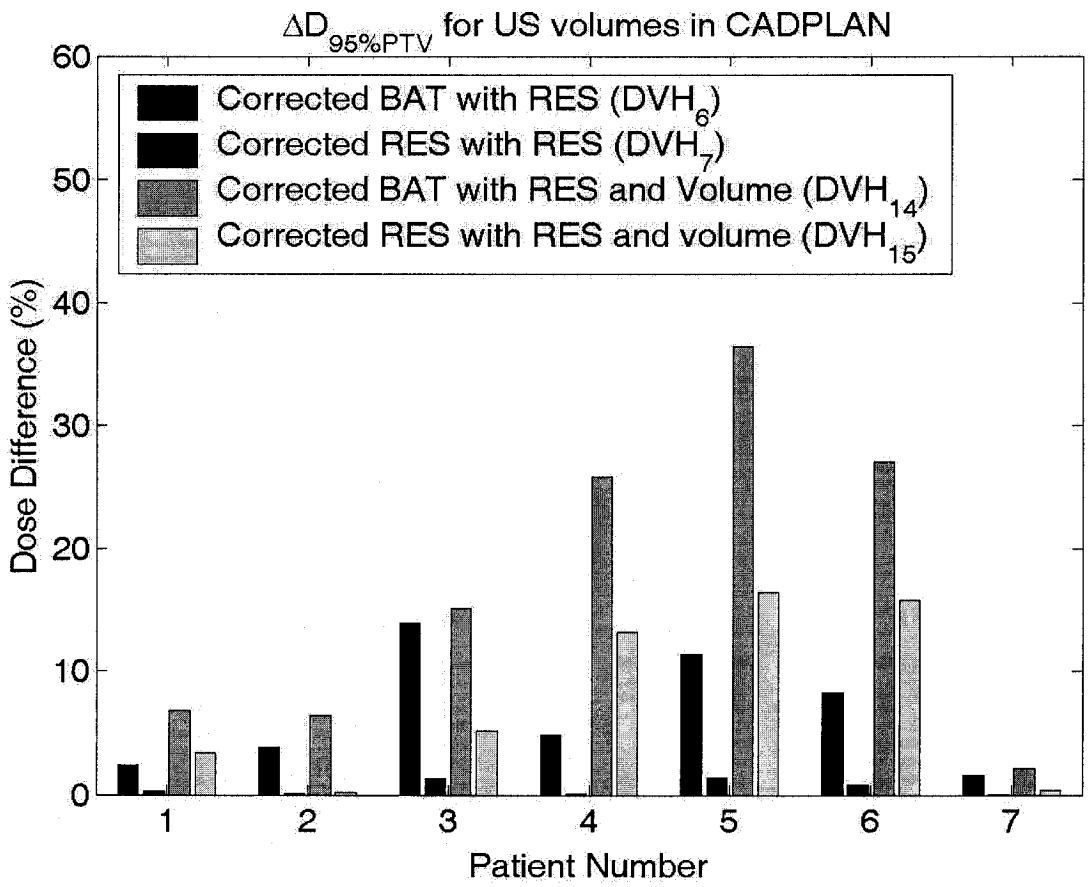

Figure 6.6: Percentage dose to 95 % of the PTV for a series of CADPLAN dose calculations including US shifts and volumes.

CADPLAN		$\triangle D_{95\%PTV}$	
		Mean ± SD (%)	**Range** (%)
Corrected	**BAT with RES** (DVH_6)	6.6 ± 4.7	1.6 to 13.9
	RES with RES (DVH_7)	0.6 ± 0.6	0.1 to 1.4
Corrected (+ US volumes)	**BAT with RES** (DVH_{14})	17.1 ± 12.9	2.2 to 36.4
	RES with RES (DVH_{15})	7.8 ± 7.2	0.2 to 16.5

Table 6.6: Statistical analysis of the dose and percentage dose difference in PTV in CADPLAN calculations including US shifts and volumes. Data for 7 patients.

The PTV dose difference seems to be related to the magnitude of the volume variation, as expected. Figure 6.7 shows the volume ratio of the average US volume over all fractions ($<V_{US\_T}>$) and the US volume at planning (V_{US_sim}). The dose degradation appears to follow the extent of the volume variation; the larger the volume, the more serious the cold spot. Patient 5 seems to be an extreme case where the shifts, patient geometry and specific dose distribution affect the dose more than predicted from volume variation alone.

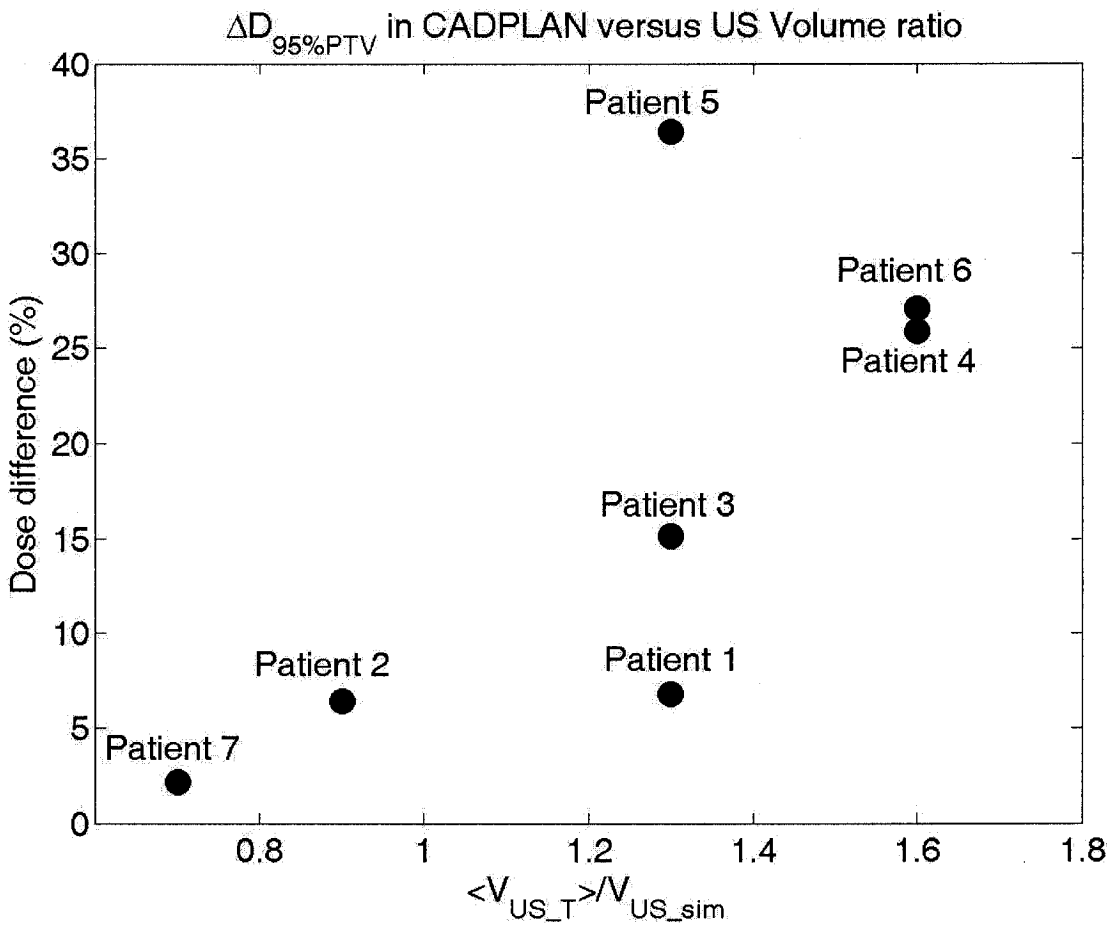

Figure 6.7: Loss of dose coverage measured by the dose difference to 95 % of the PTV as a function of the prostate US volume ratio for *Corrected BAT with RES + V* (DVH_{14}) in CADPLAN calculations.

6.2.2 XVMC

Figure 6.8 gives the XVMC DVH for the same typical patient used in section 6.2.1. As in XVMC with fixed CT volumes, the ideal situation is given by DVH_8, the *Corrected BAT with RES* by DVH_{12} and the *Corrected RES with RES* by DVH_{13}. The US volumetric information is introduced in DVH_{16} and DVH_{17}, the *Corrected BAT with RES + V* and the *Corrected RES with RES + V*, respectively.

XVMC predicts for this patient that if the BAT system was replaced by the RES, the dosimetric impact of prostate volume variation could be reduced from 17 % to 11 % (Table 6.7), not by half as predicted by CADPLAN (Table 6.5).

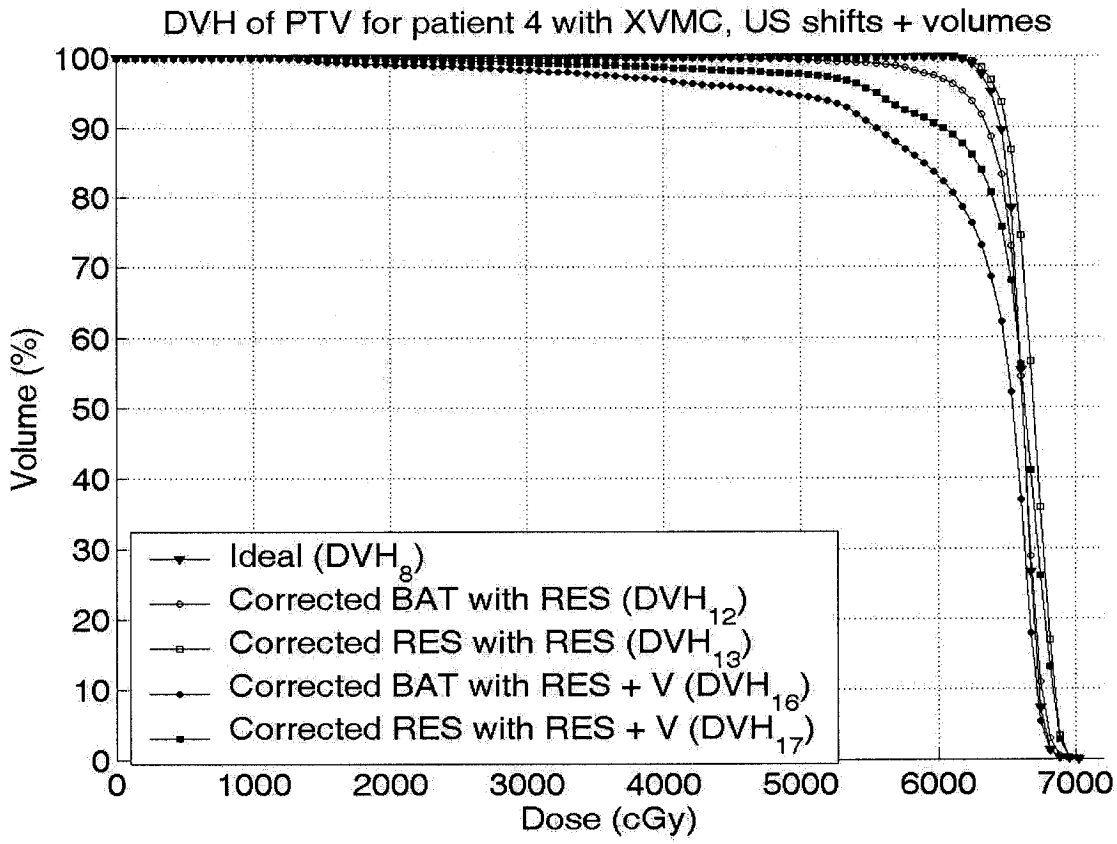

Figure 6.8: US shifts and volumes in XVMC for patient 4: Ideal position (DVH_8), Corrected BAT with RES (DVH_{12}), Corrected RES with RES (DVH_{13}), Corrected BAT with RES + V (DVH_{16}) and Corrected RES with RES (DVH_{17}) + V.

XVMC on patient 4		$D_{95\%PTV}$ (cGy)	$\triangle D_{95\%PTV}$ (%)
Ideal (DVH_8)		6394	-
Corrected	**BAT with RES** (DVH_{12})	6195	3.1
	RES with RES (DVH_{13})	6434	-0.6
Corrected (+ US volumes)	**BAT with RES** (DVH_{16})	5303	17.1
	RES with RES (DVH_{17})	5692	11.0

Table 6.7: Dose and dose difference covering 95 % of the PTV for patient 4 in XVMC including US shifts and volumes.

Table 6.8 and Figure 6.9 summarize the effects of volume variations for all patients. Although DVH_{12} and DVH_{13} represent the same cases as in Table 6.4, the displayed values differ because only 7 patients are now included in the statistics. In clinical practice, XVMC says that if we consider volume changes the degradation remaining in the PTV is 13 % (DVH_{16}). If the RES system was used for realignment instead, the dose could come to within 7 % of the planned dose.

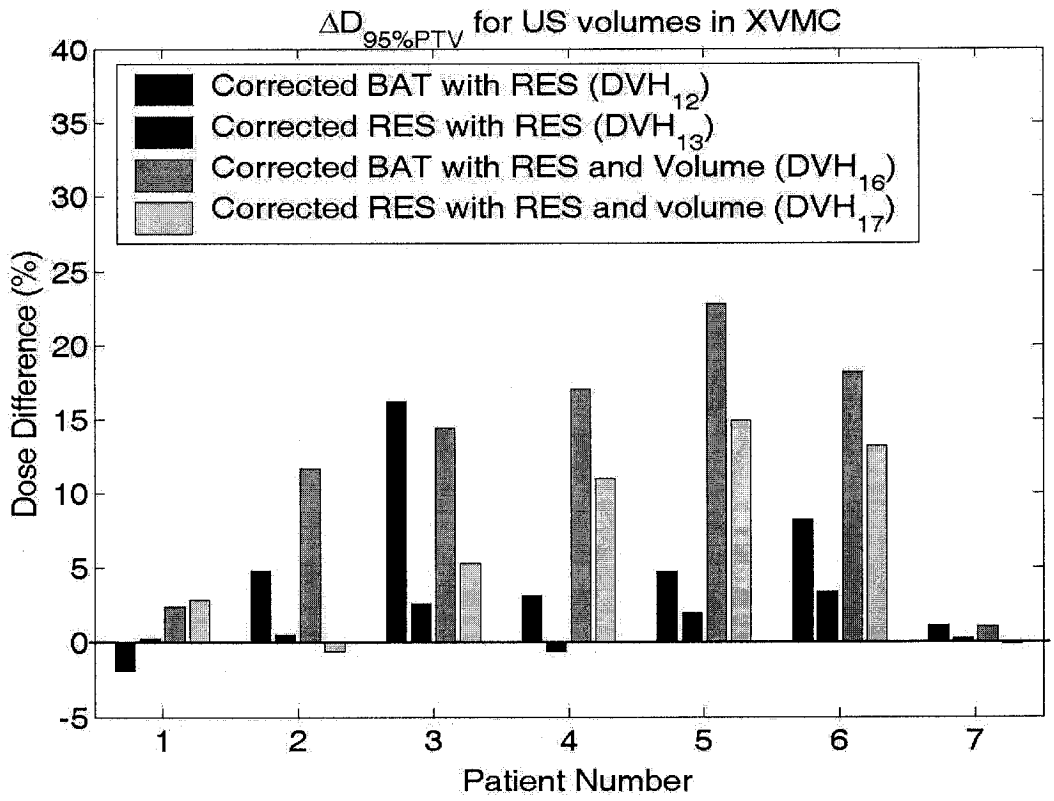

Figure 6.9: Comparison of the percentage dose to 95 % of the PTV volume for a series of XVMC dose calculations including US shifts and volumes.

XVMC		$\Delta D_{95\%PTV}$	
		Mean ± SD (%)	**Range** (%)
Corrected	**BAT with RES** (DVH_{12})	5.2 ± 5.8	-1.9 to 16.2
	RES with RES (DVH_{13})	1.2 ± 1.5	-0.6 to 3.4
Corrected (+ US volumes)	**BAT with RES** (DVH_{16})	12.5 ± 8.2	1.0 to 22.8
	RES with RES (DVH_{17})	6.6 ± 6.4	-0.6 to 14.9

Table 6.8: Statistical analysis of the dose and percentage dose difference in PTV volume in XVMC dose calculations including US volumes. Data for 7 patients.

6.2.3 Conclusion

For the clinical cases presented herein, prostate volume variations between planning time and treatment fractions seem to strongly impact the dosimetry. Replacing the BAT by the RES in the clinic could potentially improve the dosimetric coverage for prostate patients for two reasons: (1) RES offers more accurate measurements on prostate displacements and (2) RES provides volumetric information on a daily basis. Using the RES shifts and volumes in periodic adjustments to the TP might help eliminate cold spots to the target.

Scaling CT volumes to account for US volume changes, thereby neglecting shape changes, seems to be a valid approach according Deurloo *et al* [2]. By quantifying prostate shape variations in 19 patients with CT-scans during EBRT, they concluded prostate deformation to be small compared to motion. Shape changes could hence be treated as a second-order effect in IGRT.

References

[1] Cury F., Shenouda G., Souhami L., Duclos M., Faria S., David M., Corns R. and Falco T. "Comparison of BAT System and a New 3D Trans-abdominal Ultrasound-Based Image-Guided System for Prostate Daily Localization During External Beam Radiotherapy". Depts. Of Radiation Oncology and Medical Physics, McGill University Health Center. Resonant Medical Inc., Research and Development, Montreal, Canada.

[2] Deurloo K.E.I., Steenbakkers R.J.H.M., Zijp L.J., De Bois J.A., Nowak P.J.C.M., Rasch C.R.N. and Van Herk M. "Quantification of shape variation of prostate and seminal vesicles during external beam radiotherapy". Int. J. Radiat. Oncol. Biol. Phys., 61 (1), pp. 228-238, 2005.

[3] Falco T., Shenouda G., Kaufmann C., Belanger I., Procaccini C., Charrois C. and Evans M. "Ultrasound imaging for external-beam prostate treatment setup and dosimetric verification". Medical Dosimetry, 27 (4), pp. 271-273, 2002.

[4] Orgon N.P. and Tomé W.A., "The impact of daily shifts on prostate IMRT dose distributions", Med. Phys, 31 (10), pp. 2845-2848, 2004.

Chapter 7: Conclusions and future work

7.1 Summary of the work performed

Prostate motion and volume variations have been quantified based on 2D and 3D US images acquired daily during prostate RT treatments in a 2003 clinical study (section 7.1.1). Methods of patient dose calculations were compared in preparation for an evaluation on the extent to which prostate changes degrade planned dose distributions. First, dose calculations from the MGH clinical TPS have been compared to dose recalculations in both MC and the same clinical TPS with heterogeneity correction applied (section 7.1.2). Second, two different MC codes were investigated for dose accuracy and speed of computation (section 7.1.3). A previously developed MC TPS (MMCTP) was modified to include the US information. Using DVHs computed in MMCTP, the two US systems have been compared based on their ability to improve the accuracy of dose delivery (section 7.1.4).

7.1.1 Quantification of prostate variations

In agreement with previous unpublished results, a significant systematic difference seems to exist between BAT and RES assessments of prostate alignment. With either system the maximum prostate motion is around 2.5 cm in any direction, quite significant for typical prostates. A smaller lateral variance indicates that bladder and rectal fills have less effect on prostate motion in this dimension.

In terms of volumetric variations, the US volumes calculated are 1.6 times smaller than CT-volumes. The US volumes range from 36 to 70 cm^3 with an average of 48 cm^3. Except the range of volumes that varies by a factor of 2 for most patients, no other trend is observed in the change of prostate volumes over the course of therapy.

7.1.2 XVMC versus CADPLAN

From dose calculations obtained on prostate patients with XVMC and CADPLAN with and without heterogeneity correction, only MC seems to accurately model attenuation and scatter in patient heterogeneities. CADPLAN appears to only slightly better approximate MC if it uses the ETAR correction. Due to the many beams passing thought the femurs for prostate 3D-CRT at the MGH, XVMC predicts a cold spot of 1.5-5.5 % on average to 95 % of the PTV when compared to CADPLAN, except with ETAR, where this difference drops to 0.6-5.2 %. These results seem to indicate an important attenuation by bony structures in the co-planar beams used at the MGH for prostate cancer. This seems to imply the need to use MC simulations to get accurate dosimetry.

On average when compared to CADPLAN, XVMC predicts that around 17.7-37.1 % less of the bladder volume will receive 50 % of the PD, leading to less complication. On the contrary, XVMC predicts that for half of the patients, this dose will be delivered to over 2 % more of the rectum. Such hot spots on the rectum could adversely affect a RT treatment since it is the most radio-sensitive organ of the pelvic region.

7.1.3 XVMC versus DOSXYZ

On the patient with the largest discrepancy between XVMC and CADPLAN, the simplifications used in XVMC compared to DOSXYZ do not seem to significantly affect calculation accuracies. When comparing the two MC codes on the CT patient geometry, DOSXYZ and XVMC are within 1 % on the dose to 95 % of the PTV and within 0.3 % on the maximum dose.

MC simulations are then made to resemble CADPLAN results, in which patients are assumed to entirely consist of water, to evaluate the extent to which MC models heterogeneity. XVMC and DOSXYZ recalculations using only water voxels are seen to get closer to CADPLAN PTV curves than with CT voxels.

7.1.4 Dosimetric impact of prostate variations

For the symmetrical 3D-CRT plans used at the MGH for prostate cancers, a US-based system seems to be required to deliver higher radiation doses with less damage to normal organs due to prostate motion adversely affecting the dosimetry. After incorporating the daily displacements of both US systems into MMCTP, dose calculations on fixed CT volumes showed that patients would have suffered on average from a 20 % underdosage had they not been realigned daily. Realignment with RES could get the dose to the PTV back to 1 % of the planned dose, while it is currently only 14 % with the BAT.

From our results, prostate volume variations seem to strongly impact the dosimetry; the larger the prostate becomes, the more serious the cold spot. Currently in the clinic, a 13 % degradation appears to remain in the dose covering 95 % of the PTV after BAT repositioning due to changes in prostate volume. This situation might be reduced by half on this original TP using only the RES system.

Both positional and volumetric results seem to indicate that replacing the clinical BAT system by the RES could improve the dosimetric coverage for prostate patients.

7.2 Future work

In the view that prostate variations seem to strongly affect dosimetry, adaptive RT becomes an important part of an accurate TP process. By providing a new 4D dose distribution analysis tool for treatment planning, MMCTP could be used to replan a patient an optimized number of times to decrease treatment outcome complications. Dynamically replanning patients during their treatment based on US data might totally eliminate the current colds spots remaining after repositioning. This would improve local tumor control and reduce the morbidity to the OAR. Moreover, rather than scaling the CT volumes by the US volumes, newly devised TP taking the actual RES prostate shapes into account could possibly add precision to the treatment. The RES system, by offering probes for several different cancer sites, should help pioneer advances in adaptive RT protocols for head and neck, breast and other cancers.